

**TOOL DEVELOPMENT FOR ADVANCED SMALL-  
VOLUME / MICROELECTRODE VOLTAMMETRY  
AND APPLICATION**



**A Thesis Submitted in Partial Fulfilment of the Requirements for the  
Degree of Doctor of Philosophy in Chemistry  
Suranaree University of Technology  
Academic Year 2018**

การพัฒนาเครื่องมือทางโวลแทมเมตรีขั้นสูงสำหรับ  
สารปริมาณน้อย/ขั้วไฟฟ้าจุลภาคและการประยุกต์ใช้

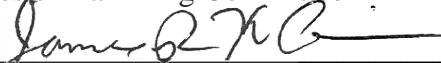


วิทยานิพนธ์นี้เป็นส่วนหนึ่งของการศึกษาตามหลักสูตรปริญญาวิทยาศาสตรดุษฎีบัณฑิต  
สาขาวิชาเคมี  
มหาวิทยาลัยเทคโนโลยีสุรนารี  
ปีการศึกษา 2561


**TOOL DEVELOPMENT FOR ADVANCED SMALL-VOLUME /  
MICROELECTRODE VOLTAMMETRY AND APPLICATION**

Suranaree University of Technology has approved this thesis submitted in partial fulfilment of the requirements for the Degree of Doctor of Philosophy.


Thesis Examining Committee

  
\_\_\_\_\_  
(Prof. Dr. James R. Ketudat-Cairns)

Chairperson

  
\_\_\_\_\_  
(Asst. Prof. Dr. Panida Khunkaewla)


Member (Thesis Advisor)

  
\_\_\_\_\_  
(Prof. Dr. Albert Schulte)


Member

  
\_\_\_\_\_  
(Asst. Prof. Dr. Sanchai Prayoonpokarach)


Member

  
\_\_\_\_\_  
(Assoc. Prof. Dr. Werasak Surareungchai)

Member

  
\_\_\_\_\_  
(Prof. Dr. Santi Maensiri)

Vice Rector for Academic Affairs  
and Internationalization

  
\_\_\_\_\_  
(Assoc. Prof. Dr. Worawat Meevasana)

Dean of Institute of Science

นายห่วยซุง ชิม : การพัฒนาเครื่องมือทางโวลแทมเมตรีขั้นสูงสำหรับสารปริมาณน้อย/  
ขั้วไฟฟ้าจุลภาคและการประยุกต์ใช้ (TOOL DEVELOPMENT FOR ADVANCED  
SMALL-VOLUME / MICROELECTRODE VOLTAMMETRY AND APPLICATION)  
อาจารย์ที่ปรึกษา : ผู้ช่วยศาสตราจารย์ ดร.พนิดา ชันแก้วหล้า, 137 หน้า.

การย่อขนาด / เคมีสีเขียว / แถบไมโครแบบแถว

ความก้าวหน้าในเทคนิคการทำอุปกรณ์อิเล็กทรอนิกส์ขนาดไมโคร และวิธีการประดิษฐ์  
อุปกรณ์ระดับไมโครและนาโน ทำให้การปรับปรุงเครื่องมือวิเคราะห์ทางเคมีไฟฟ้าให้มีขนาดเล็ก  
ลงเป็นที่ได้รับความสนใจเป็นอย่างสูง นอกจากนี้ปัจจุบันได้มีการตื่นตัวถึงปัญหาด้านสิ่งแวดล้อม  
จึงนำไปสู่ความสนใจเกี่ยวกับผลกระทบเชิงลบที่อาจเกิดขึ้นจากกิจกรรมทางวิทยาศาสตร์บนโลก  
ใบนี้

หัวข้อย่อสามเรื่องของโครงการวิจัยระดับปริญญาเอกนี้ได้ถูกจัดทำขึ้นด้วยแนวคิดหลัก  
ของการแนะนำเครื่องมือและเทคนิคที่ง่าย ประหยัด สามารถเข้าถึงได้ให้แก่ห้องปฏิบัติการวิจัยและ  
การเรียนการสอน โดยเฉพาะโครงการที่มีงบประมาณที่จำกัด ซึ่งเชื่อว่าคุณสมบัติเหล่านี้เป็นปัจจัย  
ในการผลักดันวิธีทางเคมีไฟฟ้าไปสู่ความเป็นมิตรกับสิ่งแวดล้อมด้วยประสิทธิภาพการวิเคราะห์ที่ดี  
ขึ้น

การประดิษฐ์และการประยุกต์ใช้อย่างมีศักยภาพของเซลล์เคมีไฟฟ้าขนาดเล็กแบบสาม  
ขั้วไฟฟ้าคือท่อแพลตตินัม (Pt-T) ขนาดเล็กจะถูกอธิบายไว้ในส่วนที่หนึ่งของโครงการวิจัยนี้ โดย  
เป็นการวางท่อแพลตตินัมบนขั้วไฟฟ้าทำงานในตำแหน่งตั้งตรง ท่อแพลตตินัมนี้ทำหน้าที่เป็นทั้ง  
ขั้วไฟฟ้าช่วย และเป็นที่บรรจุสารละลายตัวอย่างขนาด 30 – 60 ไมโครลิตร เซลล์เคมีไฟฟ้าจะถูกทำ  
ให้สมบูรณ์ได้โดยการใส่ขั้วไฟฟ้าอ้างอิงขนาดเล็กเข้ามาในเซลล์จากด้านบนที่เปิดไว้ เซลล์นี้แสดง  
ให้เห็นถึงความยืดหยุ่นในการเลือกขั้วไฟฟ้าทั่วไปมาประยุกต์ใช้ นอกจากนี้ยังสามารถนำมา  
ประยุกต์ใช้ในการตรวจวัดและการหาปริมาณของสารต่าง ๆ ได้หลากหลาย ตั้งแต่ ยา ฮอร์โมน  
วิตามิน สารที่สามารถเกิดปฏิกิริยารีดอกซ์ได้ อีกทั้งการประยุกต์ใช้กับเซนเซอร์ทางชีววิทยาใน  
ระดับไมโครลิตรได้

ส่วนที่สองของงานนี้อธิบายถึงการสร้างขั้วไฟฟ้าแถบทองแดงระดับไมโครแบบแถวโดย  
การประกบแผ่นทองแดงที่มีความหนาในระดับไมโครเมตรกับแผ่นอะคริลิกให้เป็นแถวซ้อนกัน  
เว้นระยะอย่างสม่ำเสมอจำนวนเจ็ดแถว ขั้วไฟฟ้านี้มีความไวสูงสำหรับการตรวจวัดไฮโดรเจนเปอร์  
ออกไซด์ (Hydrogen peroxide) และ โดพามีน (Dopamine) เมื่อเปรียบเทียบกับขั้วไฟฟ้าทองแดง



แบบแผ่นกลม ซึ่งปรากฏการณ์นี้บ่งบอกว่ามีประสิทธิภาพในการถ่ายโอนมวลสารที่มากขึ้น โดยเป็นไปตามการคาดการณ์ที่ว่ามีการแพร่กระจายของสารบริเวณรอบ ๆ แถบขนาดไมโครในลักษณะครึ่งทรงกลม

การตรวจวัดและการหาปริมาณออกซิโทซิน (OXT) ในส่วนที่สาม เริ่มจากความต้องการของกลุ่มประสาทวิทยาที่ได้มีการทำงานร่วมกัน โดยต้องการหาความเข้มข้นของ OXT ในตัวอย่างสมองของหนูทดลองจากไมโครไดอะไลซิสในระดับพิโคโมลาร์ การตรวจวิเคราะห์ทางเคมีไฟฟ้าโดยใช้เซลล์ท่อแพลตตินัมขนาดเล็ก (Pt-T) กับขั้วไฟฟ้าเพชรที่มีโบรอนเจือปนสามารถตรวจวัดออกซิโทซินที่ความเข้มข้นประมาณ 60 ไมโครโมลาร์ การวิเคราะห์หาปริมาณสารในระดับที่ต่ำกว่านี้ได้ถูกพยายามทำโดยเทคนิคอิมมูโนเซนเซอร์ทางเคมีไฟฟ้า ซึ่งเป็นที่ทราบว่าสามารถตรวจวัดสารชีวโมเลกุลได้ในระดับเฟมโตโมลาร์ อย่างไรก็ตามมีปัญหาเกิดขึ้นเนื่องจากขนาดที่เล็กของออกซิโทซิน และไม่มีโมโนโคลนอลแอนติบอดีคู่ที่เหมาะสมสำหรับการทำปฏิกิริยาทางภูมิคุ้มกันแบบแซนวิชที่มีประสิทธิภาพ และยังแก้ไขไม่ได้



มหาวิทยาลัยเทคโนโลยีสุรนารี

สาขาวิชาเคมี

ปีการศึกษา 2561

ลายมือชื่อนักศึกษา



ลายมือชื่ออาจารย์ที่ปรึกษา



ลายมือชื่ออาจารย์ที่ปรึกษาร่วม



WEI CHUNG SIM : TOOL DEVELOPMENT FOR ADVANCED SMALL-  
VOLUME / MICROELECTRODE VOLTAMMETRY AND  
APPLICATION. THESIS ADVISOR : ASST. PROF. PANIDA  
KHUNKAEWLA, Ph.D. 137 PP.

#### MINIATURISATION / GREEN CHEMISTRY / MICROBANDS ARRAY

Promoted by advancements in microelectronics and in micro- and nano-fabrication methods, the miniaturisation of electroanalytical instrumentation has been a topic of high interest. Besides, environmental problems have also alarmed, leading to high attention on the potential negative impacts of scientific activities on Mother Earth.

The three subtopics of this PhD research project were structured with the key ideas of introducing tools and techniques which are easy, economical, green and accessible to most research and teaching laboratories, especially those with limited budgets. It is believed that these properties are the factors for driving electrochemistry towards a greener practice with better analytical performance.

The making and potential application of a miniaturised 3-electrode electrochemical minicell arrangement, namely the Platinum-tube (Pt-T) minicell was described in part 1 of this thesis. Upon placement on an upright working electrode, this little gadget served both as the counter electrode and the holder of 30 – 60  $\mu\text{l}$  of sample solution. The electrochemical cell was then completed with the insertion of a mini reference electrode from the top opening. The cell demonstrated its flexibility in the choice of electrodes. It also showed a wide applicability for the detection and

quantification of various analytes ranging from drugs, hormones, vitamins, and redox labels as well as biosensing applications at the  $\mu\text{l}$  level.

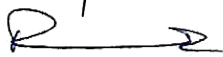
Part 2 of this work described the production of a Cu microband array electrode by sandwiching a piece of micron-thick copper foil in between acrylic plates to produce an array of seven evenly spaced microbands. This electrode demonstrated higher sensitivity for the detection of hydrogen peroxide and dopamine in comparison to a Cu disc electrode. This phenomenon suggested a more efficient mass transport mode, which agreed with the prediction of a hemicylindrical diffusion field around the vicinity of the microbands.

Oxytocin detection and quantification in Part 3 was initially driven by the need of a collaborating neuroscience group aiming at the detection of picomolar oxytocin in samples from rat brain microdialysis. Electrochemical detection in the Pt-T minicell with a boron doped diamond electrode detected oxytocin at about  $60\ \mu\text{M}$ . Lower level detection was then attempted with electrochemical immunosensing technique known for femtomolar biomolecule detection. However, the problems arising from the small size of oxytocin and the lack of suitable monoclonal antibody pair for effective sandwich immunoreaction are yet to be solved.

School of Chemistry

Academic Year 2019

Student's Signature 

Advisor's Signature 

Co-advisor's Signature 

## ACKNOWLEDGEMENTS

It is a pleasure for me to express my greatest gratitude to the following groups and individuals who have contributed either directly or indirectly to the completion of this thesis.

First, I would like to express my deepest appreciation to Prof. Dr Albert Schulte, currently affiliated to Vidyasirimedhi Institute of Science and Technology (VISTEC) for his knowledge and guidance throughout this project. I would like to thank also Asst. Prof. Dr Panida Khunkaewla, Suranaree University of Technology (SUT) for her willingness to provide academic guidance since year 2 of my PhD studies.

I am also grateful to Suranaree University of Technology for awarding me a full scholarship under the SUT-PhD Scholarship Program for ASEAN and Malaysian Agricultural Research and Development Institute (MARDI) for granting me a 3-year study leave.

A deepest acknowledgement is extended to Assoc. Prof. Dr Weresak Surareungchai as well as all members of Sensor Technology Group, King Mongkut University of Technology Thonburi (KMUTT) for their guidance and help during my attachment to their laboratory.

My heartiest thanks are extended to all members of the Biochemistry-Electrochemistry Research Unit (BECRU), School of Chemistry, Institute of Science and Center for International Affairs for their support over the past three years.

I would like to thank Ms Napapha Noeisingnoen for her help in the Thai abstract of this thesis, as well as her assistance during my stay in Nakhon Ratchasima. Besides, a special appreciation is due to Mr Thawatchai Butchat for his companion over the past year.

Last but not least, I would like to thank my family members for their moral support which is especially needed as a student residing abroad.

Wei Chung Sim



# CONTENTS

	<b>Page</b>
ABSTRACT IN THAI.....	I
ABSTRACT IN ENGLISH .....	III
ACKNOWLEDGEMENTS.....	V
CONTENTS.....	VII
LIST OF TABLES .....	XI
LIST OF FIGURES .....	XII
LIST OF ABBREVIATIONS.....	XIX
<b>CHAPTER</b>	
<b>I INTRODUCTION .....</b>	<b>1</b>
1.1 Electrochemical workstations .....	2
1.1.1 Electrochemical cells.....	3
1.1.2 Potentiostat and computer software controller .....	3
1.1.3 Electrochemical reaction.....	3
1.2 Miniaturisation in electrochemistry .....	4
1.3 Microelectrodes .....	5
1.4 Immunosensor for effective neuropeptide electroanalysis.....	9
1.4.1 Neuropeptides.....	9
1.4.2 Oxytocin .....	10
1.4.3 Electrochemical sensors .....	12

## CONTENTS (Continued)

	<b>Page</b>
1.4.4 Electrochemical immunosensors .....	13
1.5 Objectives .....	17
<b>II LITERATURE REVIEW .....</b>	<b>18</b>
2.1 Miniaturisation of electrochemical cell .....	18
2.1.1 Microliter electrochemical analysis .....	18
2.2 Band array electrode .....	21
2.2.1 Microelectrode arrays .....	21
2.3 Immunosensor for oxytocin detection .....	23
2.3.1 Detection of oxytocin .....	23
2.3.2 Electrochemical immunosensors .....	26
<b>III METHODOLOGY .....</b>	<b>31</b>
3.1 Chemicals .....	31
3.1.1 Preparation of phosphate buffer saline .....	32
3.1.2 Methylene blue-multiwall carbon nanotubes conjugate .....	32
3.1.3 Methylene blue-multiwall CNT-antibody conjugate .....	32
3.2 Electrodes and instrumentation .....	33
3.2.1 Glassy carbon electrode .....	33
3.2.2 Boron-doped diamond electrode .....	34
3.2.3 Pencil lead cylindrical electrode .....	34
3.2.4 Noble metal electrodes .....	34
3.2.5 Copper electrodes .....	34

## CONTENTS (Continued)

	<b>Page</b>
3.2.6 Glucose biosensor.....	34
3.2.7 Mini reference electrode.....	35
3.2.8 $\Omega$ -shaped Pt minicell .....	35
3.2.9 Pipette tip minicell.....	36
3.2.10 Pt-tube minicell .....	36
3.2.11 Electrode stands.....	37
3.2.12 Microband array electrode.....	40
3.2.13 Potentiostat .....	43
3.2.14 Digital Vernier calliper.....	43
3.2.15 Scanning electron microscope.....	43
3.2.16 Preparation of electrochemical immunosensor .....	44
3.3 Experimental .....	44
3.3.1 Electrochemical sensing parameters.....	44
3.3.2 Electrochemical immunosensing.....	45
<b>IV RESULTS AND DISCUSSION.....</b>	<b>46</b>
4.1 Development of miniaturised electrochemical cell.....	46
4.1.1 Tests with the $\Omega$ -shaped Pt minicell.....	47
4.1.2 Tests with the pipette tip minicell .....	51
4.1.3 Tests with the Pt-tube minicell.....	52
4.1.3.1 Simplicity of Pt-T minicell operation and working electrode compatibility.....	52



## CONTENTS (Continued)

	<b>Page</b>
4.1.3.2 Basic electrochemical performance of Pt-T minicell.....	54
4.1.3.3 Concentration stability of Pt-T minicell.....	60
4.1.3.4 General Pt-T minicell applicability .....	62
4.1.3.5 Pt-T minicell application for paracetamol quantification by pulse voltammetry .....	67
4.2 Copper Microbands Array Electrode .....	72
4.2.1 Topography of copper microband array electrode .....	72
4.2.2 Microelectrode characteristic of copper band electrode.....	76
4.2.3 Detection of hydrogen peroxide .....	78
4.2.4 Issues as a glucose biosensor.....	81
4.2.5 Solution biosensing of glucose.....	86
4.2.6 Detection of dopamine .....	89
4.3 Electrochemical immunosensor for quantification of oxytocin .....	92
4.3.1 Affinity of MB-MWCNT with blocking material.....	93
4.3.2 Sandwich immunoassay .....	97
<b>V CONCLUSIONS.....</b>	<b>100</b>
REFERENCES .....	104
APPENDICES .....	119
CURRICULUM VITAE.....	137

## LIST OF TABLES

Table	Page
2.1	List of commercially available oxytocin test kits .....24
3.1	Experimental parameters for experiment in Figure 4.12 .....44
4.1	Cathodic and anodic peak currents analysis for hexacyanoferrate(III) on a Pt wire electrode at various CV scan rates.....50
4.2	Recoveries of paracetamol in sample with a nominal concentration of 10 $\mu\text{M}$ ..... 71
4.3	Current density comparison of hydrogen peroxide calibration of copper disc and copper $\mu\text{BAE}$ using amperometry in a bipotentiostat configuration.....80

## LIST OF FIGURES

Figure	Page
1.1	A typical electrochemical workstation .....2
1.2	The twelve principles of green chemistry.....5
1.3	The three modes of mass transport .....7
1.4	Diffusional field of analyte to macroelectrode and microelectrode .....8
1.5	Structure of a neuron cell..... 10
1.6	Structure of oxytocin and its form in solution elucidated by NMR ..... 12
1.7	General structure of an antibody (Ab)..... 14
1.8	Schematic illustration of competition immunoassay and sandwich immunoassay ..... 15
2.1	Schematic illustration of the configuration of the 50 $\mu$ l hanging droplet microcell demonstrated by Jimenez <i>et al.</i> (2015).....20
2.2	Miniaturised electrochemical cell proposed by Skalová <i>et al.</i> (2018).....20
2.3	Schematic illustration of sandwich type electrochemical immunosensor with antibody immobilised via physical adsorption.....28
2.4	Structure of methylene blue.....30
2.5	Structure of single walled, double walled and multi walled carbon nanotubes .....30

## LIST OF FIGURES (Continued)

Figure	Page
3.1	List of selected common electrodes found in an ordinary electrochemical laboratory.....33
3.2	The $\Omega$ -shaped Pt minicell in operation .....35
3.3	The construction of a pipette tip minicell .....36
3.4	The making of minicell and schematic setup of minicell operation .....37
3.5	A custom-made acrylic box platform with copper coil underneath for holding electrodes with a banana plug (male connector) upright .....38
3.6	A heavy glass plate with a short glass tube section fixed at the centre designed as an accessory to hold electrodes with a flat end upright .....39
3.7	Illustration of electrodes which are light be held steadily upright with a crocodile clip clamped onto a firm retort stand .....39
3.8	Initial Cu $\mu$ BAE prototypes using different materials as the spacer .....41
3.9	Zoom-in view of the copper microbands of electrodes in Figure 3.8.....41
3.10	Illustration of construction of copper microband array electrode .....42
3.11	The making of copper microband array electrode with super glue as adhesive .....43
4.1	The operational electrochemical workstation using an $\Omega$ -shaped Pt minicell .....47
4.2	CVs of 1 mM hexacyanoferrate(III) in 0.1 M KCl on the surface of a 1 mm 250 $\mu$ m cylindrical Pt electrode in a Pt inverted- $\Omega$ minicell and a conventional 5 ml cell at scan rates varying from 2 to 100 $\text{mV s}^{-1}$ .....49

## LIST OF FIGURES (Continued)

Figure	Page
4.3	Evaluation of rate of electron transfer of hexacyanoferrate(III) at a 1 mm long Pt wire electrode of 250 $\mu\text{m}$ diameter in the inverted- $\Omega$ Pt minicell.....50
4.4	The setup of Pt-T minicell in operation.....52
4.5	Cyclic voltammograms of 12.5 mM hexacyanoferrate(III) in 0.1 M PBS (pH 7.0) in a Pt-T minicell with a 30 $\mu\text{l}$ electrolyte load for various electrodes .....56
4.6	Comparison of CV consistency of conventional 5 ml beaker cell and Pt-T minicell .....57
4.7	CVs of 1 mM hexacyanoferrate(III) in 0.1 M KCl on the surface of a 3 mm Pt disc electrode in the Pt-T minicell and a conventional 5 ml cell at scan rates varying from 2 to 100 $\text{mV s}^{-1}$ on 3 mm Pt electrode .....59
4.8	Evaluation of rate of electron transfer of hexacyanoferrate(III) at a 3 mm Pt disc electrode using Pt-T minicell.....60
4.9	Oxidative peak currents of DPV for a 30 $\mu\text{l}$ aliquot of 5 mM hexa ammineruthenium(III) solution in a Pt-T minicell over a duration of 70 min at room temperature (28°C) in the absence of solvent- saturated environment.....61
4.10	Structures of ciprofloxacin and doxorubicin .....63
4.11	Oxidation mechanism of 4-methylumbelliferone as proposed by L. Wang <i>et al.</i> (2015).....64

## LIST OF FIGURES (Continued)

<b>Figure</b>	<b>Page</b>
4.12	Minicell electrochemical experiments on drugs, hormone, antioxidant, redox label and disease-indicating oxidase biosensor .....66
4.13	Plots of current vs concentration of ciprofloxacin, doxorubicin, oxytocin, ascorbic acid, 4-methylumbelliferone and glucose for the respective experiments in Figure 4.12 .....67
4.14	DPVs showing oxidation peaks of standard solutions of PCT ranging from 1,000 to 3.124 $\mu\text{M}$ .....68
4.15	Calibration curve plot of DPV anodic peaks from Figure 4.14 against PCT concentration .....68
4.16	Schematic illustration of PCT standard solution preparation for calibration and standard addition for quantification of paracetamol in sample .....69
4.17	DPVs of quantification of PCT with nominal concentration 10 $\mu\text{M}$ by the standard addition method.....70
4.18	Standard addition plot for the quantification of PCT with nominal concentration of 10 $\mu\text{M}$ .....71
4.19	Topography of copper microband array electrode BE002 and elemental distribution analysis of a selected region of BE002 by energy dispersive X-ray spectroscopy .....73
4.20	Topography of a single copper microband of BE005 and copper disc electrode (Cu 2 mm) by scanning electron microscopy .....74

## LIST OF FIGURES (Continued)

Figure	Page
4.21	Topography of copper microband array electrode BE011 and elemental distribution of copper and carbon on the selected region of BE011 by energy dispersive X-ray spectroscopy.....75
4.22	Illustration of expected hemicylindrical diffusion mode along the microbands of a $\mu$ BAE .....76
4.23	The linear sweep voltammograms of a Cu $\mu$ BAE, a 1 mm disc and a 2 mm disc electrodes at various scan rates ranging from 5 to 50 $\text{mV s}^{-1}$ in 5 mM hexaamineruthenium(III) solution.....77
4.24	Chronoamperometric traces of hydrogen peroxide response of copper $\mu$ BAE BE002 and copper disc electrode in a bipotentiostat mode.....79
4.25	Chronoamperometric traces of hydrogen peroxide response of copper $\mu$ BAE BE005 and copper disc electrode in a bipotentiostat configuration.....80
4.26	Amperometric response of glucose detection with glucose oxidase biosensor on BE005 .....82
4.27	Plot of cathodic current against glucose concentration .....83
4.28	Amperometric trace of a glucose oxidase sensor on a $\mu$ BAE (BE005) platform with nitrogen gas purged during 1000 – 2000 s.....83
4.29	Illustration of diffusion of molecules at the immobilised glucose oxidase layer over the surface of a macroelectrode.....85

## LIST OF FIGURES (Continued)

Figure	Page
4.30	Illustration of diffusion of molecules at the immobilised glucose oxidase layer over the surface of copper microband array electrode .....85
4.31	Cathodic paint deposited along the copper microbands .....86
4.32	Amperometric trace of a series of glucose additions into 5 ml of 0.5 $\mu$ M glucose oxidase solution using $\mu$ BAE (BE011) as the sensor for enzymatically produced hydrogen peroxide .....88
4.33	Calibration curve of glucose in 5 ml of 0.5 $\mu$ M glucose oxidase solution using $\mu$ BAE (BE011) as the sensor for enzymatically produced hydrogen peroxide .....89
4.34	Cyclic voltammograms of $\mu$ BAE (BE011) and 2 mm copper disc in 0.1 M phosphate buffer (pH7.0) before used for detection of dopamine.....90
4.35	Differential pulse voltammograms of dopamine with increasing concentration from 0.2 to 2.29 mM using $\mu$ BAE BE011 and 2 mm copper disc .....91
4.36	Calibration curves of dopamine in 0.1 M phosphate buffer (pH 7.0) using $\mu$ BAE (BE011) and copper 2 mm disc electrode.....91
4.37	Differential pulsed voltammograms for the application of 0, 0.1 and 1% BSA for the blocking of SPE surface washed by flowing 3 times 1 ml of 0.05% PBST .....94



## LIST OF FIGURES (Continued)

<b>Figure</b>	<b>Page</b>
4.38	Differential pulsed voltammograms for the application of 0, 0.1, 0.5 and 1% BSA for the blocking of SPE surface and later soaked in 2 ml 0.05% PBST for 10 min.....95
4.39	Differential pulsed voltammograms for the application of 0, 0.1, 0.5 and 1% BSA for the blocking of SPE surface and later soaked in 2 ml 2% PBST for 10 min.....95
4.40	Differential pulsed voltammograms for the application of 0, 0.1, 0.5 and 1% casein for the blocking of SPE surface and later soaked in 2 ml 2% PBST for 10 min .....96
4.41	Peak current summary of various blocking and washing conditions from Figure 4.37, Figure 4.38, Figure 4.39 and Figure 4.40.....96
4.42	Differential pulsed voltammograms of the effect of coating redox label MB-MWCNT with 1% BSA .....97
4.43	Differential pulsed voltammograms of oxytocin detection with various conditions.....99

## LIST OF ABBREVIATIONS

A <sub>b</sub>	Antibody
A <sub>g</sub>	Antigen
μBAE	Microband array electrode
BDD	Boron doped diamond
BSA	Bovine serum albumin
CA	Chronoamperometry
CE	Counter electrode
CIP	Ciprofloxacin
CNT	Carbon nanotube
CV	Cyclic voltammetry or Cyclic voltammogram
DPV	Differential pulse voltammetry or Differential pulse voltammogram
DOX	Doxorubicin
EDS	Energy dispersive X-ray spectroscopy
ELISA	Enzyme-linked immunosorbent assays
GC	Glassy carbon
GOx	Glucose oxidase
IU	International unit (biological activity)
MB	Methylene blue
MWCNT	Multiwall carbon nanotube
OD	Outer diameter

**LIST OF ABBREVIATIONS (Continued)**

PCT	Paracetamol
PEEK	Polyether ether ketone
PEG	Polyethylene glycol
Pt-T	Platinum tube
RE	Reference electrode
rpm	revolution per minute
RSD	Relative standard deviation
SEI	Secondary electron imaging
SEM	Scanning electron microscopy
sqrt	Square root
S <sub>rate</sub>	Scan rate
WE	Working electrode

# CHAPTER I

## INTRODUCTION

Promoted by advancements in microelectronics and in micro- and nano-fabrication methods, the miniaturisation of electroanalysis instrumentation has been a topic of high interest, with attention given to all the three practical system components, namely the sensors, the peripherals and the two- or three-electrode electrochemical cells. Besides, environmental problems over the past decades have also raised the concern of scientists to pay more attention to the potential negative impacts of their activities on Mother Earth. In 1998, this has led to the introduction of the *Twelve Principles of Green Chemistry*, which covers various aspects in chemical synthesis (Anastas and Warner, 1998).

However, research has been focusing on technological advancement to be presented in high impact factors journals. Though most of these advancements are practical and do provide answers to certain issues, they are mostly not easily adaptable by the majority of laboratories, mainly due to the budget restrictions and sophisticated high-end facilities needed.

Thus, this PhD research project was structured with the key ideas of introducing tools and techniques which are easy, economical, green and accessible to most research and teaching laboratories, especially those with a limited budget. It is believed that these properties are the factors that will drive the industry users of electroanalysis towards a greener practice.

This PhD project focuses on the development of new electrochemical tools that can improve the workflow and performance of chemical analysis. The work is divided into three main parts, namely the miniaturisation of three-electrode electrochemical cells, the development of microband array working electrode for voltammetry and the electrochemical immunosensor for the detection of oxytocin. In this work, some of the twelve principles of green chemistry (see **Figure 1.2**), e.g. waste reduction and energy efficiency, are also addressed.

The background topics related to the scope mentioned above are introduced in the following subsections.

## 1.1 Electrochemical workstations

An electrochemical workstation is an instrumental setup and configuration that enables electrochemical experiments. A typical electrochemical workstation found in a conventional electrochemical laboratory comprises of an electrochemical cell, a potentiostat and a computer (see **Figure 1.1**).

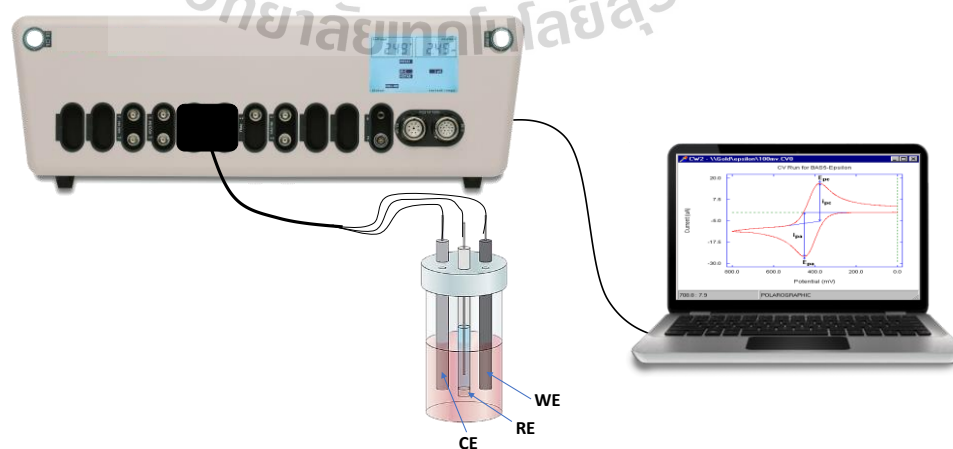


**Figure 1.1** A typical electrochemical workstation.

### **1.1.1 Electrochemical cells**

An electrochemical cell can be classified into two categories namely a device that generates electrical power from a chemical reaction and a device that performs a chemical reaction with the application of external electrical energy. The former being called galvanic cell, voltaic cell or battery, while the latter is known as an electrolytic cell.

Electrochemical cell discussed in the context here generally refers to the electrolytic cell. A typical electrochemical cell consists of the working electrode (WE), reference electrode (RE) and counter electrode (CE) immersing in an electrolyte in the 3-electrode configuration, while a 2-electrode configuration combines the reference and counter electrodes. In both cases, the electrodes are connected to a potentiostat for the application of a potential to the working electrode and current measurement for quantitative analyses of analytes.

### **1.1.2 Potentiostat and computer software controller**

A potentiostat is an electrical device that is capable of applying a potential to a working electrode with the help of a software controller, either a built-in program controller or a computer software controller. The potential applied can be either a specific constant potential relative to the reference electrode, a potential sweep profile, where the potential gradually changes at a specified scan rate, or a potential pulse profile, in which current is taken before and after a potential pulse application.

### **1.1.3 Electrochemical reaction**

Upon the application of a certain potential, an oxidation or reduction reaction of an electroactive species is expected to take place at the working electrode. Oxidation happens when an electroactive species gives up electrons to the working

electrode surface, while reduction takes place when an electroactive species gains electrons from the working electrode surface. A corresponding opposite reaction will take place at the counter electrode following the principle of charge conservation, which says that the total electrical charge in an isolated system never changes. It is the electron transfer from the working to the counter electrode that is being measured as the current of an electrochemical measurement. Usually, the surface area of counter electrode should be much larger than that of the working electrode so that it is not the limiting factor to the reaction at the working electrode. A general oxidation reaction can be presented or written as  $O + ne^- \rightleftharpoons R$ , where O and R are the oxidised and reduced species, respectively, of the redox couple. The reversed reaction is a reduction reaction.

## 1.2 Miniaturisation in electrochemistry

Miniaturisation is a growing trend in the field of analytical chemistry. Firstly, miniaturisation works on electrochemical cell aim on the reduction of sample volume, e.g. screen-printed electrode system and hanging micro-volume droplet cell (Jimenez *et al.*, 2015; Kai *et al.*, 2014; Neugebauer *et al.*, 2004; Riberi *et al.*, 2018). Secondly, miniaturisation works on electrode target on minimising the dimension of electrode for local measurement (*in situ*) on minute objects; reducing the capacitive current; reducing the effect of resistance; and increasing the signal-to-noise (S/N) ratio (J. Wang, 2006). This includes the reduction of electrode size to micro- and nano-size to be used in an electrophysiological study, for example, microelectrode as brain sensor probe for real-time monitoring of neural signal or electrical stimulation of nervous tissue (Kwon *et al.*, 2016). Lastly, the reduction of the size of electrochemical peripherals for ease of use and improved portability, e.g. hand-held battery powered devices (Xiang and Lu,

2011). Miniaturised electrochemical cells have also been reported for use in a flow-based system (Kovalcik *et al.*, 2004).

This is also in-line with the waste prevention principle, one of the twelve principles of green chemistry, which was first introduced by Anastas and Warner (1998). The twelve principles of green chemistry is a set of values that enable scientists to protect and benefit the economy, people and the Mother Earth, when they are incorporated into the design, development and implementation of chemical products and processes.

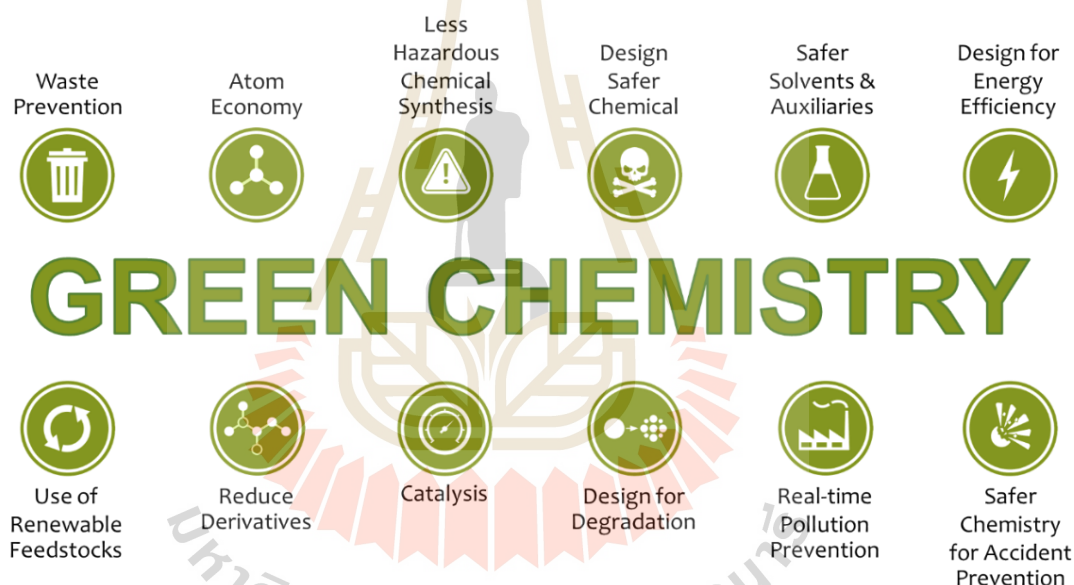


**Figure 1.2** The twelve principles of green chemistry.

### 1.3 Microelectrodes

Microelectrodes have received an explosion of interest since the 1980s and have made an impact on both fundamental and applied electrochemistry. Montenegro *et al.* (2012) reviewed that microelectrode experiments: (1) are cheap to perform and simple to carry out, (2) are based on sound fundamental principles, (3) improve greatly



the quality of experimental data, (4) facilitate a range of new experiments not feasible with large electrodes and (5) have applications in many fields of science.

Electrode process comprises the interfacial electrode reaction and mass transport phenomena. Electrode reaction refers to the physical (nonfaradaic) and chemical (faradaic) reactions that take place at the electrode surface, while mass transport involves the delivery of chemical species to the electrode surface. These processes govern the electrochemical performance of a detection scheme. (Bard and Faulkner, 2001)

Mass transport includes three main modes: (1) diffusion, a motion driven by the species concentration gradient; (2) migration, a motion of a charged species under the influence of an electrical potential gradient; and (3) convection, the hydrodynamic transport of species based on density gradient in a liquid body (natural convection) or external force (forced convection). An illustration of these modes is shown in **Figure 1.3**. Diffusion is the mode that should always be taken into consideration because during an electrochemical process, analyte will be consumed, thus creating a concentration gradient between the vicinity around the electrode surface and the bulk environment. This induces the transport of analyte from the bulk (higher concentration) to the electrode surface (lower concentration). (Scholz *et al.*, 2010; J. Wang, 2006)

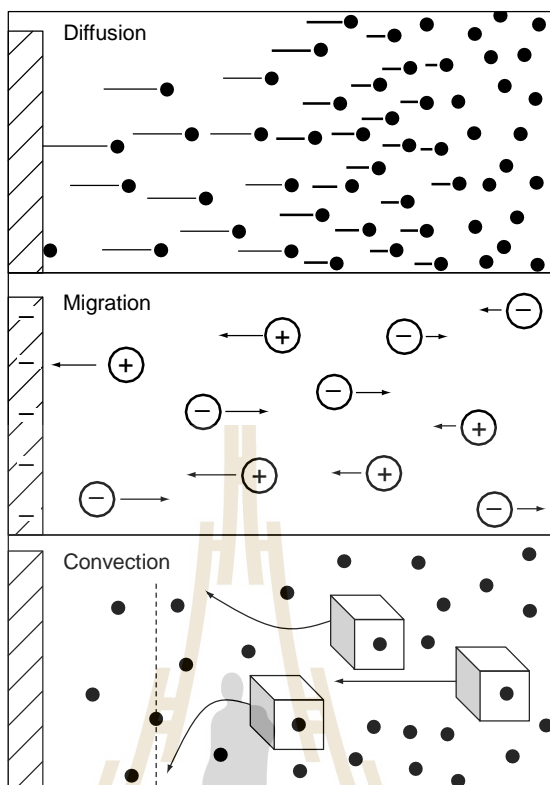


**Figure 1.3** The three modes of mass transport. (J. Wang, 2006)

The efficiency of diffusion is different for a macroelectrode and a microelectrode. **Figure 1.4** illustrates the conditions of diffusion for a macroelectrode and a microelectrode. For a macroelectrode (e.g. 3 mm disc electrode), planar diffusion dominates mass transport of analyte molecules to the electrode surface. In planar diffusion, analyte molecules are mainly travelling perpendicularly to the electrode surface. When the dimension of the disc is shrunk to micro-dimension, e.g. 10  $\mu\text{m}$  disc, radial diffusion becomes more dominant. Analyte molecules in the bulk solution diffuse to the electrode surface from all directions in a hemispherical diffusion pattern. This increases the mass flux and hence then faradaic current density. This effect is responsible for the sigmoidal shaped steady state in a cyclic voltammogram of a microelectrode.

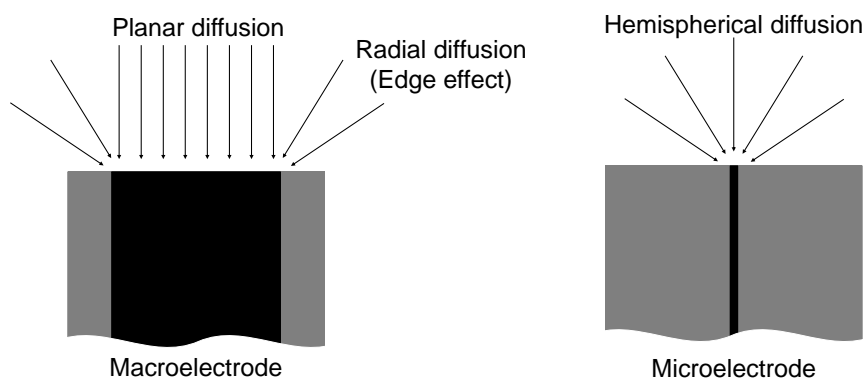


**Figure 1.4** Diffusional field of analyte to macroelectrode and microelectrode.

Today, microelectrode is generally defined as an electrode with a dimension between 0.1 to 50  $\mu\text{m}$  (Montenegro *et al.*, 2012). The smallest translates to a disc area of  $10^{-14} \text{ m}^2$ , compared to  $10^{-6} \text{ m}^2$  of a 3 mm disc electrode commonly used in electroanalytical experiments.

The beneficial properties of microelectrode are (1) improved mass transport for the delivery of analyte to the electrode surface; (2) better discrimination against charging current, which is additive to faradaic currents and distorts the experimental data; (3) decreased distortion from  $iR$  drop and thus feasibility of electrochemical analysis in highly resistive solutions, e.g. benzene, frozen acetonitrile etc.; (4) low double-layer capacitance allows high-speed voltammetric experiments for probing the kinetics of very fast electron transfer and coupling chemical reaction or the dynamic of processes such as exocytosis. (Montenegro *et al.*, 2012; J. Wang, 2006)

## 1.4 Immunosensor for effective neuropeptide electroanalysis

This sensor adaptation work aims to develop an electrochemical immunosensing scheme for the detection and quantification of oxytocin, a neuropeptide, in brain dialysate from laboratory rats at sub-picomolar concentration level.

### 1.4.1 Neuropeptides

Neuropeptides are small polypeptide molecules which consist of a short sequence of amino acids linked together by peptide bonds. They function as neuronal signalling molecules and involve in a wide range of activities of the brain and the body in specific ways. Unlike classical neurotransmitters, which are released from axon terminals by  $\text{Ca}^{2+}$ -dependent exocytosis, neuropeptides are packaged in large dense-core vesicles which are not localised to synapses. Instead, these neuropeptide vesicles are normally found in soma, dendrites and in axonal varicosities as well as nerve endings (refer **Figure 1.5** for the structure of a neuron cell).

There are more than 100 neuropeptides expressed in the form of large vesicles in different neuronal subpopulation and they can be released from all compartments of a neuron. Each of these vesicles carries a large number of neuropeptide molecules and they act at receptors with nanomolar affinity. Consider oxytocin as an example, a vesicle of oxytocin holds up approximately 85,000 oxytocin molecules (Leng *et al.*, 2008).

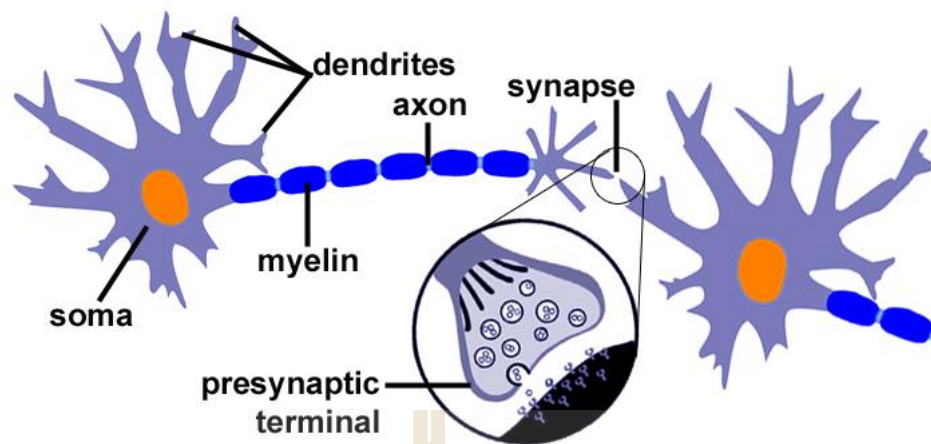


**Figure 1.5** Structure of a neuron cell.

(source: <https://medium.com/@mukulmalik/human-brain-s-f426e5bc9964> , accessed on 2017-10-03)

#### 1.4.2 Oxytocin

Oxytocin is a neuropeptide, consisting of a sequence of nine amino acids (refer **Figure 1.6**), which acts as a neurohormone, a neurotransmitter or a neuromodulator (Tarhan *et al.*, 2011). It is also known as neurohypophysial hormone as it is being secreted by the neurohypophysis for regulating various biological functions and illnesses, such as complex emotional and social behaviours and antidiuretic effects (Caldwell and Young III, 2006; Kirsch *et al.*, 2005).

When present in the bloodstream, oxytocin causes the contraction of the uterus and has been used widely to induce labour. Besides, oxytocin in the bloodstream also causes milk ejection in lactating animals. (Soloff *et al.*, 1979)

Brain oxytocin, on the other hand, has been reported to have a startling ability to evoke particular behaviours and trigger satiety and enhance sexual behaviour in animal models. Oxytocin injections in rats and sheep can trigger maternal behaviour.

In monogamous voles, oxytocin injections facilitate pair bonding, while oxytocin receptor-deficiency in mice demonstrated disturbances in social behaviour. (Leng and Ludwig, 2016)

Nonetheless, since the discovery of intranasal oxytocin crossing into the central nervous system, there are growing reports on the application of this experimental paradigm to explore the biological effect of this neuropeptide (Born *et al.*, 2002). Weisman *et al.* (2012) reported that intranasal administration induced dramatic raises of oxytocin concentration in saliva from  $6.9 \text{ pg ml}^{-1}$  at baseline to  $1265.4 \text{ pg ml}^{-1}$  15 min after the administration.

Meanwhile, other researchers have shown that administration of oxytocin via intranasal spray reduces the neuronal responses within the amygdala in the human brain (Domes *et al.*, 2010; Green and Hollander, 2010). Amygdala is a heterogeneous structure that has a central role in emotional learning and memory as well as the responsibility in the perception of emotions such as anger, fear, sadness and arousal (Balleine and Killcross, 2006; Domes *et al.*, 2007). Thus, a decrease in amygdala translates to the effect of reducing fear and arousal; increasing trust behaviour in decision making (Kosfeld *et al.*, 2005). These findings make this neuromodulator system of the brain a promising target for psychotherapeutic intervention and treatment of numerous psychiatric illnesses, for example, anxiety disorders, social phobia, autism and postpartum depression (Neumann, 2008).

Thus, a sensitive, convenient and reliable method for the quantification of oxytocin in body fluids, particularly brain dialysates, is of great demand towards a better mechanistic understanding of the function of this neurohormone. The challenge

is the ultralow concentration of the analyte in the relevant brain fluid. e.g. picomolar level upon conventional stimulation of the target brain region.

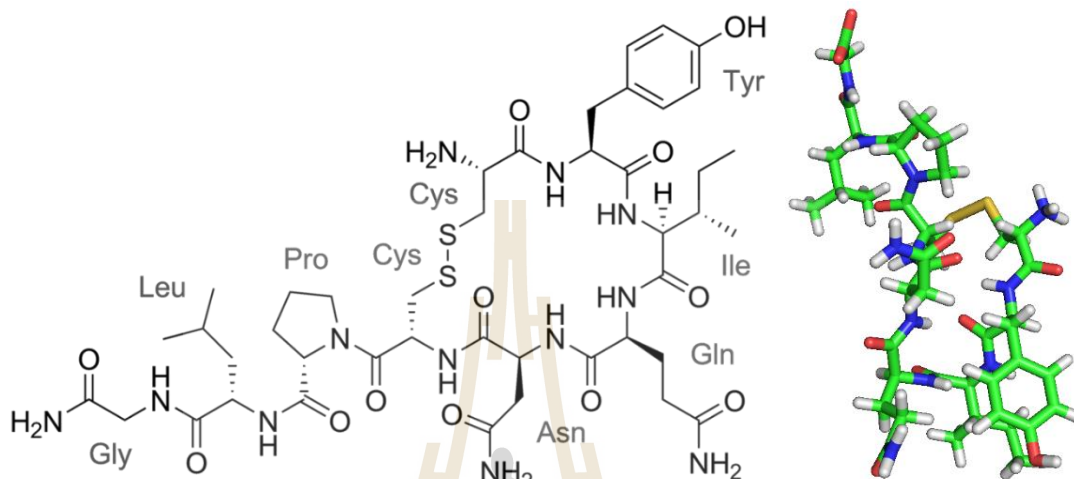


**Figure 1.6** Structure of oxytocin and its form in solution elucidated by NMR. (Koehbach *et al.*, 2013)

### 1.4.3 Electrochemical sensors

A chemical sensor is generally a tool consisting of a transducer, which transforms the response into a detectable signal on modern instrumentation and a chemically selective layer. This chemically selective layer selectively isolates the response of the analyte from its immediate environment. Depending on the property to be determined, they can be classified into electrical, optical, mass, thermal or electrochemical sensors. (Stradiotto *et al.*, 2003)

Unlike optical, mass and thermal sensors, electrochemical sensors operate at low cost, but provide remarkable detectability. Due to their simple and compact experimental design, electrochemical sensors are highly portable and accessible, and thus are of great focus in recent analytical research.



Depending on the detection technique, modern electrochemical sensors can be divided into 4 common groups: (1) potentiometric sensors, which measures the potential across interface, e.g. the membrane of a pH meter (Kimmel *et al.*, 2012); (2) chemically modified sensors, which use chemically modified electrode to detect the target analyte via amperometric or voltammetric analysis (Stradiotto *et al.*, 2003); (3) electrochemical biosensors, which consist of a biomolecule coupled to a transducer that will convert the biological activity into electrical signal (Bakker and Qin, 2006); and (4) electrochemical immunosensors, which perform immunoassays based on antigen and antibody recognition (Kimmel *et al.*, 2012).

#### 1.4.4 Electrochemical immunosensors

An immunoassay is a highly selective bioanalytical technique that detects and quantifies analytes ranging from small molecules to macromolecules in a solution using an antibody ( $A_b$ ) or an antigen ( $A_g$ ) as a biorecognition agent. It is one of the highly focused analytical techniques with more than 78,000 research works in immunosensing methodology reported since 2000 (Ju *et al.*, 2017a). Theoretically, immunoassay utilises antigen-antibody immunoreaction as well as its coupling to an appropriate transducer to produce an analytical signal. The high specificity of antigen-antibody interaction is the unique advantage of immunoassay methods.

An antibody is a Y-shaped protein (immunoglobulin) synthesised by B-lymphocytes (immune cells) upon stimulation by an antigen (refer **Figure 1.7**). It consists of the constant region (the stem of Y) and the variable region which is located on the top part of the Y structure. The variable region provides the highly selective binding to an epitope site on an antigen. Immunoassays measure the formation of antibody-antigen complexes by labelling or labelling-free format. The labelling-free



format is based on the immunoreaction to directly produce the measurable detection signal, while the labelling format uses some signalling molecules to label the immunological reagents, such as antigen or antibody, to produce a detectable analytical signal on the immunoreaction. Due to the signal transduction and amplification by using a label, higher sensitivity can also be achieved for immunoassays. (Ju *et al.*, 2017a)

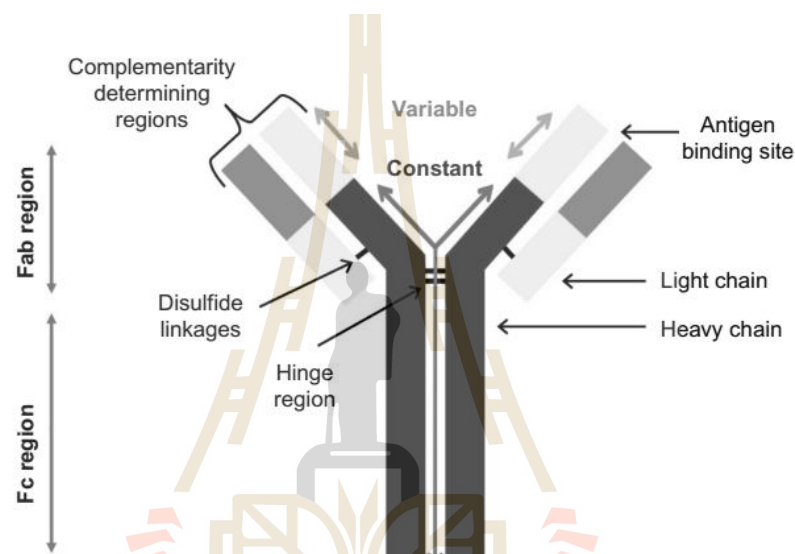


**Figure 1.7** General structure of an antibody ( $A_b$ ). (Ju *et al.*, 2017a)

There are two common immunoassay methods for immunoreaction using the labelling format, namely the competitive and sandwich methods. As illustrated in **Figure 1.8**, in a competitive immunoassay, the surface of the substrate immobilised with antibodies ( $A_b$ ) are exposed to the mixture of sample antigen ( $A_g$ ) and labelled antigen ( $A_g^*$ ). These two antigens will compete for the antibodies on the surface until an antigen-antibody binding equilibrium is established. Thereafter, the substrate surface is rinsed to remove unbound antigens and the bound label's signal is detected. The relationship between signal and antigen concentration is thus inversely

proportional for competitive assay. Sandwich immunoassay, on the other hand, captures antigen in a sample directly with the surface immobilised antibody (the capture antibody,  $A_{b1}$ ). The surface is then rinsed and exposed to the labelled detection antibody ( $A_{b2}^*$ ) as the signalling agent. The unbound  $A_{b2}^*$  is then removed by rinsing and the signal of the detection antibody is measured. Different from the competitive mode, sandwich methods give a signal that is directly proportional to the concentration of antigen in the sample. The sandwich mode also offers a greater selectivity since the cross-reacting species rarely bind to both the capture and detection antibodies. (Cox *et al.*, 2012; Ju *et al.*, 2017a)

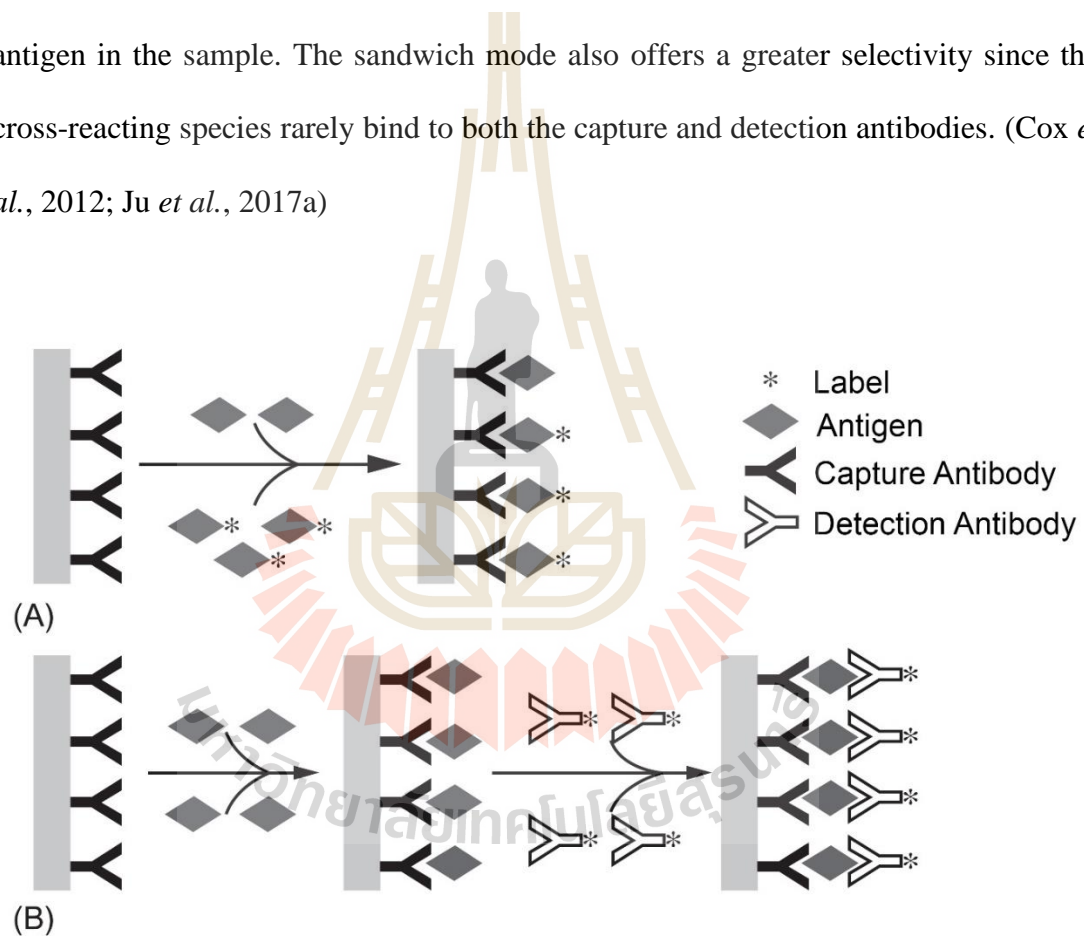
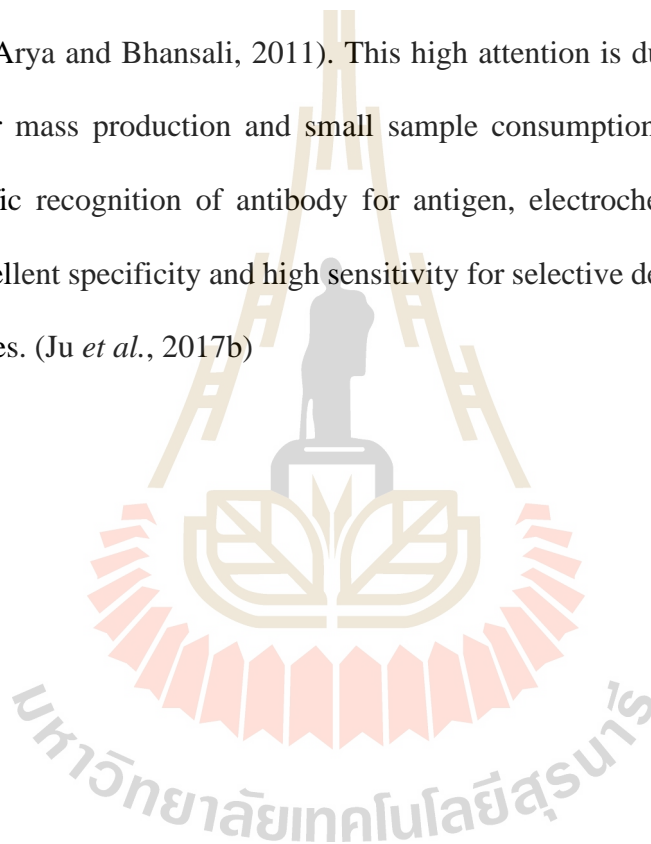


**Figure 1.8** Schematic illustration of (A) competition immunoassay and (B) sandwich immunoassay. (Ju *et al.*, 2017a)

Electrochemical immunosensors involve the coupling of immunoreactions to an electrode for producing electrical signals which is then converted to analytical data.

In comparison to other immunoassays, electrochemical immunosensors have gained enormous interest as cheap versatile bioanalytical devices for low-cost analysis and have an important contribution to the detection of protein biomarkers (Arya and Bhansali, 2011). This high attention is due to their robustness, economic for mass production and small sample consumption. Moreover, with the highly specific recognition of antibody for antigen, electrochemical immunosensor provides excellent specificity and high sensitivity for selective detection of biomarkers in real samples. (Ju *et al.*, 2017b)

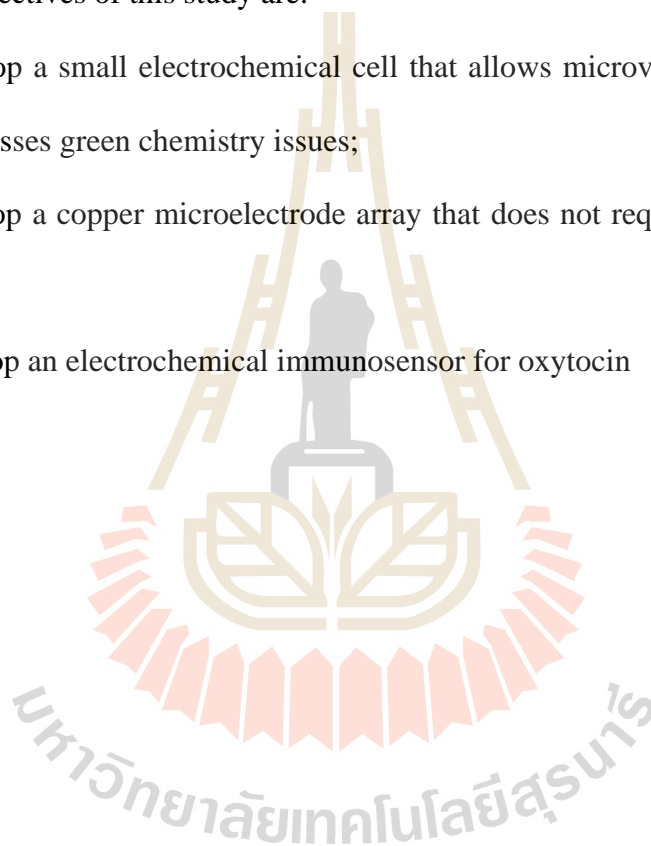


## 1.5 Objectives

This PhD thesis aimed to develop electrochemical tools or techniques which (1) are green, practical, economical and accessible to electrochemists from basically all laboratories, such as research, commercial and teaching laboratories; and (2) offer advanced analytical figures of merit (e.g linear range, sensitivity, detection limit etc.).

The main objectives of this study are:-

- a. To develop a small electrochemical cell that allows microvolume electroanalysis and addresses green chemistry issues;
- b. To develop a copper microelectrode array that does not require microfabrication; and
- c. To develop an electrochemical immunosensor for oxytocin



## CHAPTER II

### LITERATURE REVIEW

#### 2.1 Miniaturisation of electrochemical cell

##### 2.1.1 Microliter electrochemical analysis

Despite miniaturisation has been a trend in electrochemistry, the idea of miniaturisation, however, has been focussing mainly on the reduction of electrode size for (1) improved mass transport and for direct *in situ* measurement in brain (Kwon *et al.*, 2016; Lourenço *et al.*, 2016; Ward *et al.*, 2009); (2) screen-printed electrode etc.. Meanwhile, majority of the miniaturisation works on electrochemical cell were for the application in flow cell systems (Kovalcik *et al.*, 2004; Sahlin *et al.*, 2003). A combination of these two features such as screen-printed electrode fabricated micro-electrochemical cell was reported by Shitanda *et al.* (2011).

To date, reports have shown the feasibility of incorporating functional two- or three-electrode minicells within vials of nanolitre down to picolitre volume (Clark and Ewing, 1998; Clark *et al.*, 1997; Henry and Fritsch, 1999; Lenihan *et al.*, 2007). However, this is only achievable with complex microfabrication procedures and requires specially adapted working stages for the operation of such tiny assemblies which are not commonly available to normal laboratories. These requirements limit the practicability of adoption of these minicells into the routine applications in common electrochemical laboratories.

In contrast, mass-fabricated screen-printed two- or three-electrode devices (SPEs) are a convenient platform for voltammetry in 25 – 100  $\mu\text{l}$  test solutions (Barton *et al.*, 2016; Mohamed, 2016; Renedo *et al.*, 2007; Trojanowicz, 2016; Yamanaka *et al.*, 2016). The possibility of mass fabrication of screen-printed electrode has led to their use in the mass production of commercial test kits which is suitable for lay man consumer operation, e.g. glucose meter.

Despite their convenient operation, the use of SPEs raises issues in acquiring the disposable sensing strips either by in-house fabrication or expensive external purchasing for research, commercial and teaching laboratories. In-house fabrication requires expensive SPE printing facilities while the price of commercial SPE ranges from USD 1 to 10 per piece depending on the material. Nonetheless, most suppliers have a minimum unit requirement per order and stocking up SPE is not advisable as most SPEs have a shelf life. In case of active research or academic laboratories, disposable SPE can be very costly and creates massive waste (e.g. plastic strips) in the long run. This will also increase the operational cost of the laboratory.

Strategies for economic microlitre-volume electroanalysis with electrodes other than SPEs are the subject of two recent reports. Jimenez *et al.* completed a three-electrode minicell by gently introducing the slim tips of carbon or noble metal microelectrodes (as detectors) and part of a platinum (Pt) microwire (as counter-electrode) into a 50  $\mu\text{l}$  electrolyte droplet hanging from the bottom disk of an inverted glass-fritted reference electrode as shown in **Figure 2.1** (Jimenez *et al.*, 2015). Skalová *et al.* sealed the tip of a tapered glass tube with gelled agar, injected 20–50  $\mu\text{l}$  of test solution into the compartment thus formed and inserted disk-type working electrodes into the trapped sample as shown in **Figure 2.2**. In order to obtain

voltammetric data, the sensor/sample assembly was operated in a beaker with the addition of electrolyte and a reference/counter electrode (Skalová *et al.*, 2018).

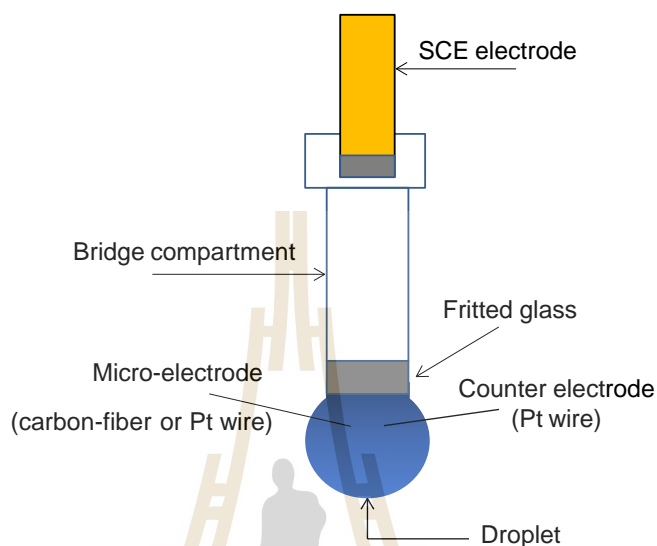


**Figure 2.1** Schematic illustration of the configuration of the 50  $\mu\text{l}$  hanging droplet microcell demonstrated by Jimenez *et al.* (2015).

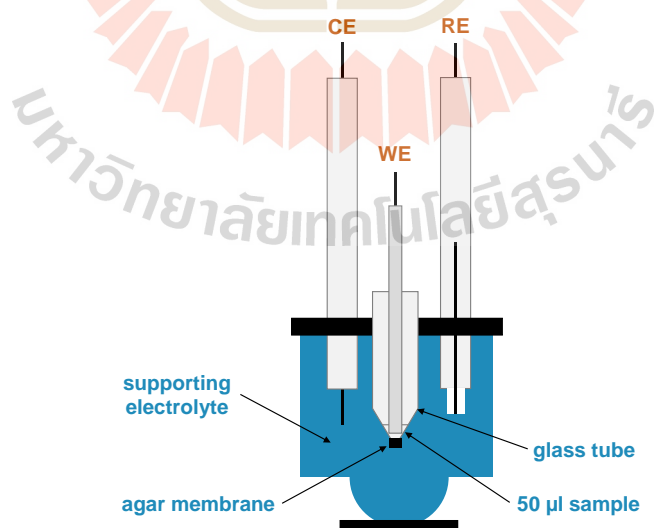


**Figure 2.2** Miniaturised electrochemical cell proposed by Skalová *et al.* (2018) which utilises agar gel to seal the tip of a glass tube for the formation of a sample chamber that is isolated from the CE and RE.

These different minicell designs resulted in the detection of a ferrocene-labelled, cell-penetrating peptide and the electrodeposition of gold nanocrystals (Jimenez *et al.*, 2015) and the accurate voltammetric determination of chemotherapeutic anthraquinone in urine (Skalová *et al.*, 2018), thus verifying the potential of microlitre voltammetry as a practical alternative to conventional measurements in millilitre-capacity beakers. The benefits of (bio-)electroanalysis satisfying the criteria of green, ecological and economic practice were also apparent. However, the suggested minicell designs are limited to work with tapered sensors that can be inserted into a small droplet, tiny cone or thin tube.

Thus, in this research project, the potential of the above ideas will be further developed into a platform which can be applied onto various commercial as well as homemade electrodes available in most electrochemical laboratories.

## **2.2 Band array electrode**

### **2.2.1 Microelectrode arrays**

The beneficial properties of microelectrodes have been of high interest over the past decades for their potential application in various analytical fields, i.e. electrochemical analysis, sensors, and microscopy. Generally, the development of microelectrode involves the miniaturisation of an electrochemical system. This gives advantages in conducting electrochemical detection in minute environment e.g. single cell analysis (Wightman *et al.*, 1991). Despite the electrochemical advantages of microelectrode, miniaturisation of electrode also at the same time requires the use of expensive potentiostat which is capable of handling picoampere current and noise-free



environment, a demand which may place limits on the portability of this type of electrochemical setup.

A microelectrode array is generally an electrode constructed through the accommodation of several to numerous numbers of microelectrodes into a single housing often microscale housing (Atighilorestani and Brolo, 2017; Elfar *et al.*, 2017; Sina *et al.*, 2017; D. Zhang *et al.*, 2009). As in electrophysiology, researchers use microelectrode arrays with multichannel signal acquisition for simultaneous monitoring of different analytes, such as a 100-microelectrode array reported by Nordhausen *et al.* (1996). Recent advancement in material science has also enabled the use of flexible material that can be deformed and fitted into the organ under study more properly without causing damage to the organ, thus allowing the introduction of a multichannel probe with single insertion of single sensor (Takeuchi *et al.*, 2003).

A microelectrode array has also other applications such as mapping of extracellular activities, such as electrogenic cell in culture and cordial synaptic projection with extracellular electrode arrays (Connolly *et al.*, 1990; Shein-Idelson *et al.*, 2017).

Microelectrode arrays could then be a solution to the above-mentioned shortcoming of a low faradaic current of ordinary single microelectrodes through magnification of faradaic current by the introduction of more detector entities without losing the beneficial microelectrode properties. However, general microelectrode arrays are fabricated in a micro-size scale through lithography, micro-moulding or dry etching technologies as well as the silicon materials (Takeuchi *et al.*, 2003). These preparations require expensive high-tech instrumentation which is not easily accessible to common electrochemical laboratory.

Above restrictions lead to the idea to produce a microband electrode array through a simple do-it-yourself (D.I.Y.) procedure, with simple tools available in an ordinary laboratory. Obviously, such a construction would be ideal for cases where the analyte is present at low concentration, sample availability is not of concern and minute in situ measurement is not required. A good model target was a copper microband electrode array, considered that Jaikaew *et al.* (2016) demonstrated nicely the potential of copper electrodes as oxidase biosensing platform which enables hydrogen peroxide detection at an interference-eliminating cathodic working potential.

## **2.3 Immunosensor for oxytocin detection**

### **2.3.1 Detection of oxytocin**

After the discovery of oxytocin in the 1920s, a bioassay was first introduced to quantify oxytocin, whereby reaction of laboratory animal was used as the determination of active oxytocin in a sample. The internationally agreed definition of 1 mg oxytocin is the quantity of oxytocin that gives 600 IU of bioactivity. It was until the 1980s, that immunoassay was started to use in the quantification of oxytocin. However, to date, the two different communities are still facing difficulty in correlating their results as they differ by two orders of magnitude. This is especially the case for non-extracted blood plasma samples due to their complex matrix which may contain enzyme oxytocinase that degrades the analyte leading to overestimation in comparison to results from bioassays. On the other hand, brain dialysate has a relatively much simpler matrix free of oxytocinase and high abundance of interfering protein molecules. (Leng and Sabatier, 2016)

Currently, there are several companies selling research test kits (see **Table 2.1**) for the quantification of oxytocin by competitive and sandwich enzyme-linked immunosorbent assays (ELISA). These kits utilise the generation of colour substance by the enzyme label on the antibody to generate an optical signal which is dependent on the oxytocin concentration in the sample. They provide an analytical solution for sample with oxytocin concentration ranging from 5.9 pg ml<sup>-1</sup> to 100 ng ml<sup>-1</sup> at a sensitivity level of 9 to 20 pg ml<sup>-1</sup>.

**Table 2.1** List of commercially available oxytocin test kits.

Product	Company	Assay Type	Detection	Sample Type	Sensitivity pg ml <sup>-1</sup>	Range pg ml <sup>-1</sup>
ab133050	Abcam	CEIA	Colorimetric	Cell culture supernatant, Milk, Urine, Serum, Plasma	15	15.6 – 1000
LS-F4411-1	LifeSpan BioSciences	CEIA	Colorimetric	Plasma, Serum		12.35 – 1000
ADI-901-153A-0001	Enzo	CEIA	Colorimetric	Cerebral spinal fluid, saliva, tissue, urine	15	15.6 – 1000
500440	Cayman Chemical	CEIA	Colorimetric	Plasma	20	5.9 – 750
ABIN2506974	Antibodies Online	CEIA	Colorimetric	N.A.	24	24 – 100,000
EU2549	FineTest	CEIA	Colorimetric	plasma, tissue homogenates and other biological fluids	<9.375	15.625 – 1000
LS-F20568	LifeSpan BioSciences	Sandwich ELISA	Colorimetric	Breast Milk, Cell lysate, Erythrocyte lysate, Plasma, Sperm and Seminal Plasma, Serum, Tissue Homogenate, Urine, Cell Culture supernatant, cerebrospinal and other biological fluids	N.A.	N.A.

Note: N.A. stands for Not Available

Although the tyrosine moieties on oxytocin are oxidisable, a property that can be utilised for quantification, the electrochemical detection of this neuropeptide is less explored. Baig and Kawde (2015) demonstrated the use of grapheme-modified graphite pencil electrode to detect L-tyrosine at  $0.07 \mu\text{M}$  with a quantitative linear range from  $0.8$  to  $60 \mu\text{M}$  by square wave voltammogram.

Meanwhile, Asai *et al.* (2016) established the possibility of oxytocin measurements by means of pulse and cyclic voltammetry at boron-doped diamond working electrodes. Boron-doped diamond electrode has low background current and capacitance, giving the superiority for potential sweep analyses. This together with its high resistance to fouling has enabled the detection of oxytocin at  $50 \text{ nM}$  level with a linear working range of oxytocin concentration from  $0.1$  to  $10.0 \mu\text{M}$  by flow injection analysis (FIA) (Asai *et al.*, 2016). However, this method requires a sophisticated instrument for the preparation of boron-doped diamond electrode. This instrument is not commonly accessible to a common electrochemical laboratory.

Apart from direct electrochemical detection, oxytocin detection by means of molecular imprinting of a conducting polymer was also reported. Synthetic receptor deposited by potentiodynamic electropolymerisation as a thin film on an Au film electrode in an electrochemical miniaturised microfluidic cell was used to selectively capture oxytocin and perform an electrochemical analysis. Linear dynamic range was  $0.06$  to  $1 \text{ mM}$  with the limit of detection at  $60 \mu\text{M}$ . (Sharma *et al.*, 2018)

As a general summary, both the commercially available ELISA kits and electrochemical detection schemes in literature are not applicable to oxytocin quantifications in samples from brain dialysis which has the analyte present at sub-picomolar level. Currently, detection of oxytocin in plasma with liquid chromatography

coupled with mass spectroscopy (2D-LC-MS/MS) has achieved a lower limit of quantification (LLOQ) of  $1.00 \text{ pg ml}^{-1}$  for human and  $50.0 \text{ pg ml}^{-1}$  for rat (G. Zhang *et al.*, 2011). This method provides quantitative results with high sensitivity and selectivity but needs expensive and bulky instrumentation and suffer from time delays between sampling and obtaining results. The highly localised facility for LC-MS/MS analysis leads to the need to transport the sample from a remote area to laboratory facilities and increases the risk of sample degradation during transportation. Instrument operation, as well as data interpretation of these high-end instrumentations, often require the expertise of competent personnel (Woods *et al.*, 2013). Besides, the lengthy sample preparation for LC-MS/MS also involves the application of chemical solution and organic solvents which are not in line with the green chemistry principles. Thus, it is worth to explore and develop a detection sensor scheme based on an electrochemical platform which can better sensitivity, accessibility and portability at a much lower start-up and instrument maintenance cost.

### 2.3.2 Electrochemical immunosensors

Immunosensors use a label or tag on the antibody to provide a highly specific signal of the antibody-antigen interaction for the detection of antibody or antigen in a sample. In the case of electrochemical immunosensor, redox active species are used as the tag for antibody to provide an electrical signal for the quantification of the analyte.

Common labels used to tag immunoreagents includes (1) enzymes, (2) noble-metal nanoparticles, (3) electrochemically or optically active agents, and (4) quantum dots (Ju *et al.*, 2017a). Besides, simple one-to-one tagging of redox active species as the signal tracing agent, researchers have also introduced the use of redox

mediator, as well as nanoparticles such as carbon nanotube as the vehicle for packing more redox active species. This bulk-to-one introduction of signal tracing species will thus generate a higher current signal at a lower analyte concentration. This application thus improves the lower limit of detection for the analyte, in comparison with the one-to-one tagging format.

In term of antibody immobilisation, there are currently: (1) physical adsorption, (2) polymer entrapment, (3) covalent binding, and (4) oriented immobilisation (Ju *et al.*, 2017a). Ojeda *et al.* (2012) demonstrated immobilisation of antibody by first introducing amine cation grafting to the surface of screen printed carbon electrode (SPCE) via oxidative voltammetric sweeps in 3 mM 4-ABA and 0.1 M lithium perchlorate ethanolic solution. After that, streptavidin was immobilised followed by the biotinylated antibody. The vacant surface of the electrode was then blocked with bovine serum albumin (BSA) and biotin before the sensor was ready to perform the competitive assay with enzyme horseradish peroxidase as the signal reporting agent.

Drop immobilisation of antibody via physical adsorption is considered the simplest method for immobilisation. Researchers have demonstrated the use of biocompatible polymer for this purpose. Polyethylene glycol (PEG), for example, has been utilised to modify the surface of screen-printed carbon electrode for the immobilisation of anti-ENO1, an antibody for lung cancer-related antigen. The immobilisation happens due to its variety of interactions with anti-ENO1, including hydrogen bonding to the side chains of the amino acid residue and to the main chain NH groups, as well as multiple coordination with positively charged amino acids. A schematic illustration of this process is shown in **Figure 2.3**. (Ho *et al.*, 2010)

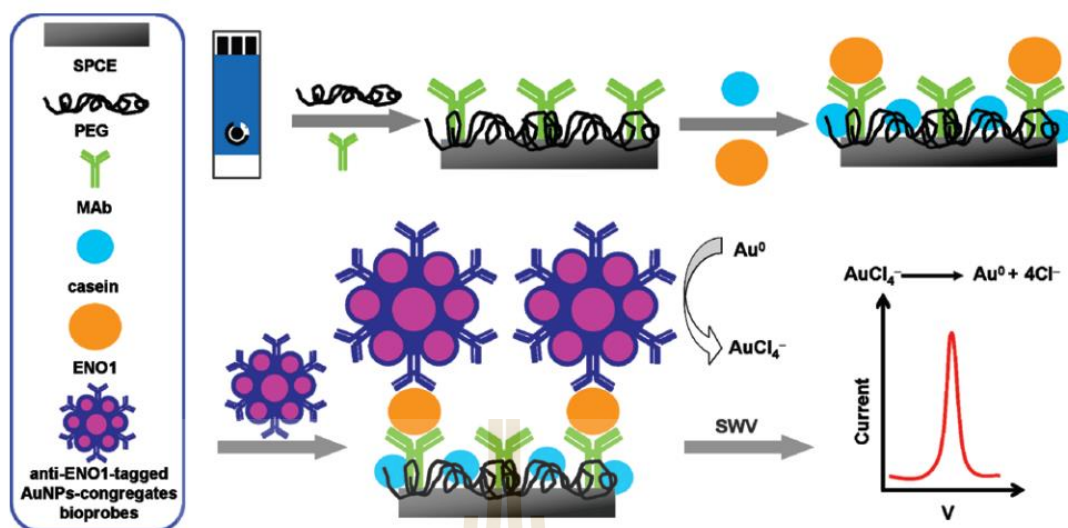


**Figure 2.3** Schematic illustration of sandwich type electrochemical immunosensor with antibody immobilised via physical adsorption. (Ho *et al.*, 2010)

Another indirect method of immobilisation of antibody is done with the use of magnetic beads. Electrochemical immunosensor for testosterone developed by Eguílaz *et al.* (2010) illustrated the use of functionalised magnetic beads and screen-printed carbon electrodes. Anti-testosterone was conjugated on magnetic beads followed by a direct competitive immunoassay involving testosterone labelled with peroxidase. The conjugate was concentrated on the screen-printed carbon electrode with a magnet. Testosterone determination was carried out by amperometry at  $-0.2$  V upon  $\text{H}_2\text{O}_2$  additions using hydroquinone as the redox mediator. Under optimised conditions, the sensor scheme gave a calibration curve with a linear range of  $5.0 \times 10^{-3}$  to  $50 \text{ ng ml}^{-1}$  and LOD of  $1.7 \text{ pg ml}^{-1}$ .

A similar application of magnetic beads was also reported by Chunglok *et al.* (2011). This research team reported a highly sensitive method for protein detection using electrochemical sandwich immunoassay with redox-modified carbon



nanotube (CNT) labels. The capture antibody is conjugated on magnetic beads while the detection antibody is tagged with the methylene blue modified multi-walled CNT (MB-MWCNT-Ab). Upon formation of capture antibody-antigen-detection antibody complex, they are washed and reaccumulated onto an SPCE with the assistance of a magnet. This scheme uses MB-MWCNT as the magnifying labels and offers a dynamic range of 0.1 to 100  $\text{pg ml}^{-1}$  which can be further improved with  $\text{Fe}(\text{CN})_6^{3-/4-}$  as a redox mediator to give a dynamic range of 5 to 100  $\text{fg ml}^{-1}$ .

The adsorption of methylene blue (**Figure 2.4**) on carbon nanotube (**Figure 2.5**) as an electrochemically functional nanostructure had been previously reported by Yan *et al.* (2005). Unlike the ordinary flat graphite, carbon nanotubes are of rolled-up graphene sheets of carbon with a sidewall curvature and a  $\pi$ -conjugative structure with a highly hydrophobic surface. These unique properties of CNTs allow the formation of  $\pi$ - $\pi$  stacking electronic interactions with the three aromatic rings of methylene blue, thus allowing the adsorption of methylene blue on CNTs. Similar  $\pi$ - $\pi$  stacking absorption of polynuclear aromatic compounds onto the side wall of CNTs has also been reported for several anthracene derivatives such as anthracene, anthraobin, 9,10-dibromoanthracene, 9,10-anthracenedicarbonitrile and 9-anthracene-methanol. (J. Zhang *et al.*, 2003)

This application of MB-MWCNT as a redox signal amplifier in an electrochemical sandwich immunoassay is a promising model to realise the quantification of sub-picomolar oxytocin in brain dialysate.



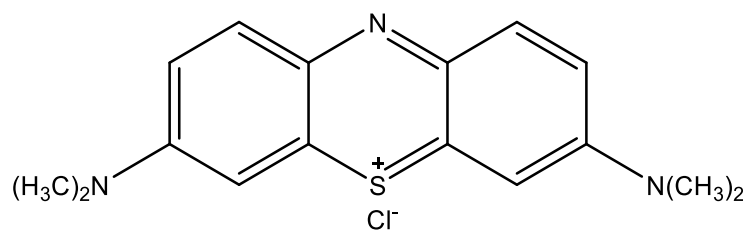


**Figure 2.4** Structure of methylene blue.

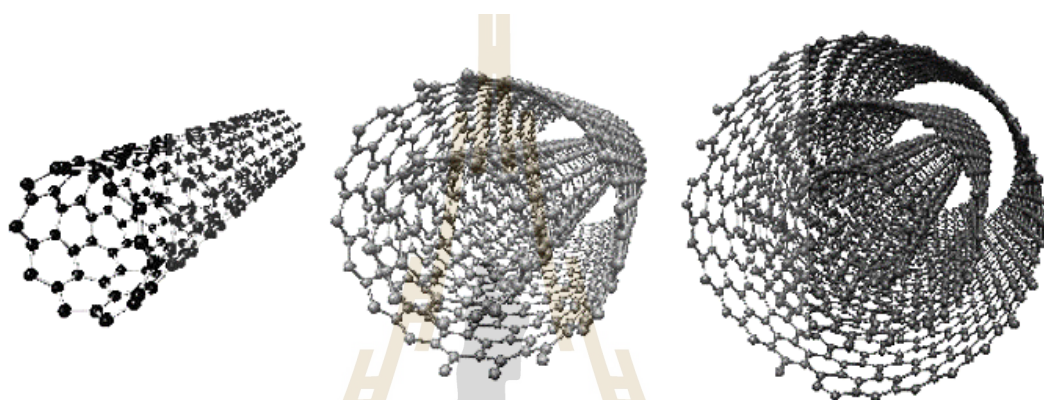


**Figure 2.5** Structure of single walled, double walled and multi walled carbon nanotubes. (Dumé, 2013)

## CHAPTER III

### METHODOLOGY

#### 3.1 Chemicals

All chemicals used in this study were of analytical grade. Ultrapure water for aqueous solution preparation was obtained from a reverse osmosis-deionization system. If not otherwise mentioned, the basis for stock solution preparation and electrolyte for most of the measurements of the study was a 0.1 M phosphate buffer that was made from a mixture of sodium phosphate monohydrate ( $\text{NaH}_2\text{PO}_4 \cdot \text{H}_2\text{O}$ ) and anhydrous dibasic sodium phosphate ( $\text{Na}_2\text{HPO}_4$ ). Stock solutions of 1 M potassium hexacyanoferrate(III) ( $\text{K}_3[\text{Fe}(\text{CN})_6]$ ), 10 mM hexaammineruthenium(III) chloride ( $[\text{Ru}(\text{NH}_3)_6]\text{Cl}_3$ ), 1 mM paracetamol (PCT), 1 mM ciprofloxacin (CIP), 0.1 mM doxorubicin (DOX), 0.1 mM 4-methylumbelliferone, 1 mM glucose and 0.5 M ascorbic acid were prepared in the 0.1 M stock phosphate buffer solution. Meanwhile, 15 mM oxytocin was prepared in the 0.1 M stock phosphate buffer solution, divided into 100  $\mu\text{l}$  aliquots and kept in vials at  $-20^\circ\text{C}$ . Glucose oxidase from *Aspergillus niger*, of specific activity  $228 \text{ U mg}^{-1}$ , was used to prepare amperometric glucose biosensors.

### **3.1.1 Preparation of phosphate buffer saline**

The 0.1 M phosphate buffer saline pH 7.0 with 0.1 M potassium chloride was prepared by dissolving 10.8660 g  $\text{Na}_2\text{HPO}_4 \cdot 2\text{H}_2\text{O}$ , 5.3836 g  $\text{NaH}_2\text{PO}_4 \cdot \text{H}_2\text{O}$  and 7.4550 g KCl in 1 litre. This solution was autoclaved before use.

### **3.1.2 Methylene blue-multiwall carbon nanotubes conjugate**

4 g MWCNT was added with 2 ml of distilled water and sonicated for 2 hr. 10 mg methylene blue together with 4 ml distilled water was added and the mixture was sonicated for 3 hr. The mixture was centrifuged at 11,000 rpm and then filtered over a 0.2  $\mu\text{m}$  cellulose membrane using a Buchner funnel with a water aspirator for suction. This process was repeated several times until the filtrate turns colourless. The MB-MWCNT residue on the filter was washed with distilled water several times and recovered for drying. This dried MB-MWCNT was redispersed in 4 ml 0.1 M PBS pH 7.0 with 0.1 M KCl for routine application.

### **3.1.3 Methylene blue-multiwall CNT-antibody conjugate**

1 ml of the MB-MWCNT prepared according to 3.1.2 was pipetted into a 1.5 ml Eppendorf tube. 20  $\mu\text{l}$  of rabbit anti-oxytocin (AB911, Merck Millipore) was added and incubated under shaking for 20 hours at 4 °C with a tube rotator. The MB-MWCNT-Ab conjugate was then harvested by centrifugation at 11,000 rpm for 30 min at 4 °C. The supernatant was collected for protein concentration determination, while the residue in the tube was further washed to remove non-adsorbed anti-oxytocin by adding 1 ml PBS buffer and centrifuged at the same condition. The process was repeated for another 4 times.

## 3.2 Electrodes and instrumentation

All electrodes used in this work and their specifications are listed below. The surfaces of all disc electrodes were thoroughly cleaned by polishing with 3 – 5  $\mu\text{m}$  alumina paste followed by 0.4  $\mu\text{m}$  alumina paste on a soft polishing mat in a continuous eight-shaped motion for 30 s, every time before performing a new measurement.

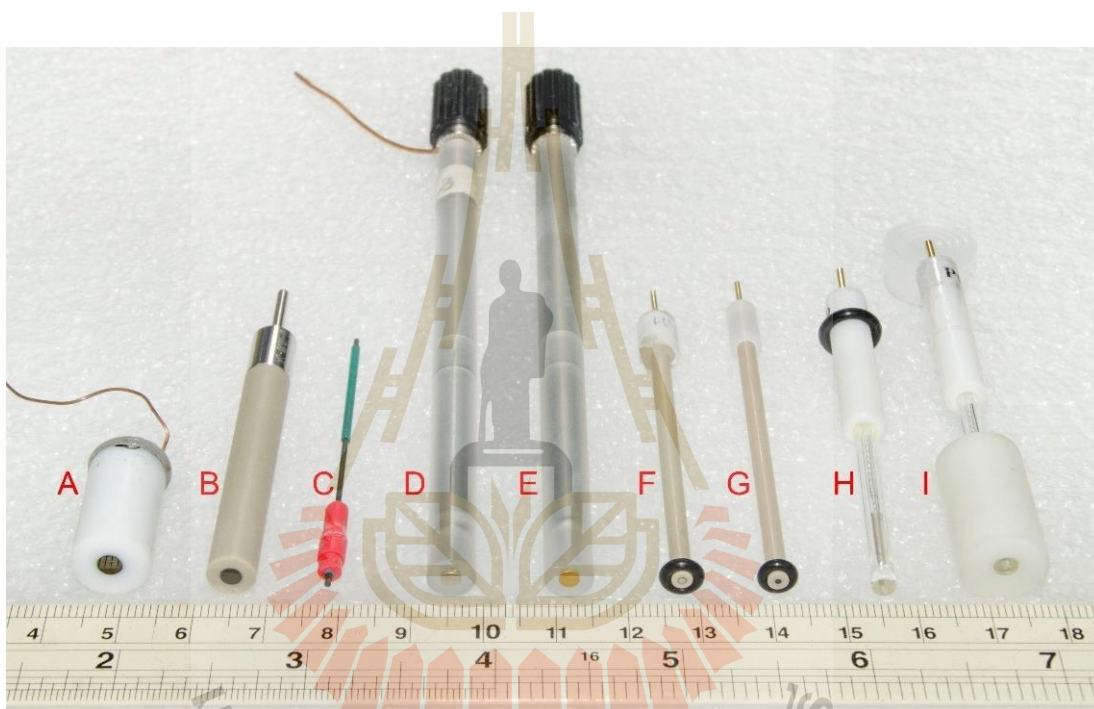


**Figure 3.1** List of selected common electrodes found in an ordinary electrochemical laboratory. The detail of each electrode is described in the following subsections.

### 3.2.1 Glassy carbon electrode

A 3 mm (**Figure 3.1A**) and a 1 mm (**Figure 3.1G**) glassy carbon (GC) disc electrodes from Metrohm AG (Herisau, Switzerland) were used in this study.

### 3.2.2 Boron-doped diamond electrode

The 3 mm disc boron-doped diamond (BDD) electrode (S/N: D-638-SA) (refer **Figure 3.1B**) used in this study was purchased from Windsor Scientific Ltd. (Slough, UK). The percentage of boron dopant was listed as 0.1%.

### 3.2.3 Pencil lead cylindrical electrode

A 2-mm-long cylindrical carbon electrode was made by insulating a 0.9 mm Pentel Hi-Polymer E 2B pencil lead with a heat-shrink tube, leaving a 2 mm portion exposed (refer **Figure 3.1C**).

### 3.2.4 Noble metal electrodes

Noble metal electrodes used in this project were 3 mm platinum (product no.: 932-0003 (refer **Figure 3.1D**)), 3 mm gold (product no.: 932-0002, OD: 7 mm, PEEK (refer **Figure 3.1E**)), 1 mm platinum (refer **Figure 3.1F**) and 10  $\mu\text{m}$  platinum (refer **Figure 3.1H** and **I**) disc electrodes from Gamry Instruments (Warminster, PA, US).

### 3.2.5 Copper electrodes

Household electrical copper wires of approximately 1 and 2 mm were used to make a copper disc electrode in this study. The diameter of these wires determined with a digital Vernier calliper. They were 1.36 and 2.23 mm, respectively. This corresponded to disc surface area of 1.45 and 3.91  $\text{mm}^2$ , respectively. The insulation of wire was stripped off revealing the conductive metal wire which was then sealed in glass dropper with epoxy glue as the adhesive.

### 3.2.6 Glucose biosensor

Five microlitres of 5  $\text{mg ml}^{-1}$  glucose oxidase (GOx) in 2 % Nafion® was dropped onto a polished 3-mm platinum disc electrode. The modified electrode

was then left drying in air at room temperature. This process was then repeated 4 times, giving a total loading of 125  $\mu\text{g}$  GOx on the conductive surface. Completed biosensors were immersed in 0.1 M sodium phosphate buffer, pH 7.0 containing 0.1 M KCl with stirring for 30 min before being transferred to a refrigerator for overnight acclimation.

### 3.2.7 Mini reference electrode

The reference electrode in all measurements was a home-made Ag|AgCl|3 M KCl electrode made by oxidising the surface of a polished Ag wire to AgCl by anodising exposure to +1.0 V in 1 M HCl solution for 5 min. The resultant Ag|AgCl wire was immersed in 3 M KCl solution in a glass Pasteur pipette with a fitted porous ceramic frit tightly fixed at the narrow tip. This porous ceramic frit, which was sealed into the tip of the glass pipette by flaming, serves as the salt bridge connecting the Ag|AgCl and electrolyte. The potential of the working reference electrode was compared against a commercial Ag|AgCl reference electrode from eDAQ (product number: ET045) and the potential difference was controlled within  $\pm 2$  mV.

### 3.2.8 $\Omega$ -shaped Pt minicell

A piece of  $5 \times 3$  mm Pt foil of thickness 0.2 mm was cut and rolled in to a  $\Omega$ -shape minicell with a diameter of 2 mm. The 3-electrode configuration is as shown in **Figure 3.2**.

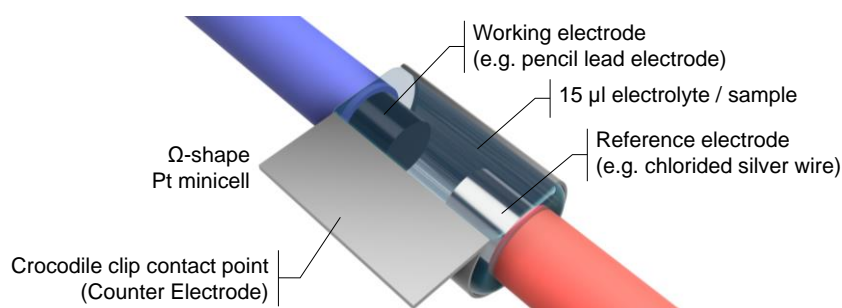


**Figure 3.2** The  $\Omega$ -shaped Pt minicell in operation.



### 3.2.9 Pipette tip minicell

An ordinary 1,000  $\mu\text{l}$  plastic pipette tip is incised and tightly plugged onto a 3 mm disc electrode with insulator housing of outer diameter of 6 mm to form a perfect seal around the electrode. The space above the 3 mm disc was used to contain approximately 100 – 150  $\mu\text{l}$  of electrolyte and sample (see **Figure 3.3**).

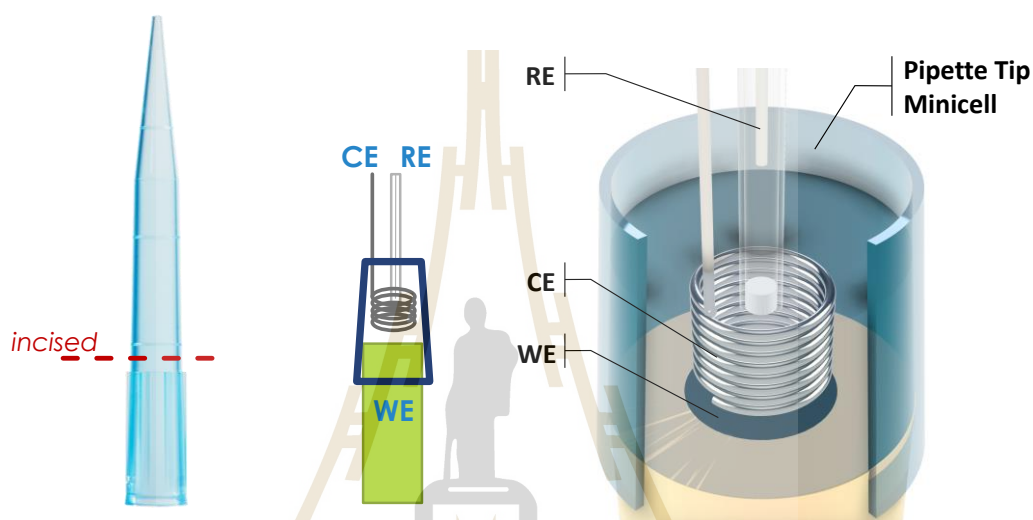


**Figure 3.3** The construction of a pipette tip minicell.

### 3.2.10 Pt-tube minicell

The construction of the proposed platinum-tube (Pt-T) minicell simply requires rolling a rectangular piece of Pt foil ( $22 \times 5$  mm, 0.2 mm thickness) along the lengthier side from one end to form a rigid cylinder of 4 mm diameter and 5 mm length. If necessary, a 3 mm rod (e.g. of Cu wire) can be used to assist in forming the shape. The remaining section (approx.  $10 \times 5$  mm) at the other end is folded to form a plane normal to the tube circumference (see **Figure 3.4**). The end product is a tubular Pt-T minicell with two open ends and a grip area for electrical connection using an alligator clip. Before use, the Pt-T minicell is cleaned by heating in a flame to bright red, then cooled. This Pt-T minicell is capable of holding up to 60  $\mu\text{l}$  of electrolyte or test solution.

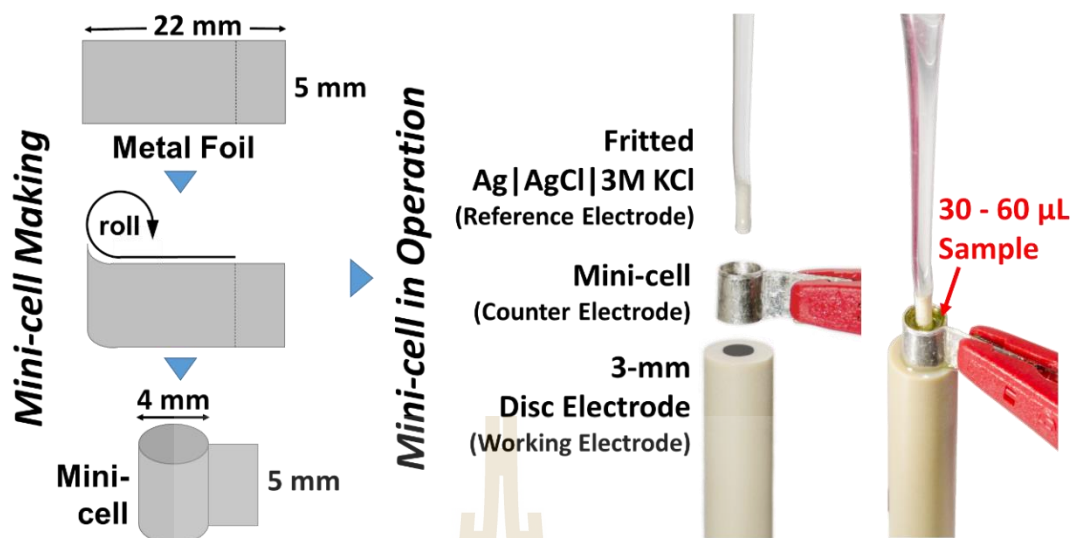


**Figure 3.4** The making of minicell and schematic setup of minicell operation.

### 3.2.11 Electrode stands

The construction of electrochemical setup using Pt-T minicell as specified in 3.2.10 requires the holding of the working electrode upright. Since there is no sealant required, a steady positioning of the working electrode is thus important to prevent leakage. Although this can be easily achieved by using any firm and stable clamp, e.g. retort stand, clamping can be a little tedious during reconstructions, this is especially significant when a numerous measurement is required for an experiment. Thus, three solutions for holding electrodes upright for the convenience of routine electrochemical analytical operation were introduced in this study.

The first accessory developed for electrodes with a male banana plug for electrical connection, e.g. electrode B in **Figure 3.1**, was a custom-made acrylic stand (**Figure 3.5**). Five pieces of acrylic plates were fixed together with hot gun glue to form a rectangular box with the dimension of  $8 \times 6 \times 4$  cm. A hole was drilled at the centre of the top surface where a copper coil with a diameter suitable for the electrode



jack was then attached underneath with hot gun glue. The copper coil was extended out from another hole one of the side surfaces. This copper coil bridges the working electrode to a potentiostat via a crocodile clip connector. Besides, it also provides a firm grip to the working electrode inserted.

The second accessory developed for electrodes with a flat end, e.g. electrodes E and F in **Figure 3.1**, was a glass holder with a heavy glass base (**Figure 3.6**). This glass holder was a section from glass test tube which was fixed onto a piece of window glass. An electrode can be placed upright into the glass holder. An electrical connection can be achieved by clipping a crocodile clip to metal screw. Alternatively, copper wire can be screwed for easy electrical connection.

The final solution used in this study is a stand with a crocodile clip (**Figure 3.7**). This is especially suitable for light-weight electrodes, e.g. electrodes A, C, F, G, H and I in **Figure 3.1**.

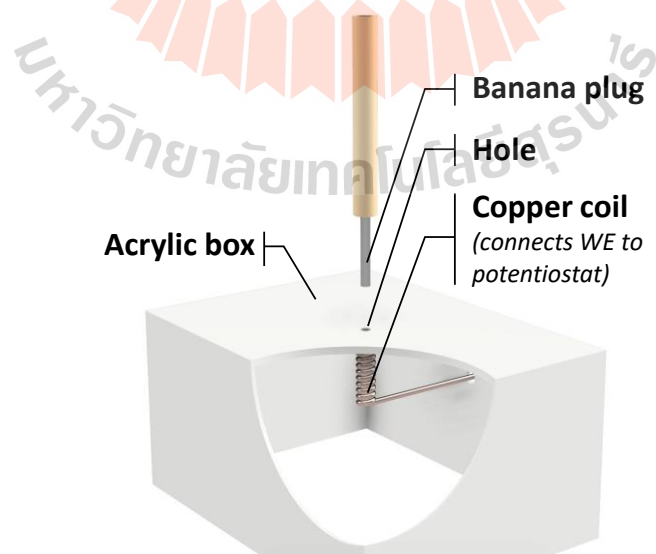


**Figure 3.5** A custom-made acrylic box platform with copper coil underneath for holding electrodes with a banana plug (male connector) upright.

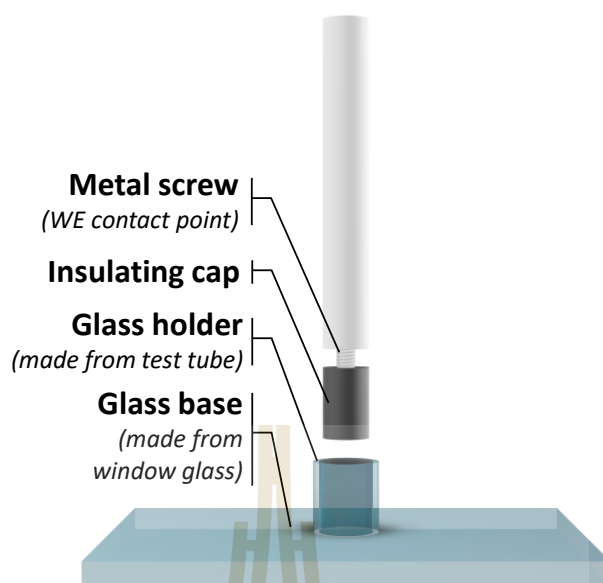


**Figure 3.6** A heavy glass plate with a short glass tube section fixed at the centre designed as an accessory to hold electrodes with a flat end upright.

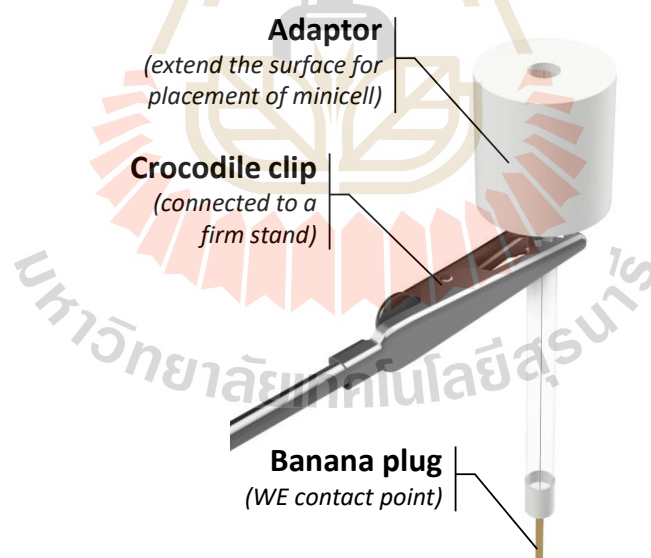


**Figure 3.7** Illustration of electrodes which are light be held steadily upright with a crocodile clip clamped onto a firm retort stand.

### 3.2.12 Microband array electrode

There were basically three generations of microband array electrode ( $\mu$ BAE) prototypes developed in this study. Initial attempts in making an easy-to-make  $\mu$ BAE were experimented by sandwiching copper foils in between different spacer materials, i.e. glass slide, plastic phone card and acrylic plate with epoxy glue as the adhesive.

**Figure 3.8** shows the five initial  $\mu$ BAE prototypes developed in this study. All five  $\mu$ BAEs were enclosed in a glass test tube to provide a rigid housing for routine application. These prototypes were classified into two generations, in which generation 1 (BE001 and BE002) and generation 2 (BE004 and BE005) used glass slides and acrylic plates as microband spacer, respectively. Zoom-in views of the microbands of the respective  $\mu$ BAEs are shown in **Figure 3.9**.

The copper microbands of BE001 as shown in **Figure 3.8** were spaced with a layer of glass slide and epoxy glue. The BE001 microbands were not straight and not uniformly spaced due to the difficulty in controlling the viscous epoxy glue in between the copper foils. Hence, the microband array was improved in BE002 with the introduction of two glass slides and reduced application of epoxy glue in between the layers. This sandwich assembly was tightly compressed together with the help of binder clips. As the thin glass slides are fragile and difficult to handle, plastic phone cards were experimented as the spacer of the sandwich assembly demonstrated in BE003.

The sandwich construction was then upgraded to clear acrylic plastic plates as the spacer. Acrylic plate is much easier to shape and it allows the wrapping of copper foil along its edges producing a continuous band as shown in BE004 and BE005 (**Figure 3.8**).

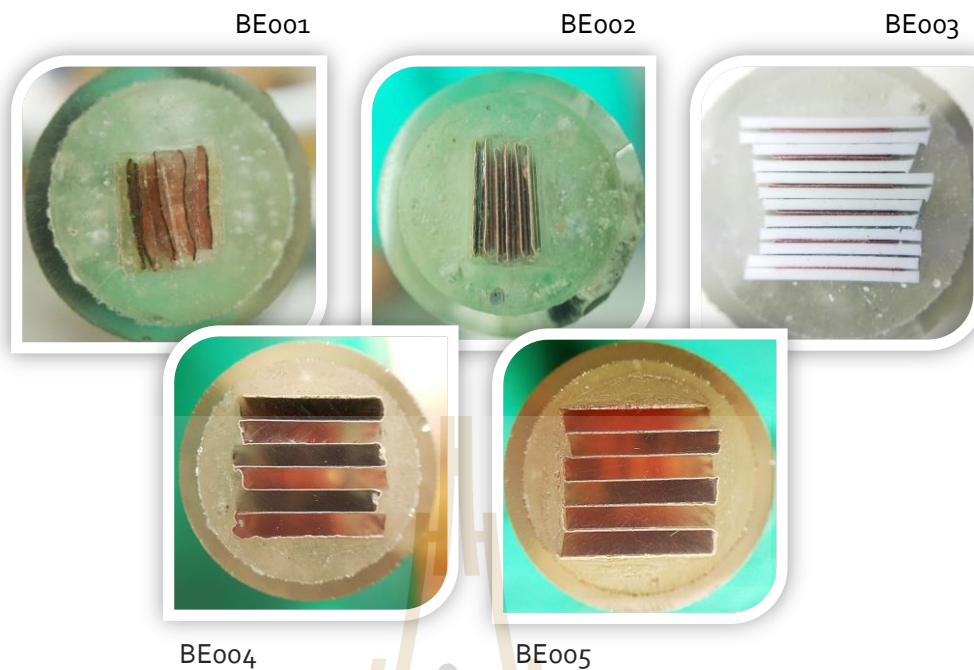


**Figure 3.8** Initial Cu  $\mu$ BAE prototypes using different materials as the spacer. The spacer for BE001 and BE002 was glass slides, BE003 was plastic phone card, while that of BE004 and BE005 was acrylic plate.

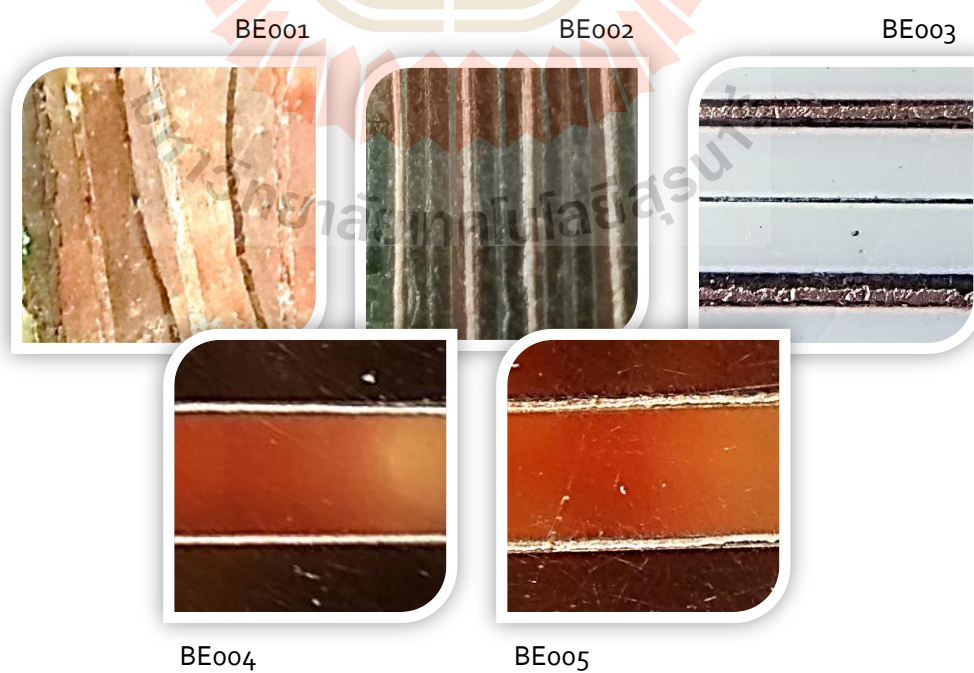


**Figure 3.9** Zoom-in view of the copper microbands of electrodes in **Figure 3.8**.

Eventually, the copper microband sandwich structure was upgraded to generation 3 where super glue was used as the adhesive instead of epoxy glue. A piece of  $30 \times 60$  mm copper foil with thickness  $25 \mu\text{m}$  was cut from a copper foil roll. Acrylic plates of  $6 \times 20$  mm (8 pieces) and  $8.5 \times 20$  mm (2 pieces) were cut from a 1 mm thick acrylic sheet. Copper foil was then folded along the long edge of the 6 by 20 mm acrylic plate using super glue as the adhesive. This sandwich structure was then left for the adhesive to get dried and hardened before enclosed with the remaining acrylic plates into a rectangular block.

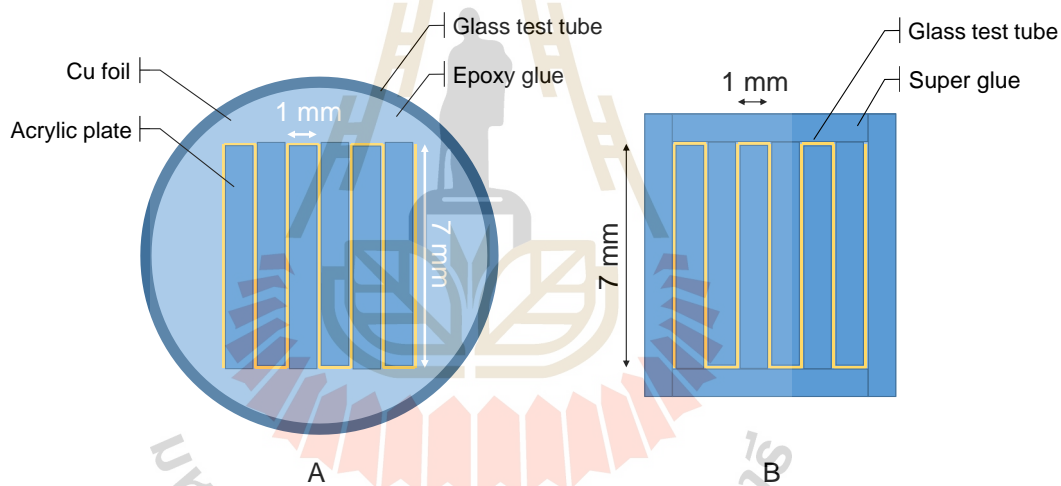


**Figure 3.10** Illustration of construction of copper microband array electrode. (A) Sandwich band structure sealed in a glass test tube with epoxy glue. (B) Sandwich band structure enclosed in acrylic plastic plate with super glue as the adhesive.



**Figure 3.11** The making of copper microband array electrode with super glue as adhesive.

### 3.2.13 Potentiostat

Electrochemical analyses in this report were conducted with a pocket-sized USB-powered 910 PSTAT mini potentiostat from Metrohm AG (Herisau, Switzerland). The selection of this potentiostat also demonstrated the portability of the system. Complementarily, Reference 600 from Gamry Instruments (Warminster, USA) was also used to support this work.

### 3.2.14 Digital Vernier calliper

Digital Vernier calliper with a measurable range 0 – 150 mm and a resolution 0.01 mm was used to measure the diameter of copper wires for the making of copper disc electrode.

### 3.2.15 Scanning electron microscope

The topography of microband array electrode ( $\mu\text{BAE}$ ) was studied with secondary electron imagery (SEI) and energy dispersive X-ray spectroscopy (EDS) using a scanning electron microscope JEOL JSM-6010LV at Suranaree University of



Technology and a JOEL JSM-7610F at Vidyasirimedhi Institute of Science and Technology.

### 3.2.16 Preparation of electrochemical immunosensor

Three-electrode carbon screen printed electrode from Quasense was soaked in distilled water for 30 min to wet the carbon electrode surface. Anti-oxytocin was then coated onto the surface by dropping 10  $\mu$ l of diluted anti-oxytocin onto the working electrode surface and incubated for a certain duration (e.g. 60 min). The SPE was then washed with the washing solution and then blocked with blocking molecules (bovine serum albumin or casein) for a certain duration (e.g. 20 min). Washing was then carried out to remove the non-adsorbed blocking molecule. This electrochemical sensor was then ready for sandwich immunoassay to capture antigen oxytocin and later the reported MB-MWCNT-Ab conjugate.

## 3.3 Experimental

### 3.3.1 Electrochemical sensing parameters

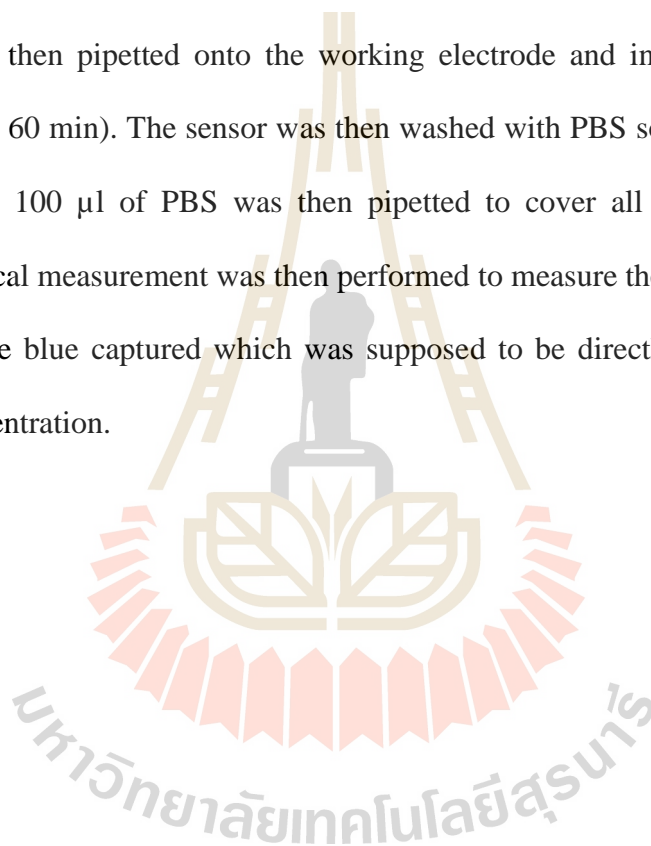
**Table 3.1** Experimental parameters for experiment in **Figure 4.12**.

Experiment	Parameters
(A)	DPV $E_{cond} -1.0$ V 10 s; $t_{equil}$ 10 s; $E_{begin} -1.0$ V $E_{end}$ 1.5 V; $S_{rate}$ 100 mV s <sup>-1</sup> ; $E_{step}$ 5 mV; $E_{pulse}$ 100 mV; $t_{pulse}$ 10 ms.
(B)	DPV $E_{cond}$ 0.0 V 10 s; $t_{equil}$ 10 s; $E_{begin}$ 0.2 V $E_{end}$ 0.8 V; $S_{rate}$ 100 mV s <sup>-1</sup> ; $E_{step}$ 10 mV; $E_{pulse}$ 25 mV; $t_{pulse}$ 50 ms.
(C)	DPV $E_{cond}$ 0.0 V 5 s; $t_{equil}$ 5 s; $E_{begin}$ 0.4 V $E_{end}$ 1.2 V; $S_{rate}$ 100 mV s <sup>-1</sup> ; $E_{step}$ 5 mV; $E_{pulse}$ 50 mV; $t_{pulse}$ 10 ms.
(D)	CV $E$ -0.5 to 1.0 V; $S_{rate}$ 50 mV s <sup>-1</sup> ; $E_{step}$ 10 mV.
(E)	CV $E$ 0.2 to 1.2 V; $S_{rate}$ 50 mV s <sup>-1</sup> ; $E_{step}$ 10 mV.
(F)	CA $E$ +600 mV

### 3.3.2 Electrochemical immunosensing

The immunosensor prepared according to **3.2.16** was then used to perform the capture antibody-antigen-detection antibody sandwich immunoreaction.

Sample containing the target antigen was pipetted onto the working electrode area of the immunosensor and incubated for a certain duration (e.g. 60 min). Then unbounded antigen was then washed off and the MB-MWCNT-Ab conjugate solution was then pipetted onto the working electrode and incubated for a certain duration (e.g. 60 min). The sensor was then washed with PBS solution and dried with nitrogen gas. 100  $\mu$ l of PBS was then pipetted to cover all the 3 electrodes. An electrochemical measurement was then performed to measure the current generated by the methylene blue captured which was supposed to be directly proportional to the antigen concentration.





## CHAPTER IV

### RESULTS AND DISCUSSION

#### 4.1 Development of miniaturised electrochemical cell

Cheap construction materials, ease of fabrication and assembly, the simplicity of operation and working electrode compatibility are determining factors for the acceptance of the proposed miniaturised electrochemical cells as 'green' substitutes for conventional beaker options.

This study is a continuation of former initiative to develop simple tools for small volume electroanalysis. A Pt  $\Omega$ -shaped minicell was previously reported by one of our former group members Sripirom (2013). The cell demonstrated the possibility of simple 15  $\mu$ l electroanalysis with a simple rolling of Pt foil into a container that acts as the counter electrode as well. Sripirom (2013) demonstrated in the  $\Omega$ -shaped minicell pharmacokinetic drug profiling in human blood following paracetamol (PCT) tablet consumption. However, the cell can only work with working and reference electrodes of small dimension and thus not compatible with most of the common disc electrodes found in an ordinary electrochemical laboratory.

Besides, the electrode transfer rate of analyte in a cylindrical counter electrode container environment in comparison to a conventional 5 ml beaker cell was not evaluated. Hence, the possibility of expanding the compatibility with common electrodes and the missing electron transfer rate in Pt  $\Omega$ -shaped minicell were investigated.

#### 4.1.1 Tests with the $\Omega$ -shaped Pt minicell

The  $\Omega$ -shaped Pt minicell was built according to 3.2.8. The  $\Omega$ -shaped Pt minicell of approximately 2 mm diameter served both as the container for 15- $\mu$ L sample solution as well as the counter electrode. Reference and working electrodes of appropriate diameter were inserted from the left- and right-hand ends of the tube with the help of micromanipulators (as illustrated in **Figure 4.1**) to complete the electrochemical cell.

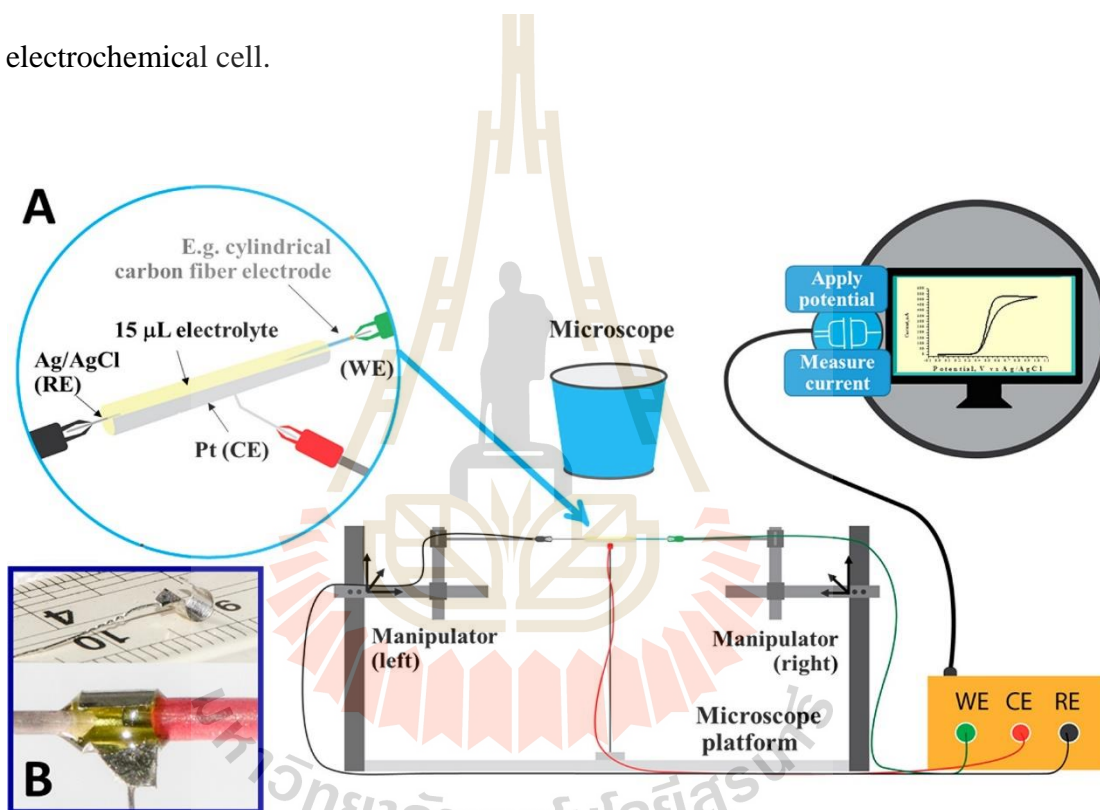


**Figure 4.1** The operational electrochemical workstation using an  $\Omega$ -shaped Pt minicell. (Sripirom *et al.*, 2018)

This study evaluated the rate of electron transfer in the previously proposed  $\Omega$ -shaped Pt minicell by Sripirom (2013). For a freshly polished and electrochemically cleaned cylindrical Pt wire electrode with a diameter of 250  $\mu$ m and

length of 1 mm, the quality of minicell voltammetry was evaluated through CV acquisition for the ferrocyanide/ferricyanide redox couple.

Cyclic voltammograms in **Figure 4.2**, recorded with scan rate,  $v$ , varied between 5 and 100  $\text{mV s}^{-1}$ . Symmetric anodic and cathodic current waves were verified for all tested scan rates. In Randles-Sevcik plots, the mined anodic ( $i_{pa}$ ) and cathodic ( $i_{pc}$ ) peak currents increased with about the same slope, consistently linear with  $v^{1/2}$ , and the statistics of a peak current analysis (**Table 4.1**) revealed the average  $|i_{pc}|/i_{pa}$  ratio for the CV set as  $1.06 \pm 0.01$  ( $n = 11$ ). As explained in **Figure 4.3**, the experimental peak separations for the various scan rates were converted into electron transfer rate constants,  $k$ , for the redox interaction of the iron species with the Pt wire electrode in the Pt inverted- $\Omega$  minicell, using the well-known Nicholson and Shain mathematical routine for the calculation (Nicholson and Shain, 1964). With  $\sim 1 \times 10^{-2} \text{ cm s}^{-1}$ , the average  $k$  for the CV data set of this minicell trial was actually well within the proposed range of  $10^{-1} > k > 10^{-5} \text{ cm s}^{-1}$  for systems with quasi-reversibility (Heinze, 1984a). The good linearity of the Randles-Sevcik plot (**Figure 4.2**) and the peak current ratio (**Table 4.1**) close to 1 confirmed quasi-reversibility of the Fe (II/III)/Pt redox was well preserved in the minicell as well.

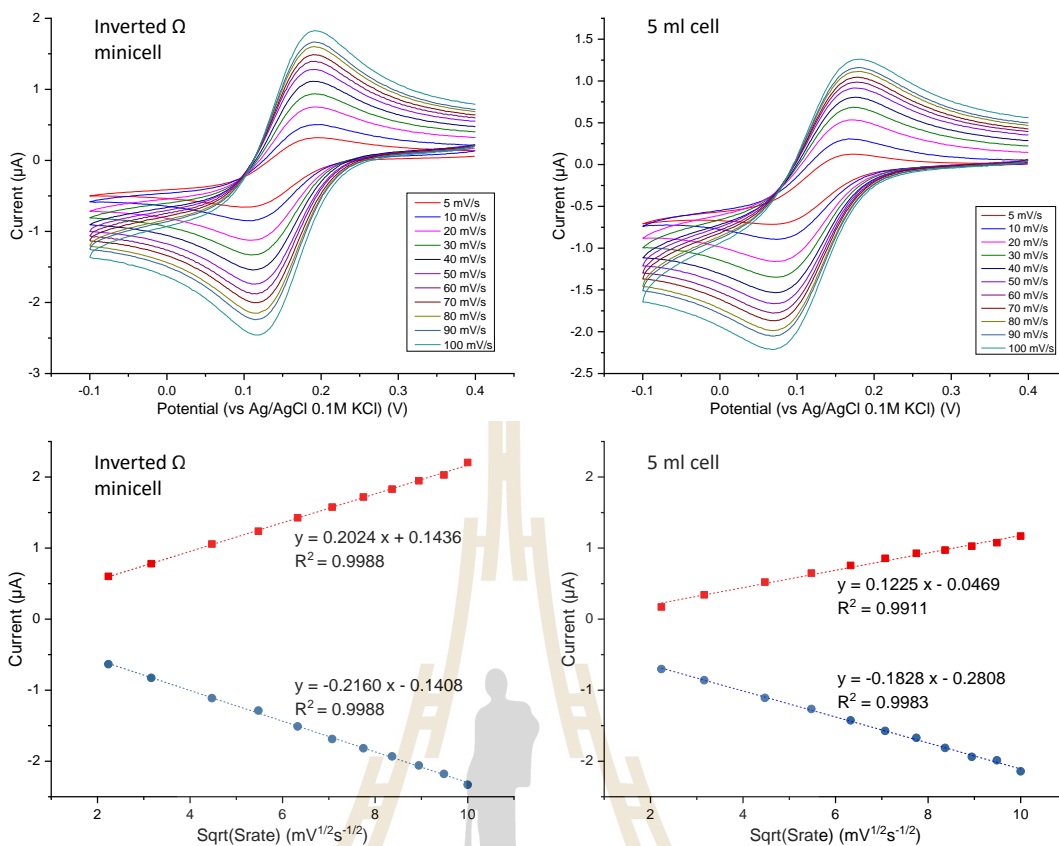


**Figure 4.2** CVs of 1 mM hexacyanoferrate(III) in 0.1 M KCl on the surface of a 1 mm  $250\ \mu\text{m}$  cylindrical Pt electrode in a Pt inverted- $\Omega$  minicell (left panels) and a conventional 5 ml cell (right panels) at scan rates varying from 2 to 100  $\text{mV s}^{-1}$ . Their respective Randles-Sevcik plots of anodic and cathodic peak currents were presented in the lower panels.

**Table 4.1** Cathodic and anodic peak currents analysis for hexacyanoferrate(III) on a Pt wire electrode at various CV scan rates.

$S_{rate}$ ( $mV s^{-1}$ )	$i_{pa}$ ( $\mu A$ )	$i_{pc}$ ( $\mu A$ )	$ i_{pc}  / i_{pa}$
5	0.6022	-0.6343	1.0533
10	0.7805	-0.8269	1.0594
20	1.0565	-1.1118	1.0523
30	1.2369	-1.2865	1.0401
40	1.4263	-1.511	1.0594
50	1.5766	-1.687	1.0700
60	1.7186	-1.817	1.0573
70	1.8295	-1.9319	1.0560
80	1.948	-2.0591	1.0570
90	2.0299	-2.1783	1.0731
100	2.2056	-2.3317	1.0572
			Avg: 1.058
			SD: 0.009

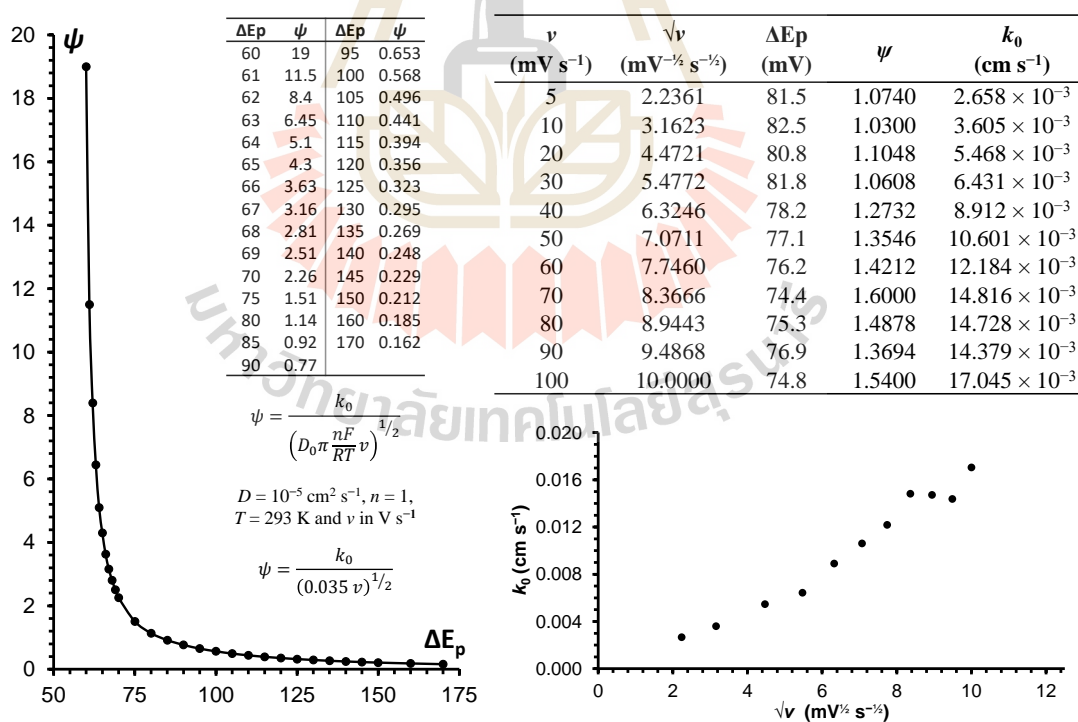


**Figure 4.3** Evaluation of rate of electron transfer of hexacyanoferrate(III) at a 1 mm long Pt wire electrode of 250  $\mu m$  diameter in the inverted- $\Omega$  Pt minicell.

#### 4.1.2 Tests with the pipette tip minicell

In the attempt to search for a cheap, easy and environmental-friendly option of forming a microlitre electrochemical cell that works with common 3 mm disc electrode, the possibility of reusing micropipette tip, a common waste material in any analytical laboratory, as the container of electrolyte and sample was explored. The detailed construction of this minicell is described in **3.2.9**. The initial attempt showed that pipette tip can form a chamber for containing electrolyte or test solution when it was capped onto a 3 mm disc electrode. Pt coil wire counter electrode and reference electrode can be dipped into the electrolyte from the top opening. This configuration was fit for electrochemical experiments.

When coupled with common commercial 3 mm disc electrode, such as BDD, Pt and Au disc electrodes in **Figure 3.1**, the cell can hold up a volume of 100 – 150  $\mu\text{l}$  suitable for the placement of Pt coil counter electrode for electroanalysis. Nevertheless, this scheme is only suitable for an electrode that has a round insulating housing of 6 – 7 mm in diameter.

Unlike the  $\Omega$ -shaped Pt minicell which works only with electrodes with small electrodes, this configuration of minicell with pipette tip required a 3 mm disc electrode. This was so that the chamber formed was large enough to contain both the Pt coil counter electrode and a miniaturised Ag|AgCl|3 M KCl reference electrode.

### 4.1.3 Tests with the Pt-tube minicell

#### 4.1.3.1 Simplicity of Pt-T minicell operation and working electrode compatibility

With the experience in handling the  $\Omega$ -shaped Pt minicell and pipette tip minicell, the two concepts were hybridised and gave the new electrochemical cell called the Pt-tube minicell.

The description in 3.2.10 explains the very simple procedure for the construction of the new version of Pt minicell. Depending on the current local price of platinum, the proposed Pt-T cell can be made at a cost of just USD 50 – 100 for a piece of 0.2 mm Pt foil. Furthermore, use of the minicell in a three-electrode arrangement requires only gentle placement on an upright working electrode of choice, pipetting of the electrolyte filling and insertion of the tip of a miniaturised reference electrode into the upper opening of the Pt-T tube which serves as the electrolyte container and counter electrode at the same time.



**Figure 4.4** The setup of Pt-T minicell in operation.



The time required between two measurements for re-assembly of a used mini cell, such as in **Figure 4.4A** or **D**, was just 2 min. This is inclusive of cleaning the Pt-T minicell by flaming and polishing, for instance, a 3-mm disk working electrode with alumina slurry, as specified in **3.2**.

An assembled Pt-T minicell was able to contain a sample of volume 30 – 60  $\mu\text{l}$  with no observable leakage, due to the capillary force of fluid within the thin cylinder. A tube diameter of 4 mm and a height of 5 mm was suitable, fitting common commercial electrode disk diameters and containing the 30  $\mu\text{l}$  sample. Minicells of significantly larger dimensions would be likely to suffer electrolyte leakage as the capillary force might fail to retain the larger liquid mass, although this was not tested. Operating the Pt-T minicell with sample volumes below 30  $\mu\text{l}$  was inconvenient since the immersion of the reference electrode from the tube top was difficult, without clear visualisation of physical contact.

**Figure 3.1** shows the eight different working electrodes that were tested with the Pt-T mini cell for various voltammetry applications. As shown in **Figure 4.4A – C**, commercial disk electrodes of diameter  $\leq 3$  mm and an outer diameter  $\geq 3.5$  mm can be easily coupled with the Pt-T minicell. Electrodes of smaller outer diameter or different geometry may also be fitted with the help of extra support, such as an O-ring (**Figure 3.1F – G**) or a short piece of a polymer rod with an appropriate perforation at the centre (**Figure 3.1I**). **Figure 4.4D** is a sketch of a minicell with an adapter while **Figure 4.4E** and **F** show, as representative examples of this approach, the functional combination of the Pt-T minicell and a Teflon rod-type adaptor with a commercial 10- $\mu\text{m}$  Pt-disc electrode of just 3 mm outer glass insulation diameter. It is worth mentioning that with tailor-made adaptors, virtually any common nano-, micro-



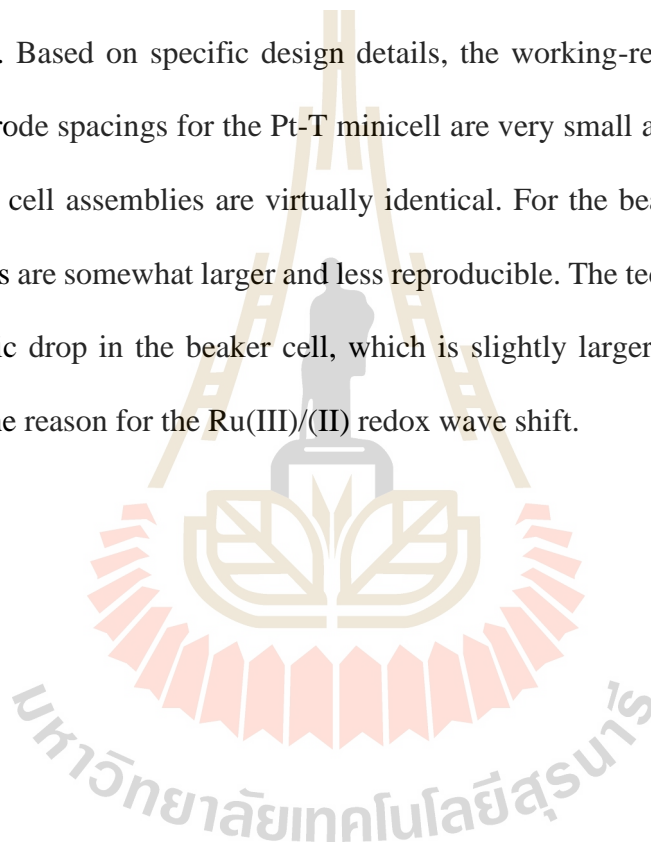
or macroelectrode form is adaptable to the Pt-T minicell, which is of the utmost importance with respect to the general applicability of the tool in electroanalysis laboratories.

#### 4.1.3.2 Basic electrochemical performance of Pt-T minicell

To evaluate the quality of electrochemical signals from standard working electrodes in the restricted electrolyte volume of the Pt-T minicell, cyclic voltammetry tests were carried out with aqueous electrolyte solutions of potassium hexacyanoferrate(III) and hexaammineruthenium(III) chloride. For comparison, trial replicates were made in a conventional beaker-type three-electrode electrochemical cell containing 5 ml electrolyte. Cyclic voltammograms (CVs) were measured with 3-mm diameter Pt, Au, boron-doped diamond and glassy carbon disk macroelectrodes, a 10- $\mu$ m-diameter Pt disk microelectrode and a 2-mm-long, 0.9-mm-diameter cylindrical pencil lead macroelectrode in the Pt-T minicell with 30  $\mu$ l of 12.5 mM hexacyanoferrate(III) in 0.1 M PBS, pH 7. For all except the pencil lead electrode the current-potential traces showed the peak-shaped or sigmoidal waves that are characteristic of hexacyanoferrate(III) voltammetry at disk-shaped noble metal and macro- and micro-electrodes (**Figure 4.5**). The absence of well-shaped peaks in CVs with the pencil-lead sensor, used here without special preceding surface activation, reflected the poorer redox sensitivity of the electrode material, which is a composite of graphitic carbon powder and a polymer binder, rather than the poor performance of the minicell system.

Two sets of three hexaammineruthenium(III) CVs were taken with a 3 mm boron-doped diamond disk electrode with 5 ml of solution in the beaker cell and 30  $\mu$ l in the Pt-T minicell. In each case, electrodes were reassembled, and the

electrolyte was refilled between individual CV runs. The Pt-T mini cell delivered almost superimposable CVs, while in the beaker small but noticeable peak shifts occurred between individual runs and the voltammograms did not exactly overlap each other (**Figure 4.6**). Also, the separation of anodic and cathodic peak maxima was a little greater for scans in the beaker cell, which can be attributed to effects related to ohmic ( $iR$ ) drop and electrochemical reversibility of electron transfer inherent in the design of the two cells. Based on specific design details, the working-reference and working-counter electrode spacings for the Pt-T minicell are very small and thus the CVs from the repetitive cell assemblies are virtually identical. For the beaker option, however, these spacings are somewhat larger and less reproducible. The technical details suggest that the ohmic drop in the beaker cell, which is slightly larger than that in the Pt-T minicell, is the reason for the Ru(III)/(II) redox wave shift.



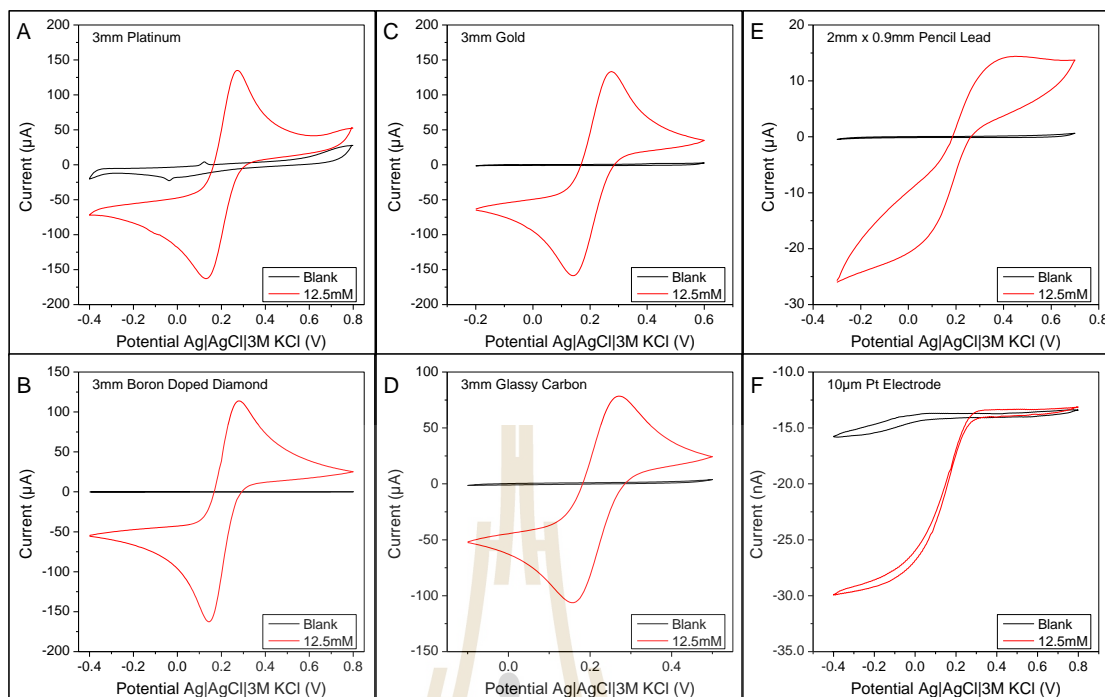


**Figure 4.5** Cyclic voltammograms of 12.5 mM hexacyanoferrate(III) in 0.1 M PBS (pH 7.0) in a Pt-T minicell with a 30  $\mu$ l electrolyte load for various electrodes: (A) a 3-mm-diameter platinum disk electrode, (B) a 3-mm-diameter boron-doped diamond electrode, (C) a 3-mm-diameter gold disk electrode, (D) a 3-mm-diameter glassy carbon disk electrode, (E) a 2-mm-long 0.9-mm-diameter cylindrical pencil lead electrode and (F) a 10- $\mu$ m-diameter Pt disk electrode. Black traces represent measurements in hexacyanoferrate(III)-free supporting electrolyte.

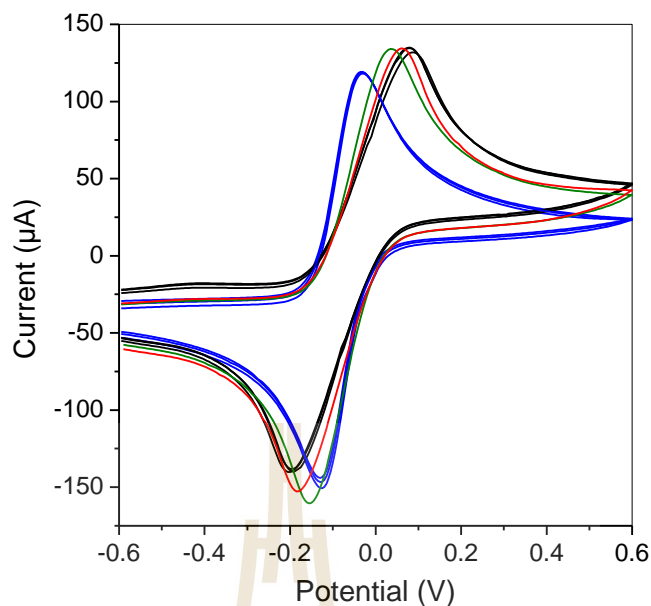


**Figure 4.6** Comparison of CV consistency of conventional 5 ml beaker cell and Pt-T minicell. All CVs were obtained in 30  $\mu\text{l}$  of 10 mM hexaammineruthenium(III) in 0.1 M phosphate buffer, pH 7.0, with a BDD electrode. The blue lines are from 3 scans of 3 cell reconstructions in Pt-T minicell. CVs from a conventional 5 ml beaker cell were presented in three different colours: black lines for the 3 scans in single constructions, while red and green lines for scans recorded in 2 reconstructions.

To compare electrochemical reversibility for sensor operation in the large- and small-volume systems, a series of CV experiments were performed with 1 mM hexacyanoferrate(III) / 0.1 M KCl, with a 3 mm Pt disk electrode in a 5 ml beaker and with the 30  $\mu$ l Pt-T mini- cell, with scan rates from 2 to 100  $\text{mV s}^{-1}$ . Hexacyanoferrate(III) is often used as a stable quasireversible model system for the characterisation of new electrode materials and of mass transfer kinetics in electrochemical reactors.

The CVs obtained, together with their peak current analyses, are presented in **Figure 4.7**. For both CV sets, cathodic ( $i_{pc}$ ) and anodic ( $i_{pa}$ ) peak currents were directly proportional to the square root of scan rate. Peak separations for the two cell options varied between  $\sim 70$  and  $\sim 100$  mV, while the average ratios of  $i_{pa}/i_{pc}$  were 1.39 and 1.08, respectively for the 5 ml beaker and Pt-T minicell. Using standard methodology (Heinze, 1984b; Nicholson, 1965), peak separations were converted to electron transfer rates ( $k$ ) which were  $\sim 0.009$  and  $\sim 0.015$   $\text{cm s}^{-1}$  as the mean values for hexacyanoferrate(III) redox in the beaker and mini cell, respectively. Both cell systems showed pronounced linearity of the Randles-Sevcik plot, an  $|i_{pa}|/i_{pc}$  close to 1 and rate constant values within the required range of  $10^{-1}$  to  $10^{-5}$   $\text{cm s}^{-1}$ . The detailed calculation of this conversion is given in **Figure 4.8**. This agrees with the expected quasi-reversibility of the redox interaction of dissolved hexacyanoferrate(III) with Pt, though the mini cell produced a slightly better result. The minimal manifestation of ohmic  $iR$  drop, excellent reproducibility of voltammetric response and superior quasi-reversibility were identified as valuable properties of the Pt-T mini cell and thus made it a promising alternative for practical applications.

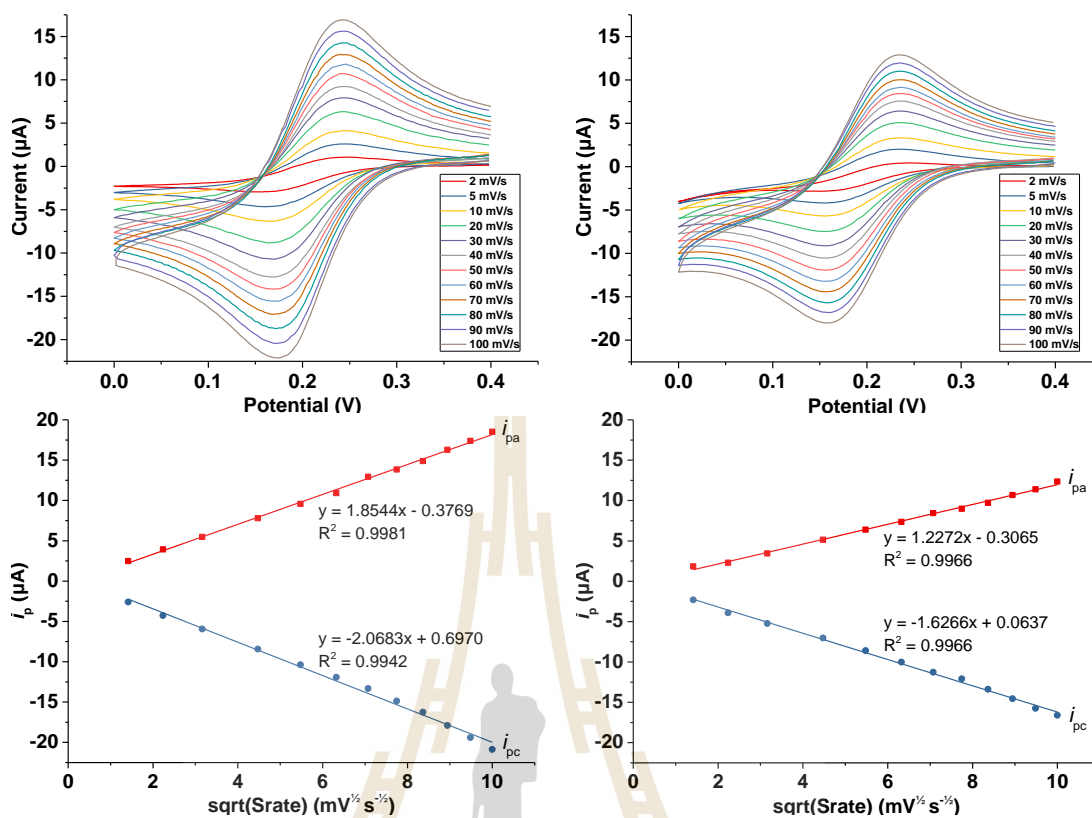


**Figure 4.7** CVs of 1 mM hexacyanoferrate(III) in 0.1 M KCl on the surface of a 3 mm Pt disc electrode in the Pt-T minicell (left panels) and a conventional 5 ml cell (right panels) at scan rates varying from 2 to 100  $\text{mV s}^{-1}$  on 3 mm Pt electrode. Their respective Randles-Sevcik plots of anodic and cathodic peak currents were presented in the lower panels.

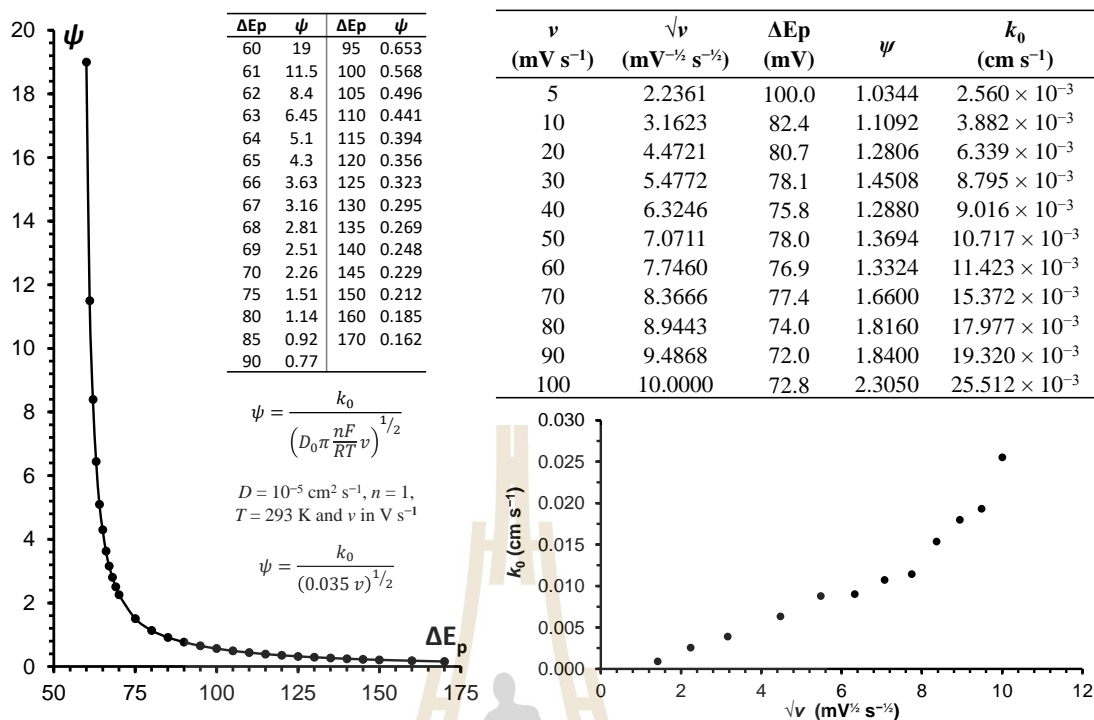


**Figure 4.8** Evaluation of rate of electron transfer of hexacyanoferrate(III) at a 3 mm Pt disc electrode using Pt-T minicell.

#### 4.1.3.3 Concentration stability of Pt-T minicell

Solvent evaporation is a critical factor for electroanalysis in a small volume as it may significantly affect concentrations of dissolved species in the remaining electrolyte and hence disturb the response stability of the working electrode. In order to evaluate the effect of evaporation, 30  $\mu\text{l}$  of 5 mM hexaammineruthenium(III) was pipetted into the Pt-T mini cell over an integrated 3 mm Pt disk electrode and a series of DPVs was measured at 5 min intervals for the first 30 min and 10 min intervals for the next 40 min. This evaluation was conducted without using a solvent-saturated atmosphere or any other measure to protect against solvent loss. Plots of the observed peak currents as a function of time showed that the electrochemical cell configuration was able to maintain a relatively consistent peak current for the first 30 min (**Figure**

4.9). The DPV peak current increased significantly after that. The mean peak current for the initial 30 min was 51.18  $\mu\text{A}$  with an RSD at 1.54%.

This result is a valuable side-effect of the special Pt-T mini cell design as the only opening at the top of the cell is largely blocked by the fritted glass tip of the inserted reference electrode, thus minimising the surface area of the solution body in contact with the surrounding. It is worth to note that the current stability which represents the stability of analyte concentration over a period of 30 min is long enough for common electrochemical analyses.

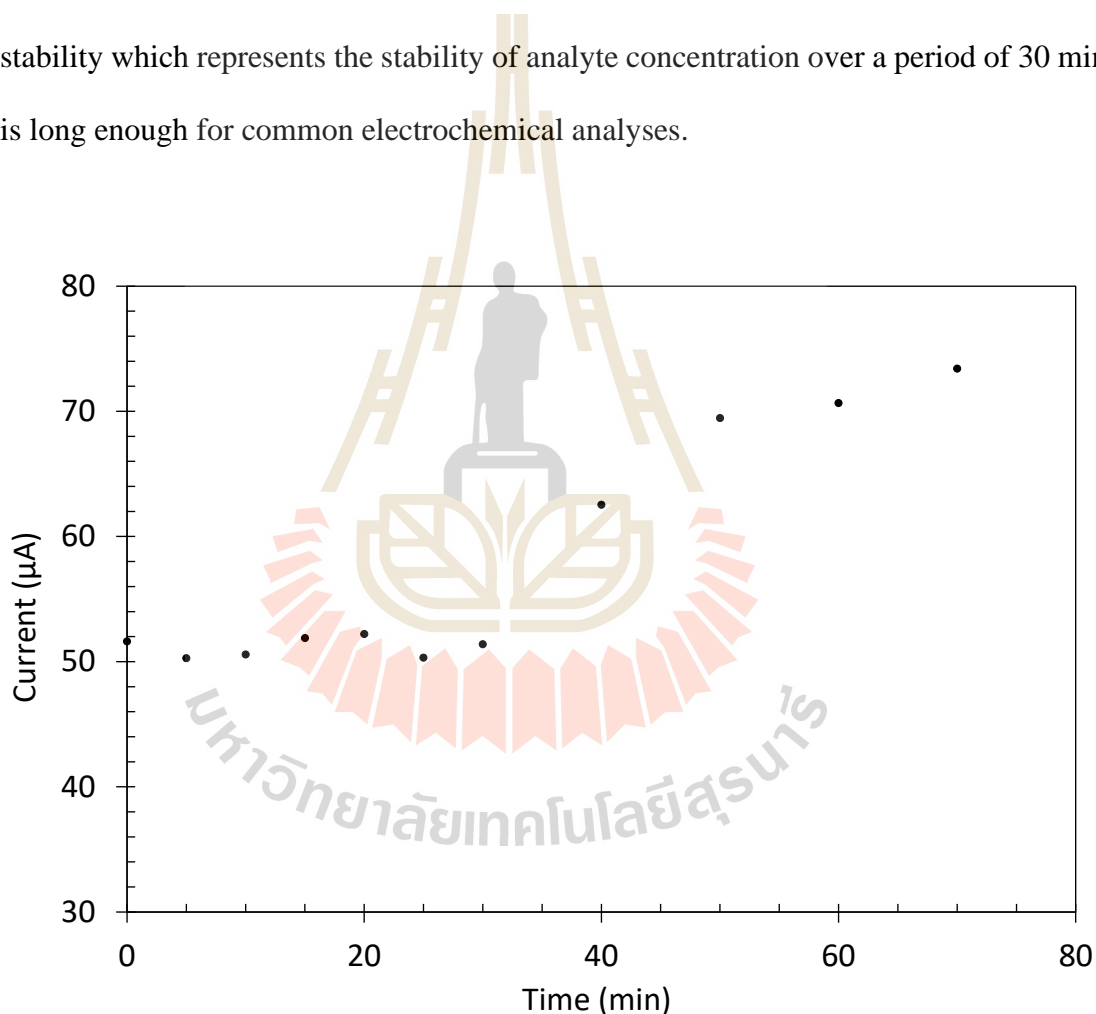


**Figure 4.9** Oxidative peak currents of DPV for a 30  $\mu\text{l}$  aliquot of 5 mM hexaamineruthenium(III) solution in a Pt-T minicell over a duration of 70 min at room temperature (28°C) in the absence of solvent-saturated environment.



#### 4.1.3.4 General Pt-T minicell applicability

To be an attractive routine laboratory tool for 'green' electroanalysis, a miniaturised electrochemical cell must have the potential to deal, cheaply and easily, with the detection of a wide range of analytes with oxidisable and/or reducible structures. To demonstrate such general applicability, chemicals with importance to human body function and health, pharmaceuticals and clinical disease diagnostics were chosen. This demonstration is relevant, as life science samples are usually of limited size and low target analyte concentration, thus, small-volume screening is a good analytical option.

Ciprofloxacin<sup>®</sup>, an antibiotic (Davis *et al.*, 1996), and doxorubicin<sup>®</sup> a cancer chemotherapy drug (Jemelková *et al.*, 2009), were chosen to evaluate the practical performance of the Pt-T minicell in the detection of drugs. Ciprofloxacin is also reportedly a frequently detected fluoroquinolone antibiotic in the aquatic environment which may induce antibiotic resistance due to long term exposure (Shen *et al.*, 2018). Doxorubicin is a widely prescribed and effective anticancer agent (Tardi *et al.*, 1996). However, its therapeutic potential is limited by a frequently irreversible and often fatal side of congestive heart failure (Swain *et al.*, 2003; Von Hoff *et al.*, 1979). **Figure 4.10** shows the molecular structures of ciprofloxacin and doxorubicin indicating their redox active functional groups.

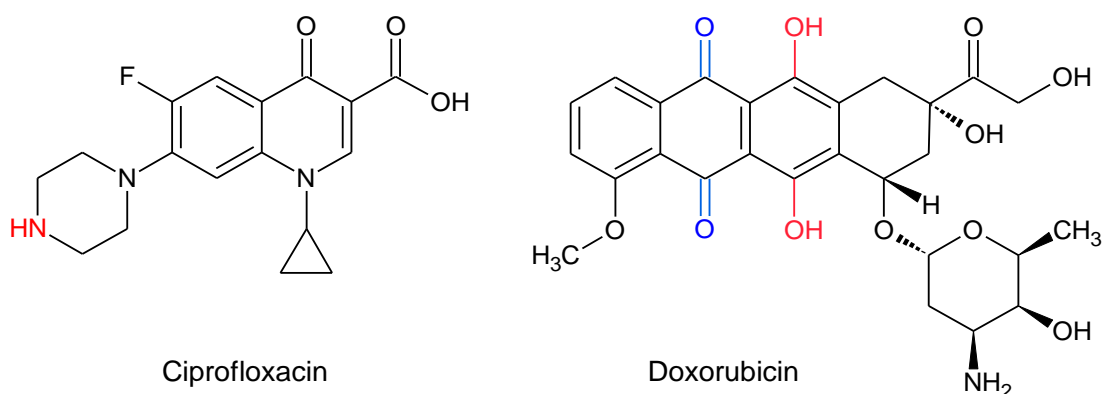


**Figure 4.10** Structures of ciprofloxacin and doxorubicin. Functional groups labelled in red are oxidisable and blue are reducible.

In addition, the device was evaluated with oxytocin, a neuropeptide regulating childbirth and various emotions (Carson *et al.*, 2013); ascorbic acid, an antioxidant that is essential to human health through its roles in collagen biosynthesis, iron absorption, radical scavenging and immune response activation (Arrigoni and De Tullio, 2002); and 4-methylumbelliferone, a drug used in bile therapy, as an ingredient of UV protection creams and a redox-active label of synthetic substrates in optical or electrochemical enzyme activity assays (Coelho *et al.*, 2013; Marathe *et al.*, 2013).

The oxidisable tyrosine moiety of this nonapeptide are responsible to the oxidation peak observed in DPVs presented in **Figure 4.12C**. Meanwhile, the CVs of ascorbic acid shown in **Figure 4.12D** demonstrated the irreversible oxidation properties of ascorbic acid forming dehydroascorbic acid. 4-Methylumbelliferone was oxidisable leading to the CVs in **Figure 4.12E**. The oxidation mechanism of methylumbelliferone is shown in **Figure 4.11** below.

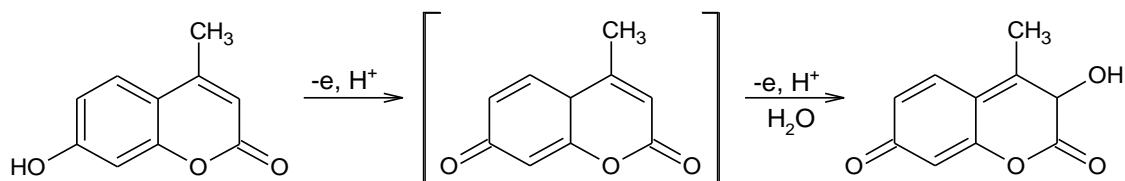


**Figure 4.11** Oxidation mechanism of 4-methylumbelliferone as proposed by L. Wang *et al.* (2015).

Finally, the suitability of the proposed Pt-T minicell for enzyme-based bioelectroanalysis of disease markers was evidenced with the amperogram of glucose biosensing. The by-product hydrogen peroxide from the conversion of glucose to gluconic acid was oxidised at the Pt electrode beneath the immobilised enzyme glucose oxidase producing a quantifiable faradaic current.

**Figure 4.12** shows the minicell DPVs of ciprofloxacin, doxorubicin and oxytocin; CVs of ascorbic acid and 4-methylumbelliferone; and amperograms from the glucose biosensor. The DPVs and CVs of 30  $\mu\text{l}$  samples of drugs, hormone and the redox label in 0.1 M PBS, pH 7 were recorded with a 3 mm boron-doped diamond electrode. Meanwhile, the CVs of ascorbic acid and the amperograms from the biosensor were recorded respectively with a 1 mm Pt disk electrode and a 3 mm Pt disk electrode with a thin surface film of GOx-loaded Nafion. The currents of these individual experiments were plot against their respective analyte concentration as shown in **Figure 4.13**.

The DPVs for the two drugs and the hormone in **Figure 4.12A**, **B** and **C** all display well-formed anodic peaks, with current directly proportional to the respective compound concentration (**Figure 4.13A**, **B** and **C**). In the CVs of ascorbic acid and 4-methylumbelliferone in **Figure 4.12D** and **E**, the concentration-dependent

anodic peak currents are evident (**Figure 4.13D and E**) but equivalent reduction peaks are vague, which agrees with the known irreversible nature of the related interfacial charge transfer processes for these two compounds. As expected in a potential step experiment, all five amperometric glucose oxidase biosensor recordings in **Figure 4.12F** start with the onset of a large but fast-decaying capacitive current spike. The plateau currents were faradaic currents contributed by the oxidation of hydrogen peroxide that was generated continuously in the biosensor's active surface coating by the enzyme-catalysed reaction. This current is directly proportional to the glucose concentration in the blank and standard samples and thus can be utilised for quantitative analysis. This was evidenced with the plot of biosensor current against glucose concentration which was linear up to about 5 mM (**Figure 4.13F**).

The results above were clear evidence for the suitability of Pt-T minicell in analytical applications for drug, hormone, antioxidant and redox label voltammetry. It also showed good compatibility with enzyme-based biosensing schemes. Heavy metal stripping voltammetry (Sripirom *et al.*, 2018) and electrodeposition (Jimenez *et al.*, 2015), which were successfully performed in other miniaturised three-electrode electrochemical cells with microlitre volumes, should also be feasible in the proposed Pt-T assembly used in this study. With the evidence presented above, it is apparent that the Pt-T minicell possesses the important characteristic of general applicability in electroanalysis.

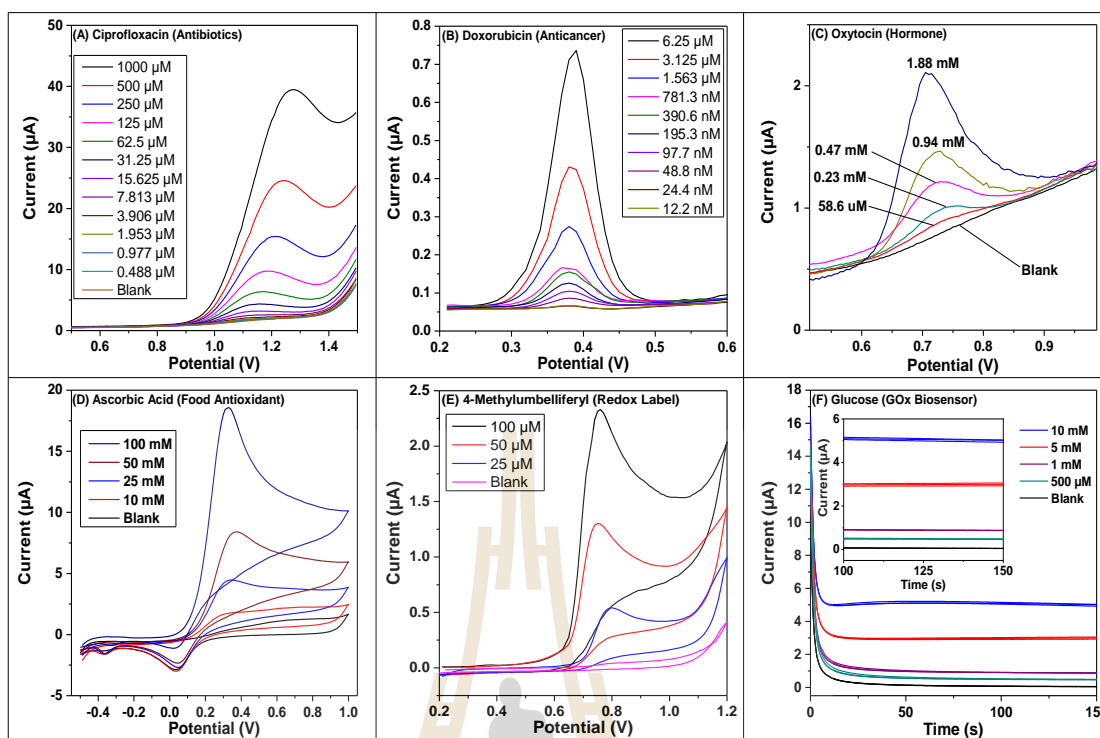


**Figure 4.12** Minicell electrochemical experiments on drugs, hormone, antioxidant, redox label and disease-indicating oxidase biosensor. (A) DPVs of ciprofloxacin with a series of 2-fold concentration dilution from 1000 to 0.49  $\mu\text{M}$ . (B) DPVs of doxorubicin with a series of 2-fold dilutions ranging from 6.25  $\mu\text{M}$  to 12.2 nM. (C) DPVs of oxytocin with a series of 2-fold dilutions from 1.88 mM to 58.6  $\mu\text{M}$ . (D) CVs of 0 to 100 mM ascorbic acid on a 1 mm Pt electrode. (E) CVs of a 0 to 100  $\mu\text{M}$  4-methylumbelliferyl (redox label). (F) Amperograms of 0, 0.5, 1, 5 and 10 mM glucose solutions obtained at +600 mV with a GOx biosensor (see 3.3 for detailed parameters for cyclic and differential pulse voltammogram data acquisition). Unless otherwise specified, all analytes were in 0.1 M PBS pH 7.0.

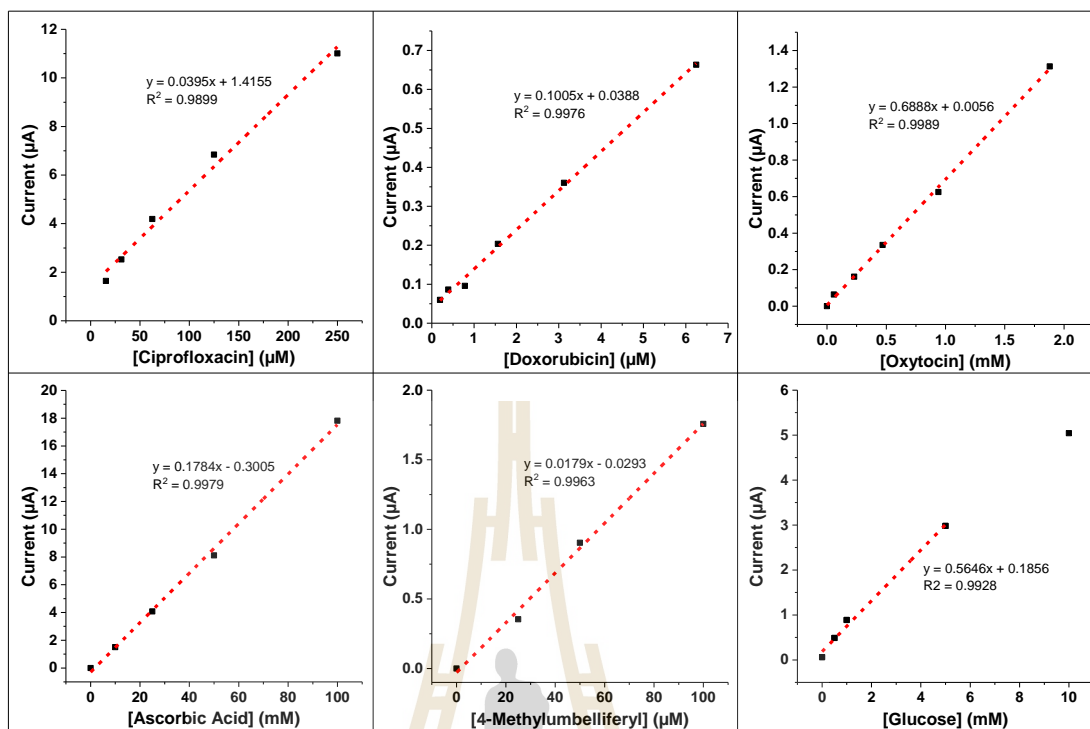


**Figure 4.13** Plots of current vs concentration of (A) ciprofloxacin, (B) doxorubicin, (C) oxytocin, (D) ascorbic acid, (E) 4-methylumbelliferone and (F) glucose for the respective experiments in **Figure 4.12**.

#### 4.1.3.5 Pt-T minicell application for paracetamol quantification by pulse voltammetry

DPVs of paracetamol (PCT) at concentrations (**Figure 4.14**)

ranging from 1000 µM with a series of two-fold dilutions to 3.124 µM were performed with the following parameters:  $E_{\text{cond}}$  0.2 V,  $t_{\text{cond}}$  10 s,  $t_{\text{equil}}$  10 s,  $E_{\text{begin}}$  0.2 V,  $E_{\text{end}}$  1.2 V,  $S_{\text{rate}}$  0.1 V s<sup>-1</sup>,  $E_{\text{step}}$  5 mV,  $E_{\text{pulse}}$  0.15 V,  $t_{\text{pulse}}$  10 ms. The calibration curve for paracetamol (**Figure 4.15**) plotted from these peak currents indicates that the BDD electrode coupled with Pt-T mini cell had a dynamic range up to 250 µM with a linear correlation of 0.9998.

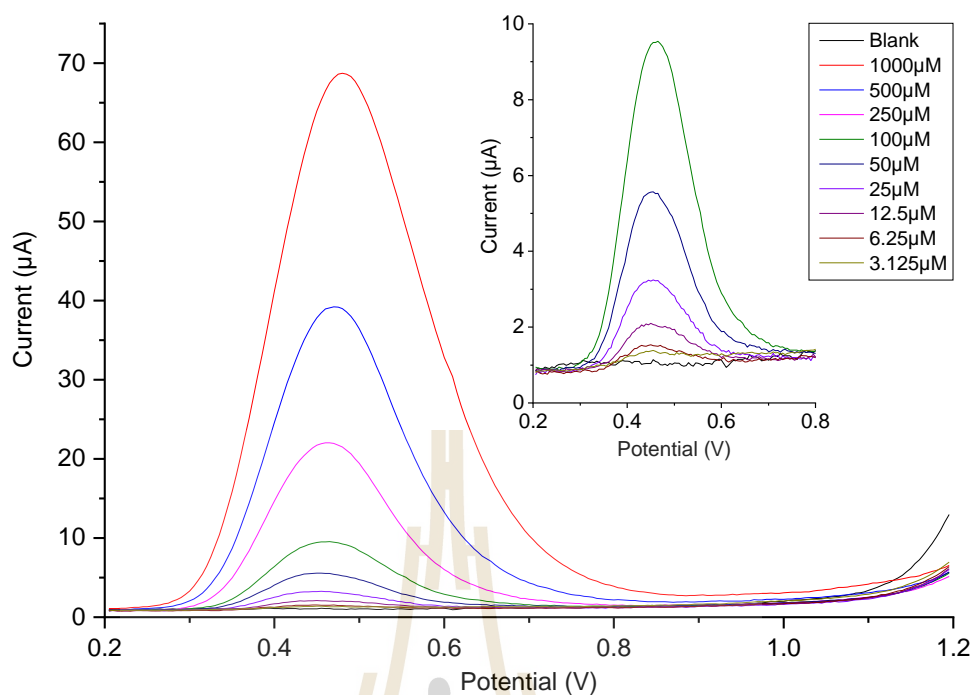


**Figure 4.14** DPVs showing oxidation peaks of standard solutions of PCT ranging from 1,000 to 3.124 μM. Measurements were performed in the Pt-T mini cell with a 30 μl load of supporting electrolyte buffer.

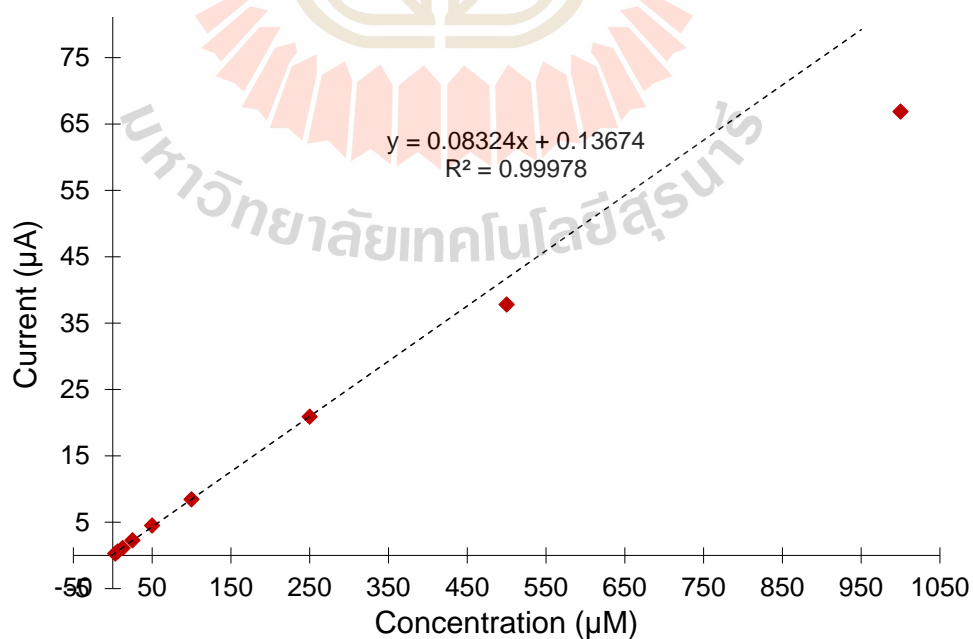


**Figure 4.15** Calibration curve plot of DPV anodic peaks from **Figure 4.14** against PCT concentration.

Due to the small volume, the conventional standard addition method for the quantification of analyte in the Pt-T mini cell was not practical, as even a small addition of standard solution to the sample would affect the analyte concentration adversely. Therefore, equal volumes of sample and standard solutions of various concentrations were mixed prior to the electrochemical detection by DPV. A detailed illustration of this sample preparation is provided as **Figure 4.16**. Since equal volumes were mixed, the initial concentrations of both sample and standard concentrations were halved.

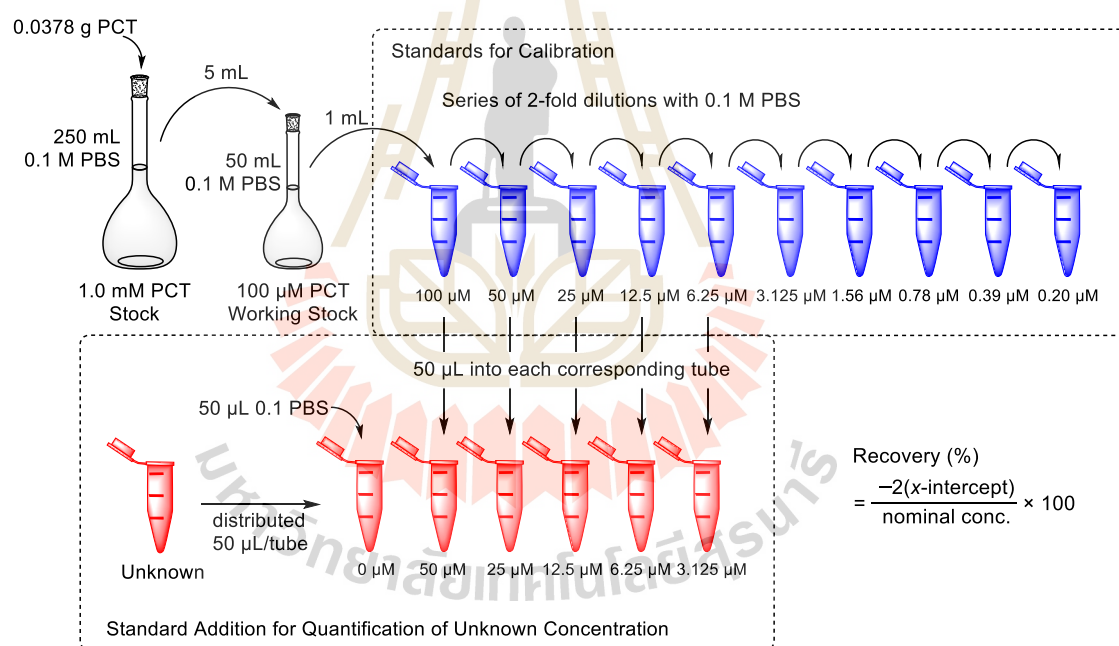


**Figure 4.16** Schematic illustration of PCT standard solution preparation for calibration and standard addition for quantification of PCT in sample.



The DPVs of this standard addition experiments are shown in **Figure 4.17**. As shown in **Figure 4.18**, the paracetamol sample with a nominal concentration of 10  $\mu\text{M}$  produced a standard addition plot that intercepted at  $-4.9801 \mu\text{M}$  at the x-axis. Since the concentration of paracetamol was halved, the x-intercept was thus translated into a sample concentration of 9.96  $\mu\text{M}$ . This demonstrated a recovery of 99.6%. Repetitions of the recovery experiment with 10  $\mu\text{M}$  paracetamol gave a mean recovery at 98.11% with RSD 6.60% ( $n=5$ ) (refer **Table 4.2**). Similarly, a sample of 50  $\mu\text{M}$  paracetamol had a mean recovery of 100.67% with RSD 6.97% ( $n=3$ ).

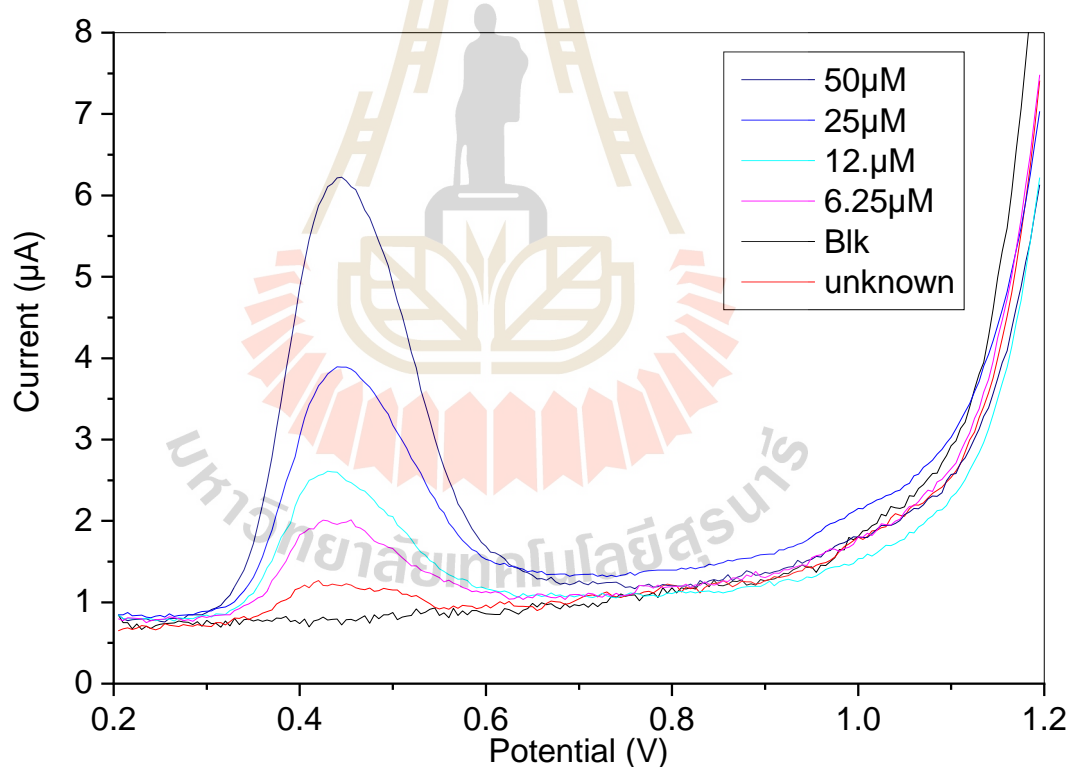


**Figure 4.17** DPVs of quantification of PCT with nominal concentration 10  $\mu\text{M}$  by the standard addition method.

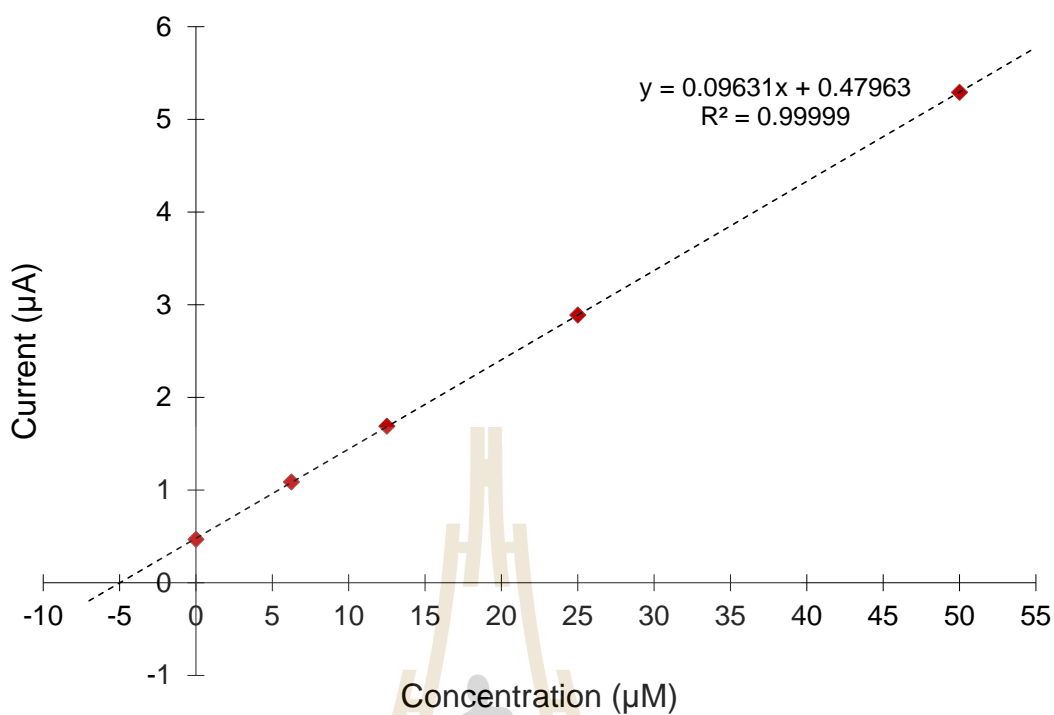


**Figure 4.18** Standard addition plot for the quantification of paracetamol with nominal concentration of 10 µM.

**Table 4.2** Recoveries of paracetamol in sample with a nominal concentration of 10 µM.

Nominal Conc. of Unknown (µM)	No. of Std. Add. Points	Linear Relationship	R <sup>2</sup>	Rec. (%)
10	5	$y=0.09631x+0.47963$	0.99999	99.60
10	5	$y=0.09898x+0.44925$	0.99895	90.78
10	5	$y=0.09176x+0.42523$	0.99992	92.68
10	5	$y=0.10163x+0.51128$	0.99977	100.62
10	5	$y=0.09592x+0.51243$	0.99796	106.85

These evaluations on the Pt-T minicell showed that the minicell was a good solution for green electroanalysis. The Pt-T minicell had a high adaptability to various common electrodes found in an ordinary electrochemical laboratory. The minicell also demonstrated high suitability for analytical work with various drugs and sensing scheme.

## 4.2 Copper Microbands Array Electrode

Microelectrodes are famous for their beneficial properties which are (1) improved mass transport; (2) better discrimination against charging current; (3) decreased distortion from  $iR$  drop; (4) low double-layer capacitance. Applications of microelectrodes usually involve ultra-low current at nanoampere level or lower which requires the use of advanced low-noise potentiostats. This study explored the possibility of preparing a microband array electrode with increased active area without using any advanced but less accessible microfabrication technology.

### 4.2.1 Topography of copper microband array electrode

Topographic image from scanning electron microscopy of BE002 (**Figure 4.19A**) showed that the making of the microscopic band electrode structure by sandwiching 25  $\mu\text{m}$  thin copper foils in between two 150  $\mu\text{m}$  thick glass slides produces a relatively straight and evenly spaced set of microbands. However, breakages of glass slides were also observed due to the fragile characteristic of thin glass. This was also the difficulty and inconvenience of this microband array construction scheme.

The use of glass slide was later replaced by the use of 1 mm acrylic plates as the spacer between the parallelly aligned microbands. Incorporation of the more durable acrylic allowed the wrapping of copper foil in a continuous S-shape

manner, thus increasing the cross-sectional copper microband surface area of the sandwich construction. The products were Cu microband electrode structures coded BE004 and BE005 as shown in **Figure 3.8**.

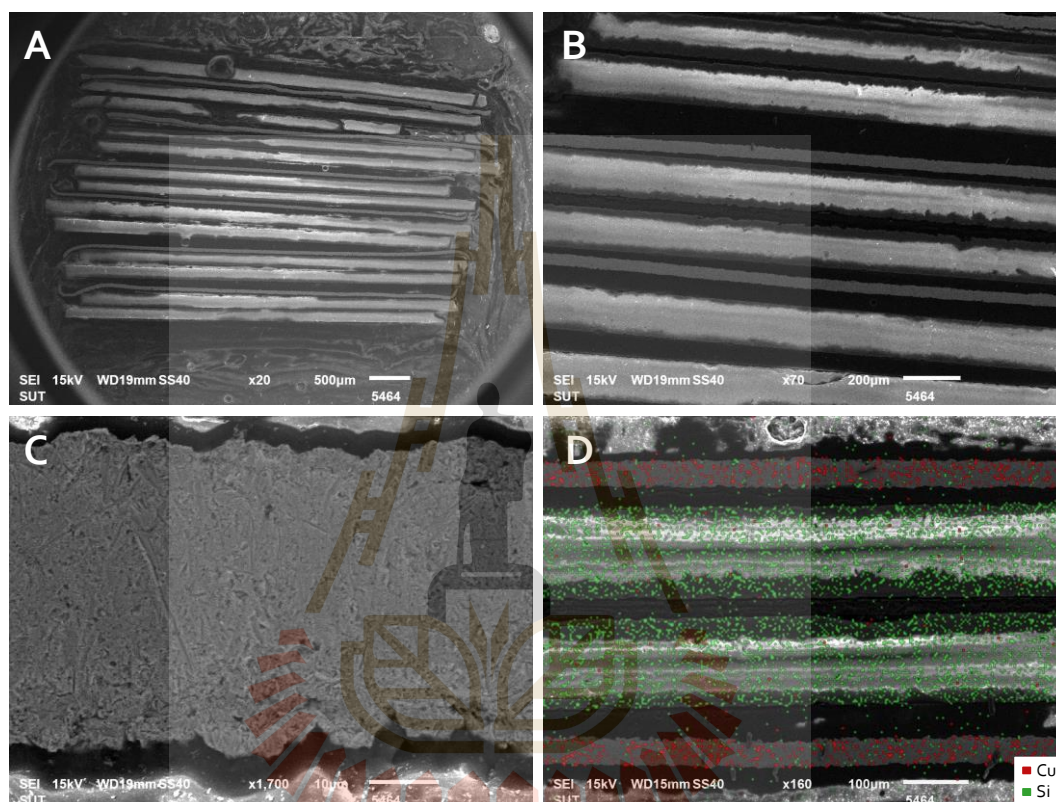


**Figure 4.19** Topography of copper microband array electrode BE002 (A – C) and elemental distribution analysis of a selected region of BE002 by energy dispersive X-ray spectroscopy (D).

The thickness of the microband of BE005 was estimated to be 37  $\mu\text{m}$  based on the scanning electron microscopy image (**Figure 4.20**). This was thicker than the thickness of copper foil probably due to abrasion against sandpaper and polishing against alumina slurry which smears the surface area of the metallic microband. Meanwhile, the diameter of the 2 mm copper disc electrode used as a macroelectrode

comparison was estimated to be 2.23 mm, which was consistent with the thickness of wire measured with a digital Vernier calliper. The surface area of copper microband of BE005 was estimated to be 0.021 cm<sup>2</sup>. This was approximately half of that of the comparative copper disc electrode which had a surface area of 0.039 cm<sup>2</sup>.

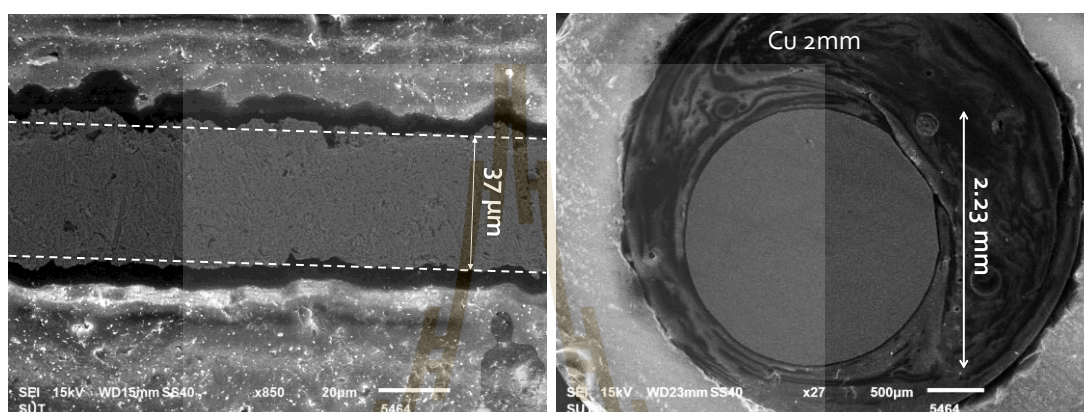


**Figure 4.20** Topography of (A) a single copper microband of BE005 and (B) copper disc electrode (Cu 2 mm) by scanning electron microscopy.

It is worth to be noted also that epoxy glue used for the generation 1 and generation 2 tends to form air bubble during the mixing of its two mixing components, i.e. resin and hardener. Besides, the epoxy material also tends to deform after a prolong usage with repetitive the exposure to solutions and dryness. Hence, epoxy glue was replaced with super glue in the development of generation 3  $\mu$ BAE. Super glue or more specifically cyanoacrylate glue is a class of strong fast-acting adhesives with industrial, medical, and household uses. The acryl groups in the resin polymerise instantly in the presence of water molecules to form long and strong polymer chains. Since almost every object has at least a tiny amount of moisture on its surface, super glue is thus an adhesive suitable for sticking generally everything.



Super glue formed strong chemical bonds that held the  $\mu$ BAE sandwich structure rigidly together. The polished cross-sectional surface of this third generation  $\mu$ BAE looked smooth with very little air bubbles. The whole assembly looks like a unibody where the copper foil had been fully incorporated into a plastic insulation body. This is also observed under a scanning electron microscope where there was less trench around the copper microband (see SEM image in **Figure 4.21**) which was obvious in the SEM images of the previous generation prototypes.

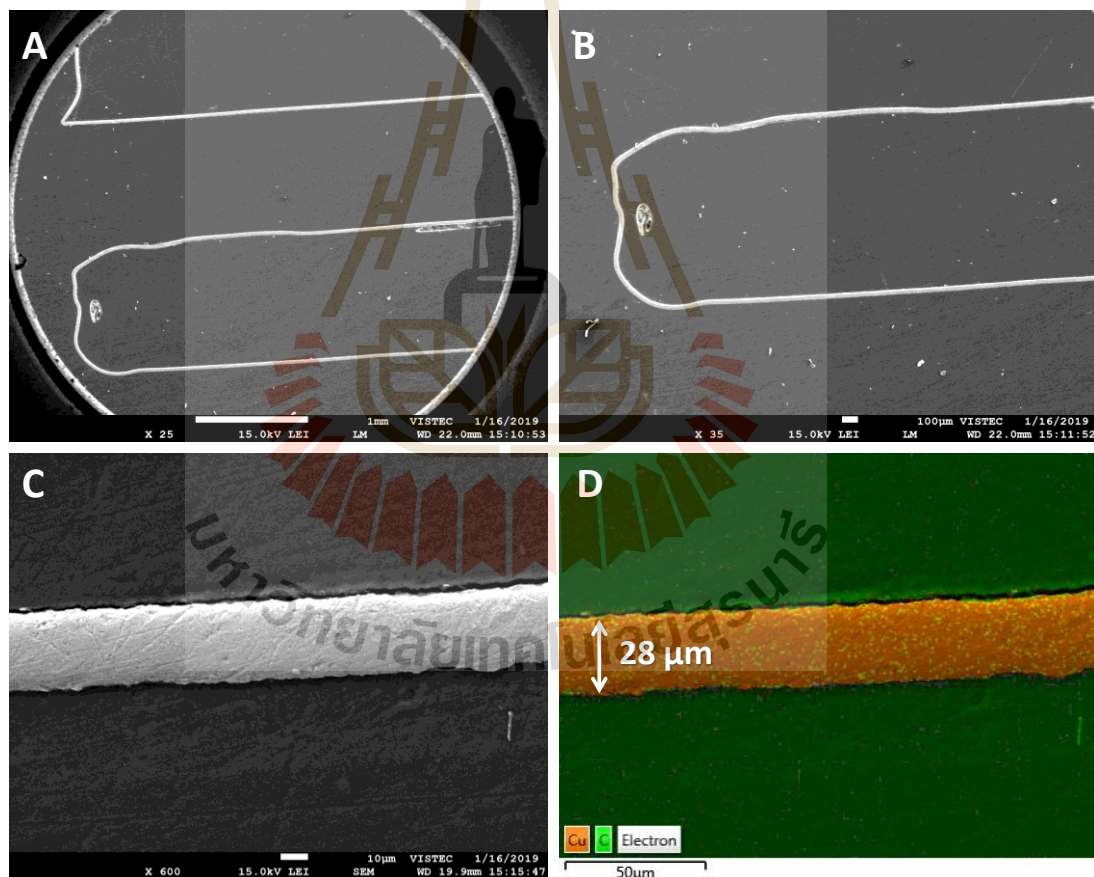


**Figure 4.21** Topography of copper microband array electrode BE011 (A – C) and elemental distribution of copper and carbon on the selected region of BE011 by energy dispersive X-ray spectroscopy (D).

The band thickness of this third-generation prototype was found to be 28  $\mu\text{m}$  which was 9  $\mu\text{m}$  thinner than that of the second-generation prototype. This was certainly an effect of the rigid polymer formed by the super glue adhesive which reduced the smearing of copper microband during abrasion against sandpaper and alumina slurry.

#### 4.2.2 Microelectrode characteristic of copper band electrode

Hemispherical diffusion of the analyte to a microelectrode is the phenomena that contribute to the higher current density on a microelectrode. It was expected that a microband structure was equivalent to a series of microdiscs aligned continuously into a line. Thus, the hemispherical fields of individual microdiscs eventually merge together forming a hemicylindrical diffusion field (see **Figure 4.22**).

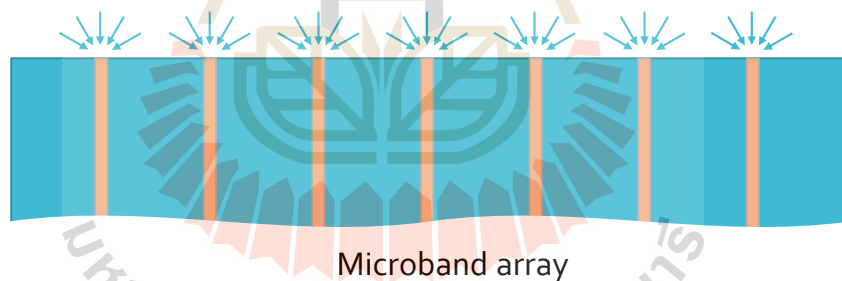


**Figure 4.22** Illustration of expected hemicylindrical diffusion mode along the microbands of a  $\mu\text{BAE}$ .

In order to confirm if the hypothetical hemicylindrical diffusion takes place when redox activity happens at the microbands array, linear sweep voltammetry was conducted against 5 mM hexaamineruthenium(III) chloride at different scan rates ranging from 5 to 50  $\text{mV s}^{-1}$  using BE011 in comparison to 1 mm and 2 mm disc electrodes.

**Figure 4.23** shows the linear sweep voltammograms of the third-generation  $\mu$ BAE prototype, BE011, in comparison to two macrodisc electrodes. BE011 demonstrated microelectrode behaviour at low scan rates 5 and 10  $\text{mV s}^{-1}$  with a transition from microelectrode to macroelectrode behaviour between 10 – 15  $\text{mV s}^{-1}$ . Microelectrode behaviours were observed where at low scan rate, there was an establishment of a steady state current which was an indication of thickening of Nernst diffusion layer due to the depletion of hexaamineruthenium(III) species.

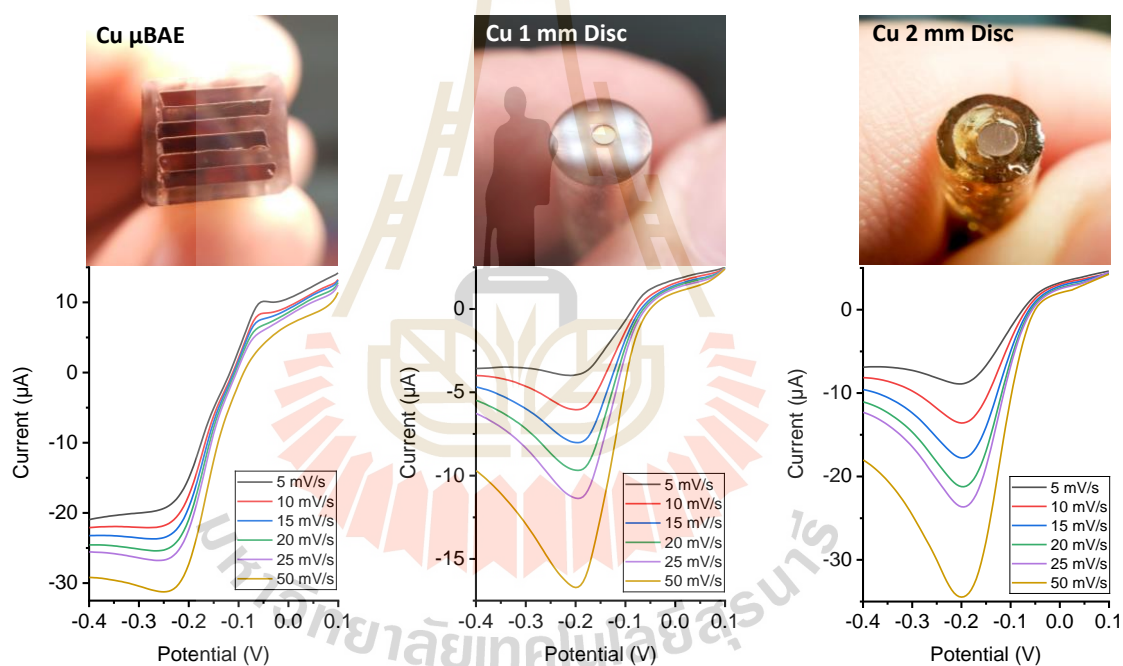


**Figure 4.23** The linear sweep voltammograms of a Cu microband array electrode ( $\mu$ BAE), a 1 mm disc and a 2 mm disc electrodes at various scan rates ranging from 5 to 50  $\text{mV s}^{-1}$  in 5 mM hexaamineruthenium(III) solution.

In comparison, no steady state current was established even at scan rate as low as 5  $\text{mV s}^{-1}$  for both 1 mm and 2 mm copper disc electrodes. This is an indication of a thickening of Nernst diffusion layer as hexaamineruthenium(III) species was



reduced and depleted. This reduction of species concentration was indicated by the drop of reductive current forming a reduction peak in the linear sweep voltammogram for both the macrodisc electrode tested.

#### 4.2.3 Detection of hydrogen peroxide

Hydrogen peroxide is the by-product of enzymatic activity of oxidase enzyme under aerated environment. Somasundrum *et al.* (1996) demonstrated the suitability of copper electrodes as the sensor for hydrogen peroxide detection by direct reduction using anodic amperometry mode.

In this study, the electrochemical performance of the copper microband array electrodes (BE002 and BE005) for the detection of hydrogen peroxide was evaluated in comparison to a normal disc electrode. This experiment was conducted in a bipotentiostat mode using a pocket-size Metrohm PSTAT.

Both BE002 and BE005 demonstrated higher sensitivity to hydrogen peroxide in comparison with a 2 mm disc electrode conducted in a simultaneous measurement using bipotentiostat mode. Amperometric traces for BE002 and 2 mm disc copper electrodes in **Figure 4.24** gave linear plots of reduction current against hydrogen peroxide concentration with  $R^2$  of 0.994 and 0.998, respectively. The sensitivity of BE002 was  $0.82 \mu\text{A } \mu\text{M}^{-1} \text{cm}^{-2}$ , thirteen times much higher than that of a 2 mm copper disc electrode at  $0.06 \mu\text{A } \mu\text{M}^{-1} \text{cm}^{-2}$ .

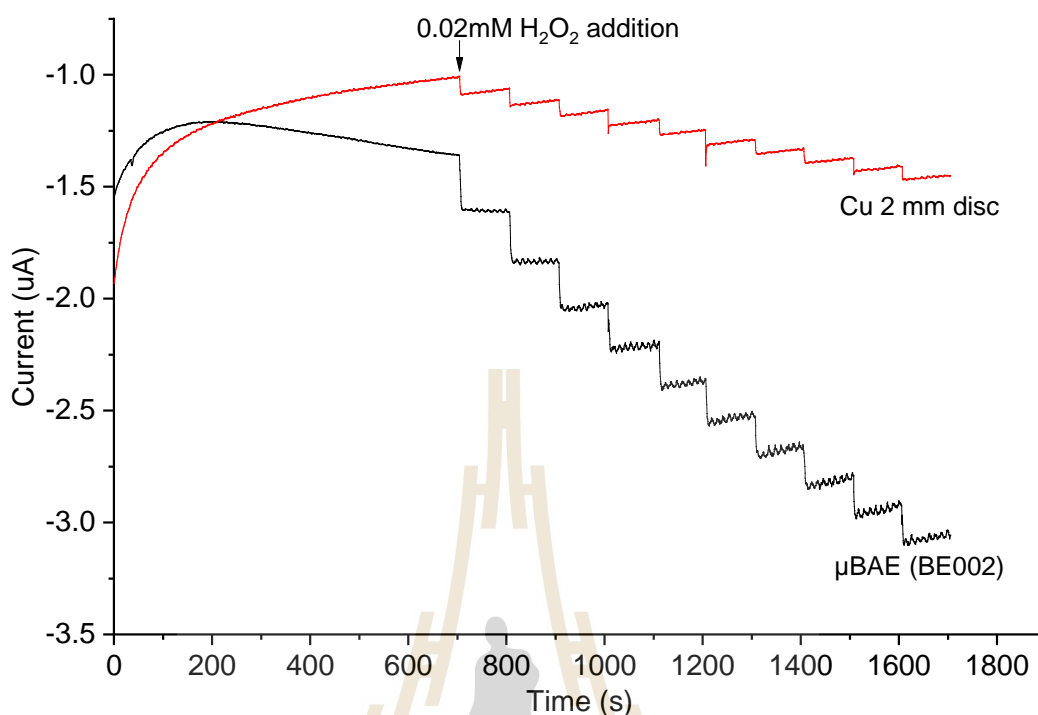


**Figure 4.24** Chronoamperometric traces of hydrogen peroxide response of copper  $\mu$ BAE BE002 and copper disc electrode in a bipotentiostat mode.

The triplicate amperometric traces of hydrogen peroxide calibration (see **Figure 4.25**) of the second generation prototype of  $\mu$ BAE, BE005 and 2 mm copper disc electrodes in bipotentiostat configuration produced similar responses with average current densities of  $0.6883$  and  $0.1272 \mu\text{A } \mu\text{M}^{-1} \text{cm}^{-2}$ , respectively as shown in **Table 4.3**.

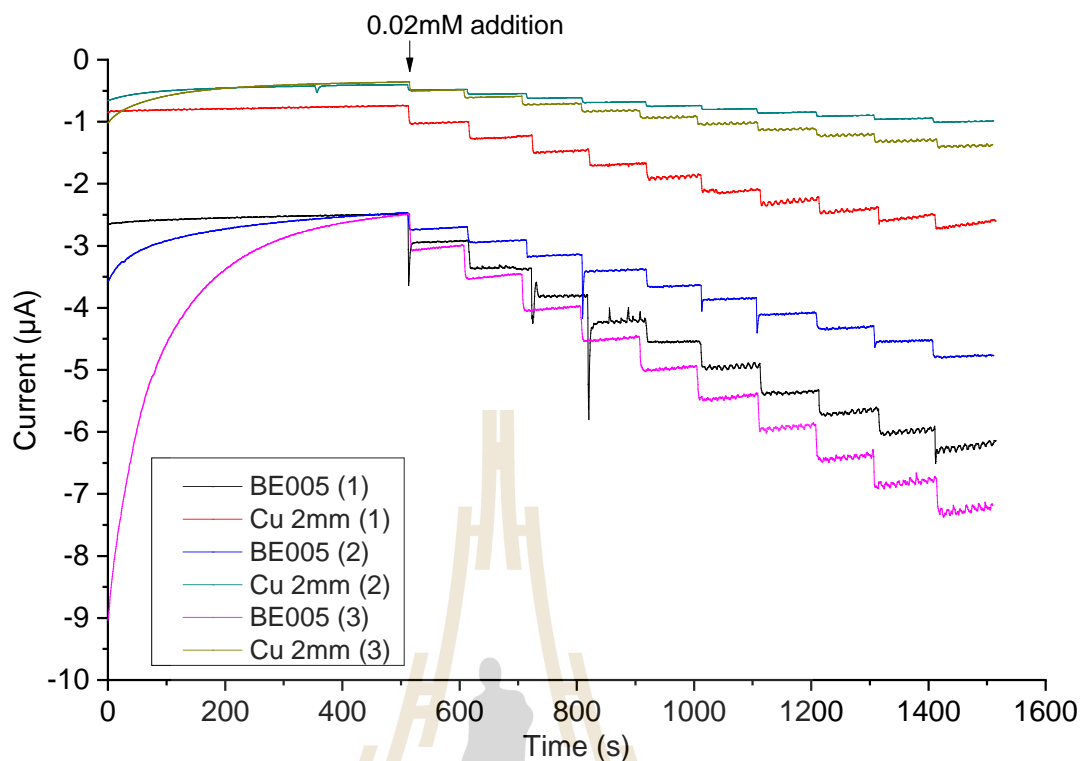


**Figure 4.25** Chronoamperometric traces of hydrogen peroxide response of copper  $\mu$ BAE BE005 and copper disc electrode in a bipotentiostat configuration.

**Table 4.3** Current density comparison of hydrogen peroxide calibration of copper disc and copper  $\mu$ BAE using amperometry in a bipotentiostat configuration.

Repetition	Cu 2 mm		Cu $\mu$ BAE (BE005)	
	Linearity $R^2$	Current density ( $\mu\text{A } \mu\text{M}^{-1} \text{cm}^{-2}$ )	Linearity $R^2$	Current density ( $\mu\text{A } \mu\text{M}^{-1} \text{cm}^{-2}$ )
1	0.995	0.2161	0.996	0.7217
2	0.995	0.0603	1.000	0.4378
3	0.997	0.1051	1.000	0.9055
Average		0.1272		0.6883

#### 4.2.4 Issues as a glucose biosensor

The higher sensitivity to hydrogen peroxide of BE005 indicated the possibility of development of an oxidase biosensor with higher sensitivity to a substrate analyte. This hypothesis was based on a previous report on the successful development of glucose oxidase biosensor on a 2 mm copper disc electrode made from domestic electric wire (Jaikaew *et al.*, 2016).

BE005 was polished according to the protocol described in 3.2. Two 50  $\mu\text{l}$  aliquots of equal volume mixture of 20  $\text{mg ml}^{-1}$  GOx and 10% Nafion were dropped and dried consequently on the electrode surface. The biosensor was then left in stirring 0.1M phosphate buffer solution for 15 min for acclimatisation before it was evaluated for its capability in glucose quantification.

**Figure 4.26** shows an amperometric trace of this glucose oxidase biosensor held at  $-0.15$  V in a series of glucose concentration addition. Initially, the sensor established steady-state current at  $-5.6$   $\mu\text{A}$ , however, the cathodic background current dropped upon addition of glucose at 500s with subsequent glucose additions at an interval of 200 s. The plot of current decrement against glucose (**Figure 4.27**) demonstrated a curve with a linear relationship up to 2.0 mM. This decrement of cathodic current reached saturation at glucose concentration over 2.2 mM where the glucose biosensor gave no response to further addition of glucose concentration. The slope of the linear region of the plot is expected to be correlated to the rate of enzymatic activity that generates the redox active hydrogen peroxide.

The background current was suspected to be from the reduction of dissolved oxygen in the electrolyte solution. In order to confirm this hypothesis, nitrogen purging for deaeration was performed to observe the change of background

current. Amperometric trace in **Figure 4.28** showed that the cathodic background current reduced significantly from  $-6.5$  to  $-0.1 \mu\text{A}$  immediately after the purging of nitrogen was applied. This effect started to disappear as soon as the purging stopped and cathodic current increased slowly back to approximately the current level before deaeration. The slow return of cathodic current was an indication of slow dissolution of oxygen in the surrounding into the electrolyte. This also confirmed that the background current was contributed by the dissolved oxygen in the electrolyte solution.

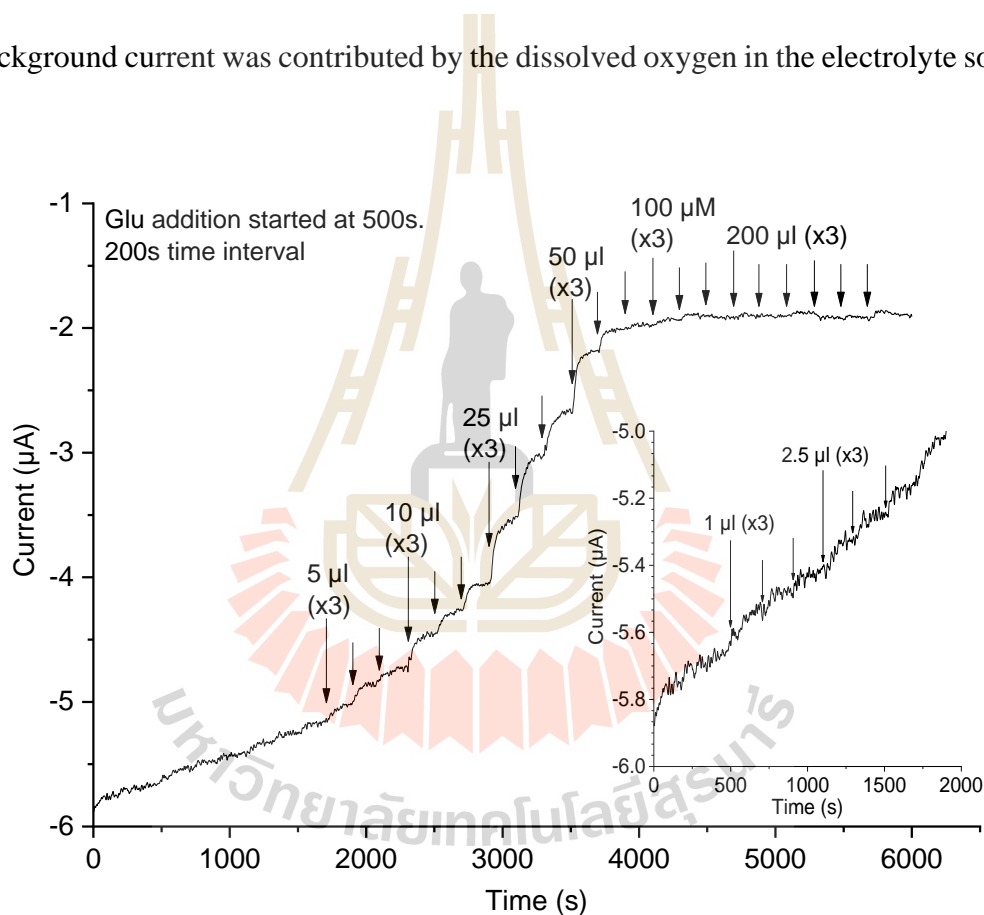


**Figure 4.26** Amperometric response of glucose detection with glucose oxidase biosensor on BE005.

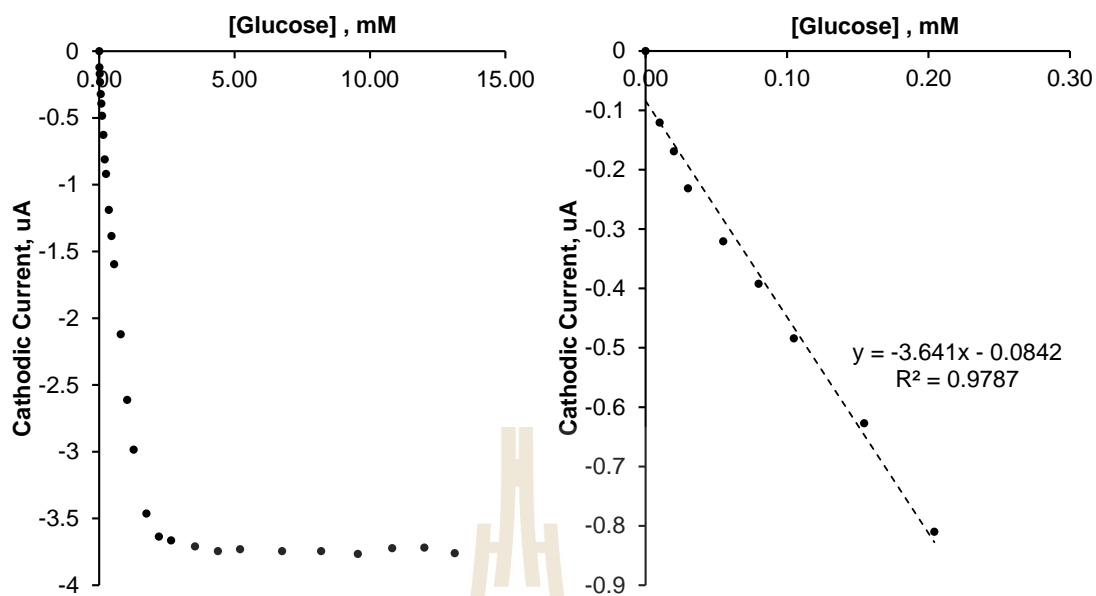


**Figure 4.27** Plot of cathodic current against glucose concentration.

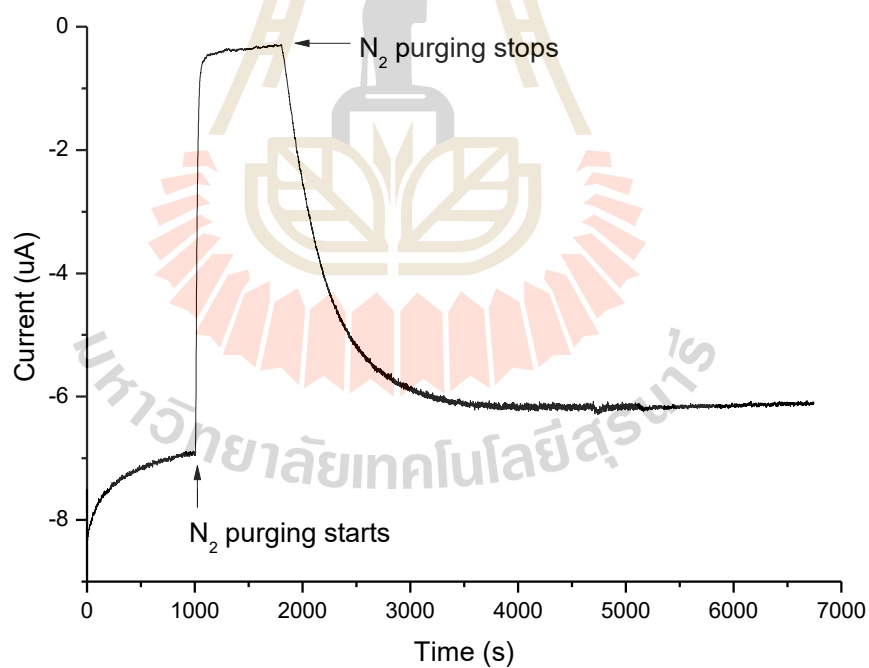


**Figure 4.28** Amperometric trace of a glucose oxidase sensor on a  $\mu$ BAE (BE005) platform with nitrogen gas purged during 1000 – 2000 s.

The confirmation of the source of background current had led to the understanding of what could happen in the Nafion polymer layer coated on a  $\mu$ BAE. Unlike a copper disc electrode, where all glucose oxidase and Nafion mixture coated were on top of the electrode active surface, in the case of  $\mu$ BAE, only very few GOx molecules were actually immobilised directly on the copper microband surface. This means that despite the enzymatic activity of glucose oxidase might have taken place actively in the presence of glucose and hydrogen peroxide generation happened in the polymer layer, very few of these hydrogen peroxide molecules were at the close vicinity of the copper microbands. Since the mass transportation of the neutral hydrogen peroxide molecule to the copper microband in the polymer layer was solely based on diffusion, a very limited amount of hydrogen peroxide molecule could have impacted and reduced at the cathodic copper microband surface. Most of the hydrogen peroxide molecules could have diffused away from the copper microbands.

Meanwhile, due to massive consumption of oxygen by the enzymatic activity of glucose oxidase over the whole electrode surface, a reduction of background cathodic current ( $I_{\text{red}}$ ) from the reduction of dissolved oxygen was observed instead. Eventually, when a new equilibrium between the transport of dissolved oxygen and glucose into the polymer layer as well as the consumption of oxygen for the regeneration of glucose oxidase was established, the current stabilised. This apparent faradaic current was the summation of cathodic current from the reduction of dissolved oxygen and hydrogen peroxide generated. This was observed as the individual amperometric step for each addition of glucose concentration shown in **Figure 4.26**.

On the other hand, most hydrogen peroxide molecules generated are able to diffuse to and reduced at the copper disc electrode (as in **Figure 4.29**). The gain

of cathodic current from hydrogen peroxide thus surpasses the drop in cathodic current from dissolved oxygen and results in an overall gain of cathodic current.

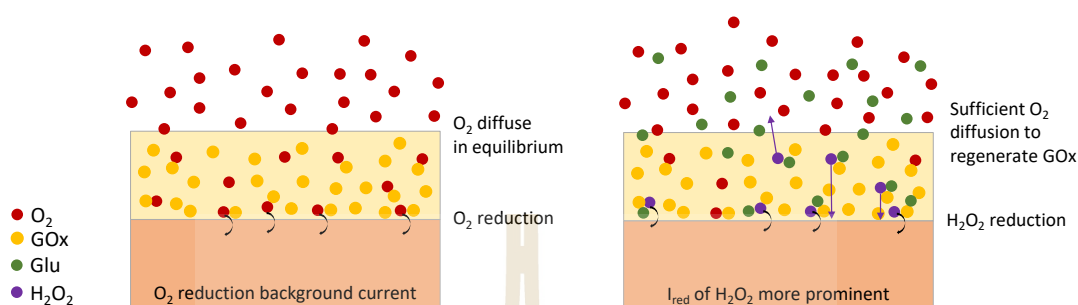


**Figure 4.29** Illustration of diffusion of molecules at the immobilised glucose oxidase layer over the surface of a macroelectrode.

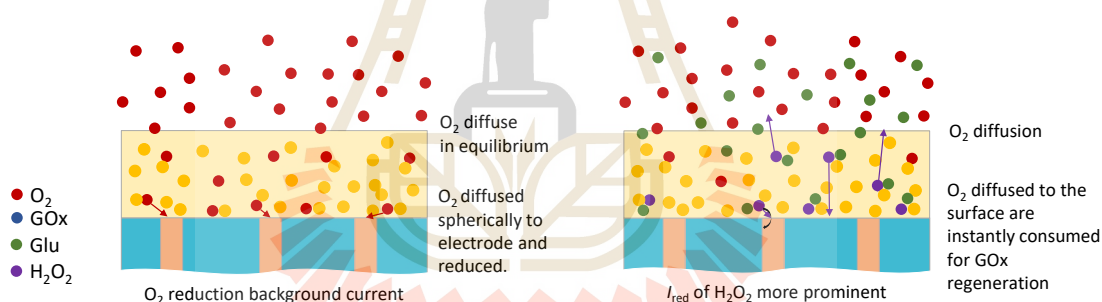


**Figure 4.30** Illustration of diffusion of molecules at the immobilised glucose oxidase layer over the surface of copper microband array electrode.

**Figure 4.30** illustrates that glucose oxidase immobilisation, by coating a mixture of GOx and Nafion, was masking the microband array. This means that the big GOx biosensor surface was seeing the analyte glucose in a macroelectrode manner. Diffusion of glucose from the bulk solution to the enzyme was driven by planar diffusion, thus losing the beneficial hemicylindrical diffusion properties of the microbands. Besides, the hydrogen peroxide molecules generated within the enzyme



film have less probability of reaching the relatively small area of the copper microband array. Meanwhile, the effect of global reduction of dissolved oxygen in the GOx film due to the regeneration of the enzyme were more prominent than the contribution of cathodic current from hydrogen peroxide generation. Thus, a step-like decrement of background current of dissolved oxygen as in **Figure 4.26** was observed whenever an aliquot of standard glucose solution was added.

Localised immobilisation was thus attempted by first depositing cathodic electrodeposition paint along the microbands (as in **Figure 4.31**) and enzyme molecules were later chemically fixed onto the paint by a cross-linker. However, the polymer did not adhere to the surface firmly enough and disappear after being soaked in 0.1 M phosphate buffer solution pH 7 for 6 hr.



**Figure 4.31** Cathodic paint deposited along the copper microbands.

#### 4.2.5 Solution biosensing of glucose

Despite having difficulty as discussed in **4.2.4** for the preparation of biosensor using  $\mu$ BAE by immobilising glucose oxidase onto the electrode surface,  $\mu$ BAE showed possibility of being utilised as a sensor for biosensing in solution or enzymatic activity monitoring in solution. **Figure 4.32** showed the amperometric trace

of a series of 25, 50, 100 and 200  $\mu\text{l}$  of 10 mM glucose additions at 500 s intervals into a beaker containing 5 ml of 0.5  $\mu\text{M}$  glucose oxidase recorded using a  $\mu\text{BAE}$  (BE011) held at  $-0.15\text{ V}$ .

The initial additions of glucose solution gave a series of step-like current responses within 500 s after each addition. This showed that the glucose added was fully converted into gluconolactone with hydrogen peroxide as the by-product which was reduced at the  $\mu\text{BAE}$ . The full conversion of glucose was indicated by the constant current which represented the constant hydrogen peroxide concentration in the test solution. It was observed with the first addition of 200  $\mu\text{l}$  of 10 mM glucose, the cathodic current increased linearly and did not reach a constant current indicating a constant generation of hydrogen peroxide during throughout the 500 s. This showed that the enzyme molecules were at a maximum rate of conversion and required a longer time to fully convert all the glucose molecules added. The maximum rate of conversion of glucose oxidase in the solution was also limited by the availability of dissolved oxygen for enzyme regeneration.

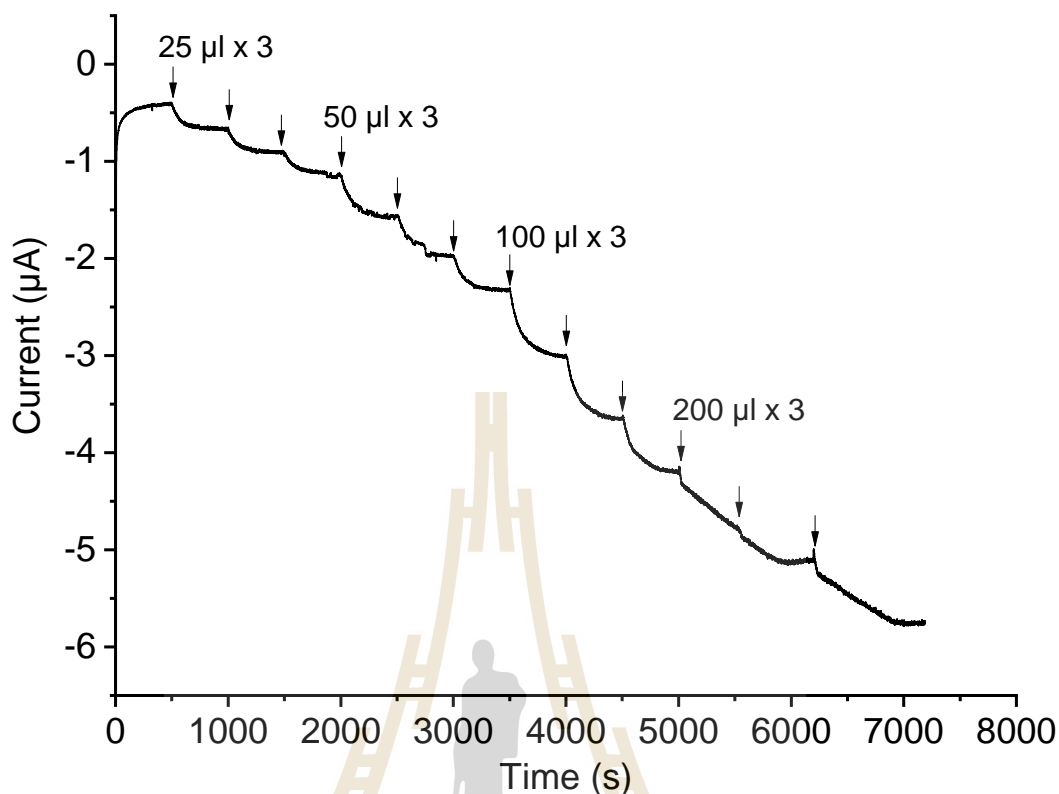


**Figure 4.32** Amperometric trace of a series of glucose additions into 5 ml of 0.5  $\mu\text{M}$  glucose oxidase solution using  $\mu\text{BAE}$  (BE011) as the sensor for enzymatically produced hydrogen peroxide.

**Figure 4.33** showed the calibration plot of current against glucose concentration added into the 5 ml of 0.5  $\mu\text{M}$  glucose oxidase solution. The plot demonstrated a linear relationship between the current and glucose concentration with a linear regression of 0.9964. The good linearity showed that the  $\mu\text{BAE}$  was able to measure glucose indirectly by detecting the by-product hydrogen peroxide from the enzymatic activity of glucose oxidase.

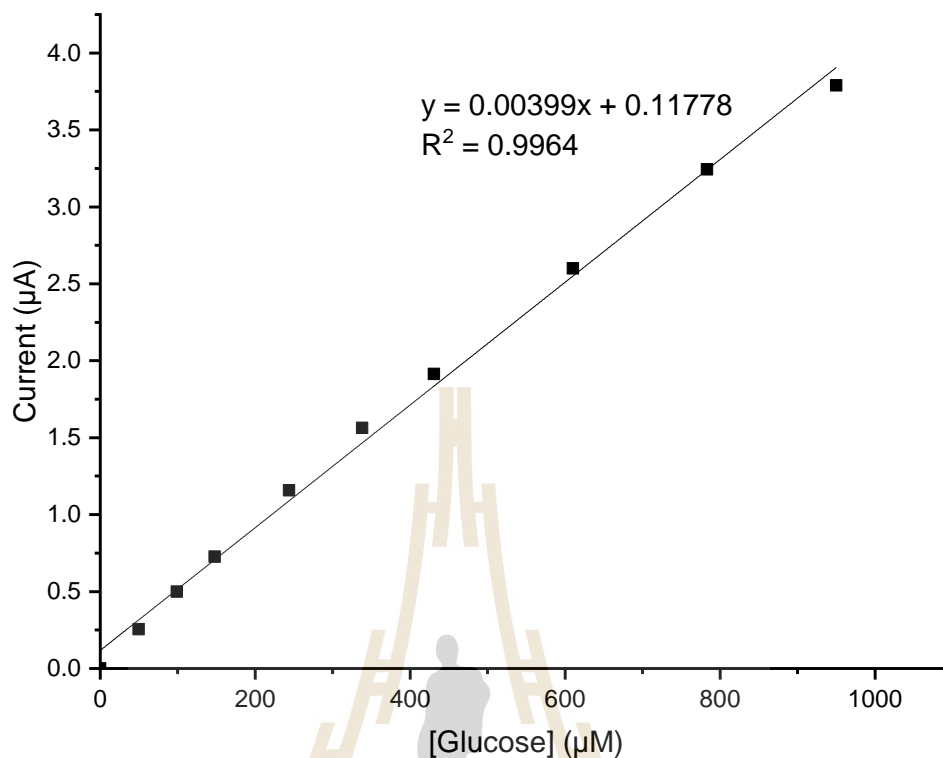


**Figure 4.33** Calibration curve of glucose in 5 ml of 0.5 µM glucose oxidase solution using µBAE (BE011) as the sensor for enzymatically produced hydrogen peroxide.

#### 4.2.6 Detection of dopamine

Dopamine is a catecholamine neurotransmitter which transfers message in the central nervous system (Xu *et al.*, 2014). Electrochemical sensor using copper oxide nano-rice, prepared by the facile precipitation method, for simultaneous determination of dopamine and uric acid by amperometry and differential pulse voltammetry techniques were reported earlier by Krishnamoorthy *et al.* (2018). Hence, Cu µBAE was tested for its ability to detect dopamine.

The third generation µBAE was first treated with 20 cyclic voltammetry scans from 0.0 to 0.5 V (see **Figure 4.34**) for Cu(II) oxide formation at

the copper surface (Drogowska *et al.*, 1992). The  $\mu$ BAE electrode was then used for the detection of dopamine by differential pulse voltammetry. **Figure 4.36** shows the plot of oxidation peak current against concentration extracted from the voltammograms in **Figure 4.35**. The  $\mu$ BAE gave a linear response for dopamine concentration ranged from 0.2 to 2.29 mM with a linear regression  $R^2$  of 0.9899. The sensitivity of  $\mu$ BAE to dopamine was  $312.02 \mu\text{A mM}^{-1} \text{cm}^{-2}$  with RSD 8.38% in comparison to  $237.04 \mu\text{A mM}^{-1} \text{cm}^{-2}$  with RSD 12.12% of a 2 mm copper disc electrode.

This indicated the suitability of copper  $\mu$ BAE for the measurement of dopamine with sample concentration within the dynamic range stated above. More importantly, this dopamine along with hydrogen peroxide tests proved that the metal microband array electrode design is practical with improved analytical sensitivity.

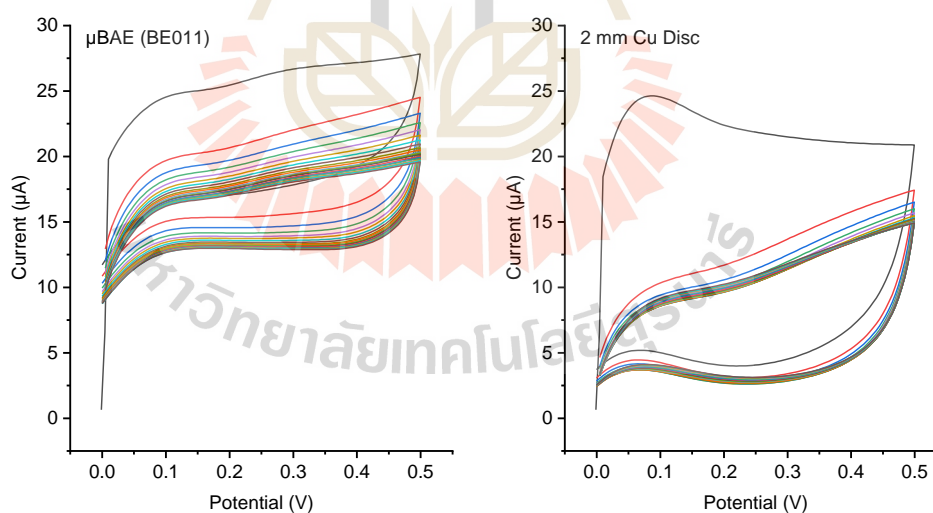


**Figure 4.34** Cyclic voltammograms (20 scans,  $S_{\text{rate}} 50\text{mV s}^{-1}$ , step size 5 mV) of  $\mu$ BAE (BE011) and 2 mm copper disc in 0.1 M phosphate buffer (pH7.0) before used for detection of dopamine.

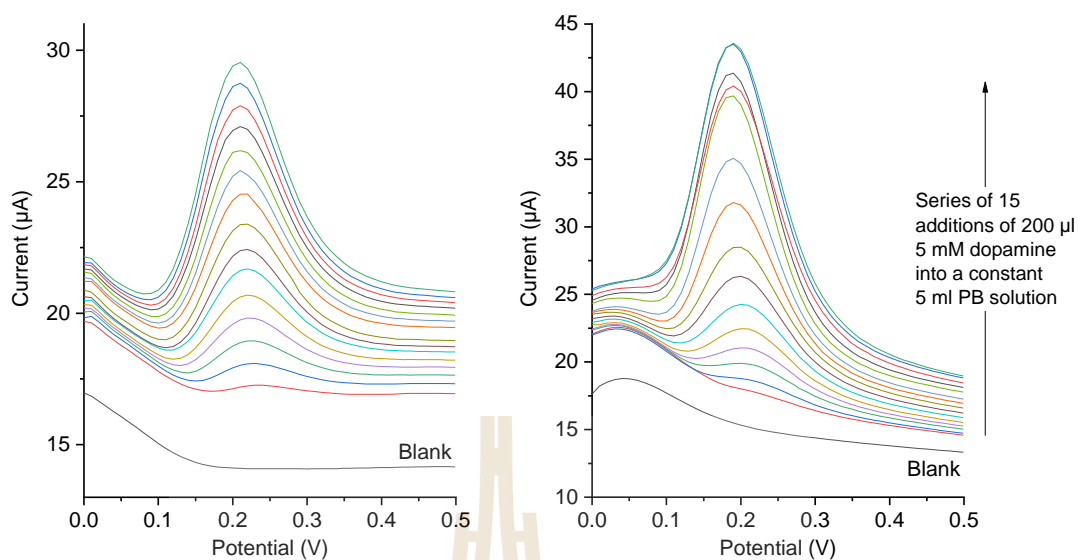


**Figure 4.35** Differential pulse voltammograms of dopamine with increasing concentration from 0.2 to 2.29 mM using  $\mu$ BAE BE011 and 2 mm copper disc.

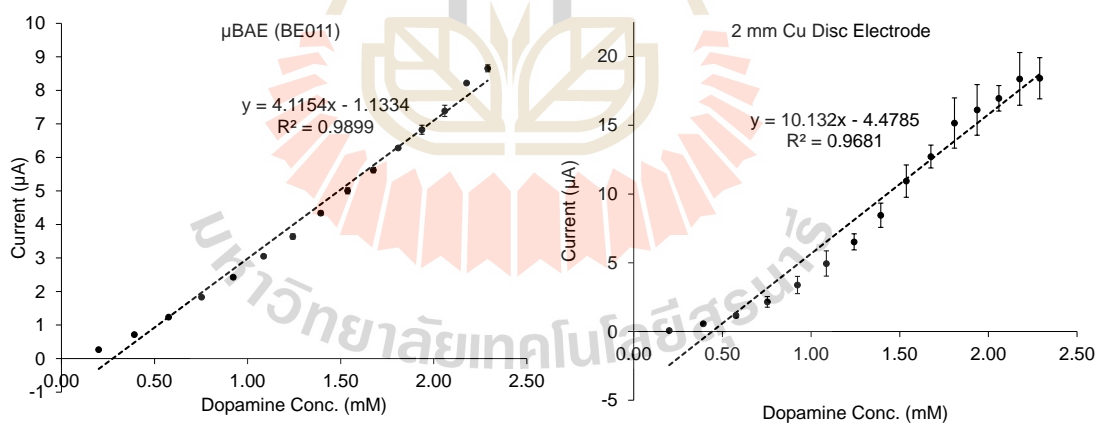


**Figure 4.36** Calibration curves of dopamine in 0.1 M phosphate buffer (pH 7.0) using  $\mu$ BAE (BE011) and copper 2 mm disc electrode.

These findings showed that a microband array electrode can be constructed with simple lamination of metal foil with micrometre thickness in between

acrylic plastic plates with super glue as the adhesive. The resultant microband array electrode demonstrated microelectrode properties at a scan rate of  $10 \text{ mV s}^{-1}$  or lower. However, the accurate enzyme immobilisation onto the microband was still a challenge to preserve the microelectrode properties. Nevertheless, the  $\mu$ BAE demonstrated usability as a sensing platform for solution biosensing and direct measurement of dopamine.

### **4.3 Electrochemical immunosensor for quantification of oxytocin**

The idea of developing a test method for oxytocin was initially driven by a problem faced by one of our collaborator Professor Dr. Mike Ludwig from the University of Edinburgh. Prof. Ludwig is involving in neuro behaviour studies related to hormonal oxytocin release into brain fluid/dialysate from rat at an extremely low picomolar level. He was all the while using GCMS as the quantification method and was thinking of switching to a greener, cheaper and easier method for mass quantification that could be applied at the site of animal testing. His idea was in line with the concept of this thesis and was therefore taken up as a challenge to develop a method using electrochemistry as the detection scheme for the pM hormone target screening.

In section **4.1**, oxytocin detection and quantification were tested via direct electrochemical detection with a boron-doped diamond disc electrode. However, the detection level, though inline with the performance level of similar published voltammetric approaches, could only reach a lowest level of detection at  $58.6 \mu\text{M}$ .

A femtomolar detection of biomolecule by electrochemical immunosensing was previously reported in several scientific reports. Chunglok *et al.* (2011) for instance,

demonstrated that magnetic-bound sandwich immunoreaction in combination with utilisation of MB-MWCNT-Ab as the current amplifying redox label allowed the detection of mouse IgG at  $5 \text{ fg ml}^{-1}$  level. Attempts were made to exploit the possibility of using MB-MWCNT-Ab for electrochemical immunosensing of oxytocin at ultralow level. Carbon screen printed electrodes were used as the sensitive electroanalytical platform for electrochemical immunosensor preparation. The required MB-MWCNT and MB-MWCNT-Ab conjugates were prepared according to the procedure specified in 3.1.3.

#### 4.3.1 Affinity of MB-MWCNT with blocking material

Blocking against the adsorption of finally detected redox label is one of the important steps in immunosensor preparation. The purpose is to block the free space on the electrode surface so to remove or reduce the effect of non-specific interaction of analyte and detection molecule with the surface. Initial adaptation of sensor preparation showed indifference between blank and standard oxytocin solutions. This observation was suspected to be a result of non-specific adsorption of MB-MWCNT on the blocking molecule BSA.

In order to confirm this non-specific interaction between MB-MWCNT and BSA, three sets of SPEs coated respectively with  $5 \mu\text{l}$  of 0, 0.1 and 1% BSA in PBS (0.1M KCl) for 20 min were exposed to  $7.5 \mu\text{l}$  of  $1 \text{ mg ml}^{-1}$  MW-MWCNT conjugate in 0.1 M PBS (0.1 M KCl) for 60 min. Washing was done with 3 times 1 ml of 0.05% PBST followed by 2 times 1 ml 0.1 M PBS (0.1M KCl) before the electrochemical measurement was done.

**Figure 4.37** shows that SPEs coated with 0.1 and 1% BSA gave a significantly higher signal at 277.0 and 258.0 nA, respectively, as compared to 206.1



nA given by SPEs coated with no BSA. This result signifies that MB-MWCNT has higher affinity to BSA coated SPE, compared to the SPEs coated with no BSA.

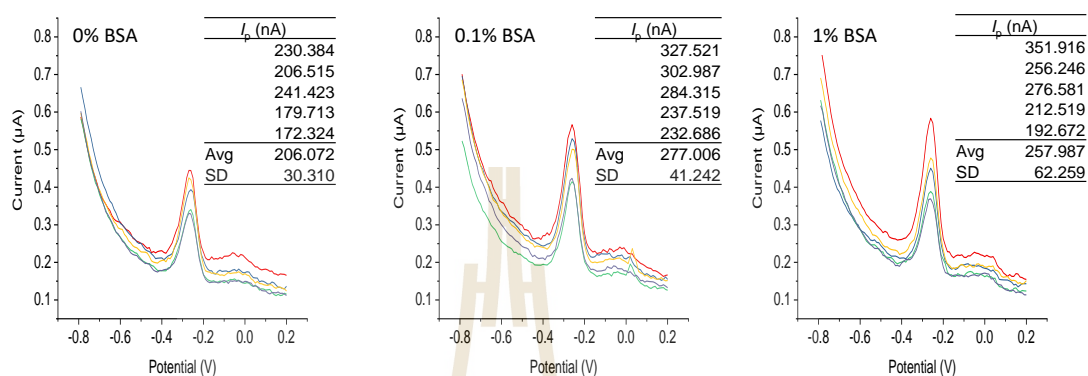


**Figure 4.37** Differential pulsed voltammograms for the application of 0, 0.1 and 1% BSA for the blocking of SPE surface washed by flowing 3 times 1 ml of 0.05% PBST.

There was no significant improvement even when the washing condition was changed to soaking the SPEs in 2 ml of 0.05% PBST for 10 min followed by a 1 ml 2% PBST and 2 times 1 ml 0.1 M PBS (0.1 M KCl) flushes. The result in **Figure 4.38** showed that the carbon material of the SPE itself has an affinity to the MB-MWCNT conjugate. An extreme soaking with 2 ml 2% PBST for 10 min also showed a similar result as presented in **Figure 4.39**.

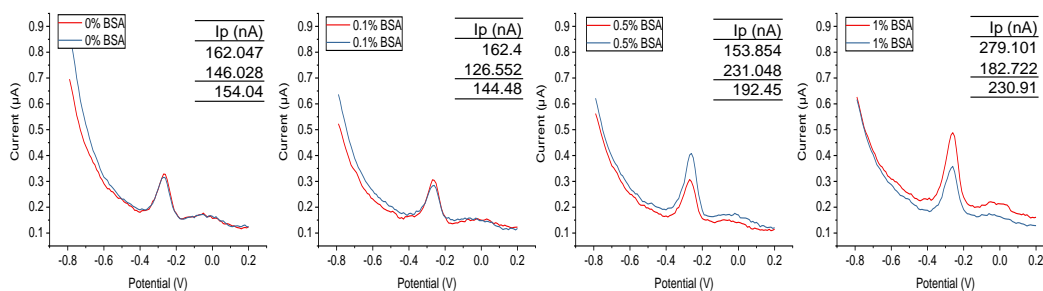


**Figure 4.38** Differential pulsed voltammograms for the application of 0, 0.1, 0.5 and 1% BSA for the blocking of SPE surface and later soaked in 2 ml 0.05% PBST for 10 min.

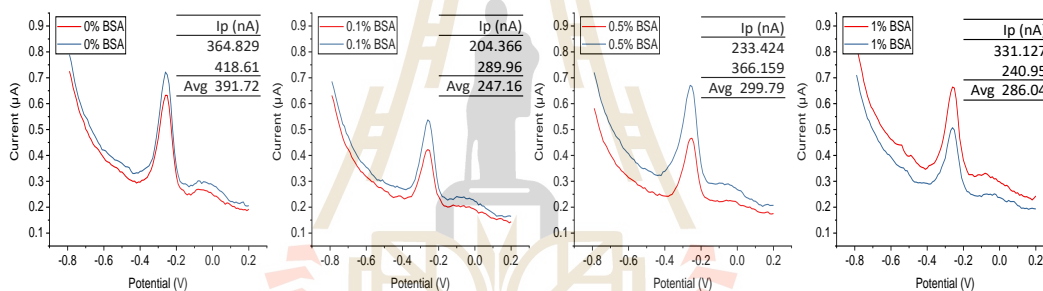


**Figure 4.39** Differential pulsed voltammograms for the application of 0, 0.1, 0.5 and 1% BSA for the blocking of SPE surface and later soaked in 2 ml 2% PBST for 10 min.

Another compound casein was evaluated for its appropriateness as a blocking molecule for this immunosensor. The result shown in **Figure 4.40** gave a similar trend to that of BSA. However, in this experiment, the soaking solution turned bluish after 10 min indicating detachment of methylene molecules from the electroactive label MB-MWCNT conjugate during the soaking process. The current responses of these attempts were summarised in a bar chart as shown in **Figure 4.41**.

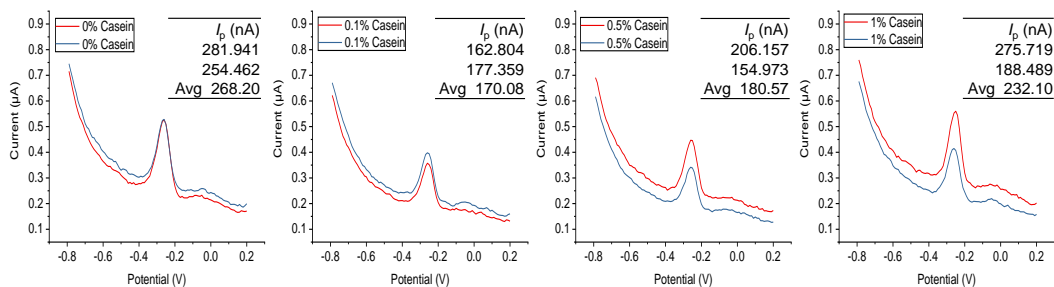


**Figure 4.40** Differential pulsed voltammograms for the application of 0, 0.1, 0.5 and 1% casein for the blocking of SPE surface and later soaked in 2 ml 2% PBST for 10 min.

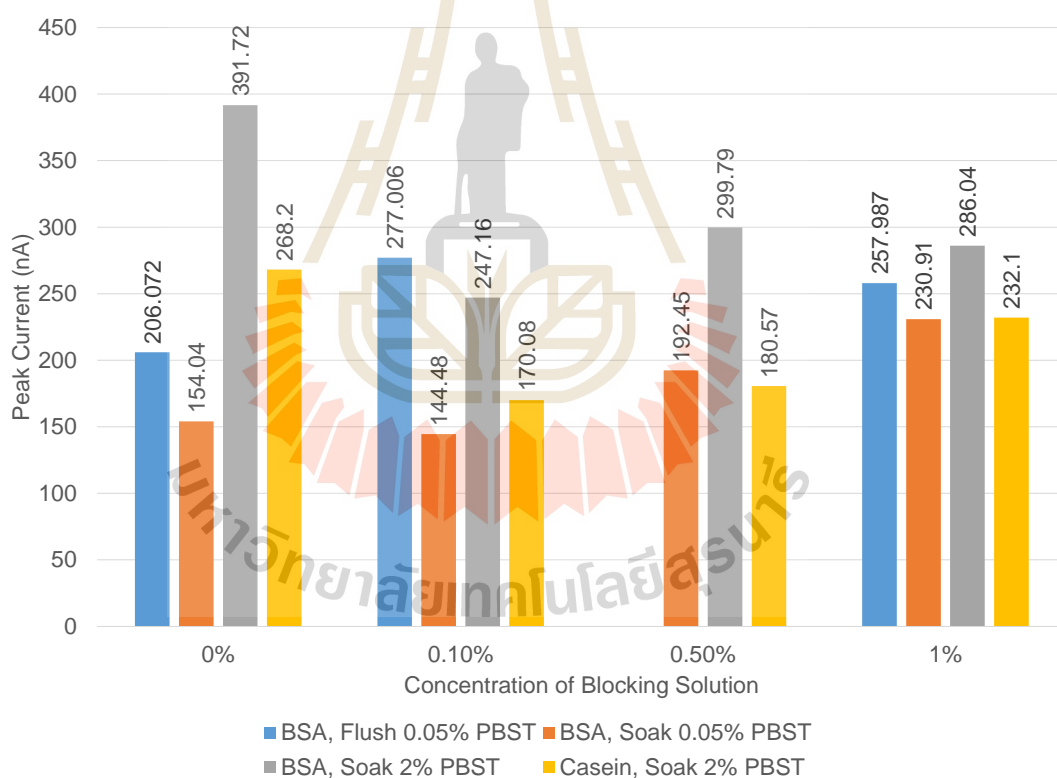


**Figure 4.41** Peak current summary of various blocking and washing conditions from **Figure 4.37**, **Figure 4.38**, **Figure 4.39** and **Figure 4.40**.

The non-specific interaction of bovine serum albumin and the MB-MWCNT could be due to the electrostatic charge attraction, since BSA is a negatively charged protein while methylene blue is a positively charged molecule. It was also attempted to reduce this electrostatic attraction by coating the MB-MWCNT conjugate with 1% BSA so that the overall positive charge of the conjugate could be reduced. Nonetheless, the resulting DPVs in **Figure 4.42** showed that there is no significant reduction in the non-specific interaction between BSA coated on the SPE and the MB-MWCNT coated with BSA.

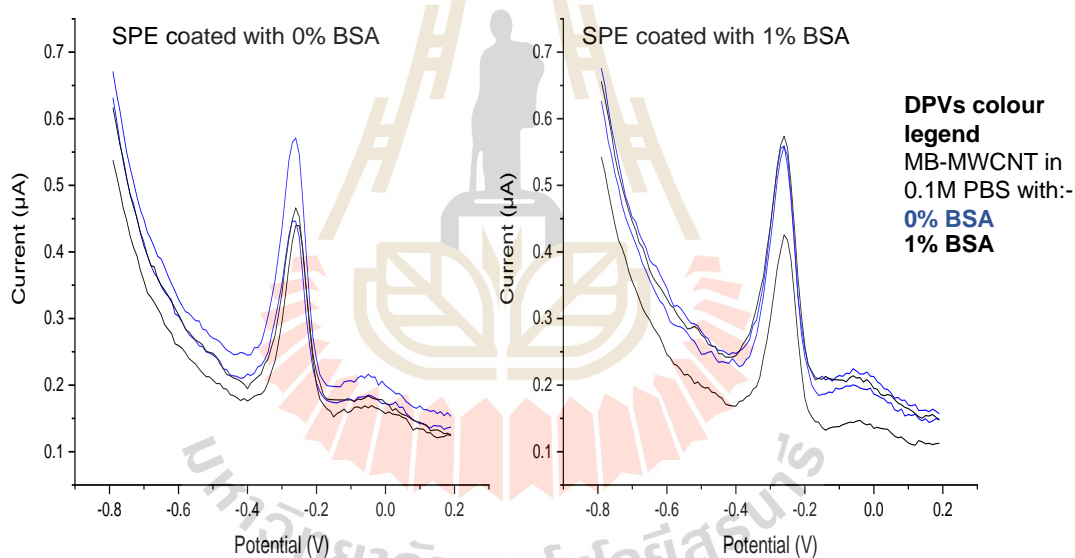


**Figure 4.42** Differential pulsed voltammograms of the effect of coating redox label MB-MWCNT with 1% BSA.

#### 4.3.2 Sandwich immunoassay

Duplicate differential pulsed voltammetric results of 0, 0.1 and 5  $\mu\text{g ml}^{-1}$  oxytocin in different conditions were shown in **Figure 4.43**. Antioxytocin was dropped onto the working electrode for adsorption at a 10:1000 dilution factor. Direct

adsorption of oxytocin onto the carbon SPE gave the lowest signal indicating no significant attachment of oxytocin onto the SPE. In the case where no capture antibody coated on the surface of SPE, but the surface was blocked with BSA, DPV signal was seen even with no target oxytocin. When this was compared with the full sandwich experiment, the blank signals were similar to sensors with no capture antibody. These blank signals were due to the non-specific interaction between the MB-MWCNT label and the blocking BSA molecules as the effect explained in section **4.3.1**.



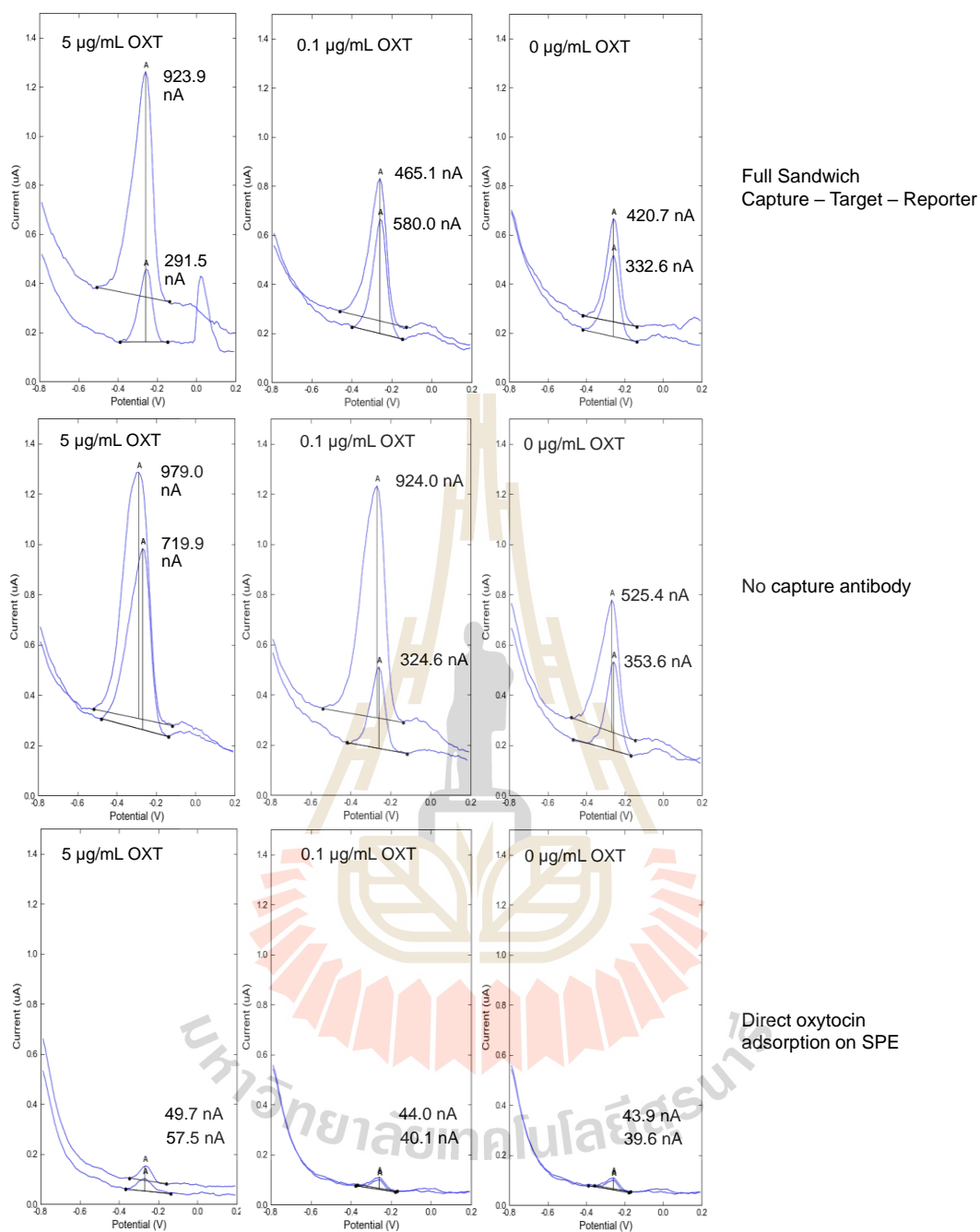


**Figure 4.43** Differential pulsed voltammograms of oxytocin detection with various conditions.

## CHAPTER V

### CONCLUSIONS

This study has successfully developed a home-made three-electrode miniaturised electrochemical cell capable of performing good-quality electroanalysis in 30 – 60  $\mu$ l sample volume. The Pt-T minicell serves as both the counter electrode and the sample container. In a three-electrode configuration, the working electrode was held vertically face up. Pt-T minicell was then rested on the electrode surface and the miniaturised reference electrode lowered down into the top opening of the minicell.

The described Pt-T mini-cell is well suited to routine electroanalysis in general laboratories, especially those with low budgets and no access to high-end facilities for sensor fabrication. The mini-cell is also a good option for analytes of low sample availability, high molecular weight, high toxicity or low concentration that cannot be further diluted for assay in conventional beaker-type cells. Additionally, the mini-cell facilitates waste-reducing and chemical-sparing small-volume 'green' analytical work.

The general applicability of the mini-cell was assessed with a series of electrochemical test runs with different electrodes and analytes. Disk-shaped Pt, Au, boron-doped diamond and glassy carbon macroelectrodes, a rod-shaped pencil lead electrode and a Pt disk microelectrode all produced normal hexacyanoferrate(III) voltammograms, validating the general electrode operability. The good concentration-dependence relationship demonstrated for drugs, hormone, antioxidant and bioassay redox tag voltammetry and accurate substrate estimation with a glucose biosensor

verified the wide analyte suitability of the proposed Pt-T mini cell, while the near-ideal recovery rates during paracetamol assays in the adapted standard addition mode gave a clear indication of the potential of mini-cell operation for quantitative electroanalysis.

Accordingly, the device is well suited to routine electroanalysis in general and especially to use in laboratories with low budgets and no access to high-end facilities for sensor manufacture and manipulation. This minicell is especially important for samples with low sample availability, low concentrations that cannot be subjected to further dilution, as required in conventional beaker-type cells, of high molecular weight or of high toxicity. It not only enables processing of samples with these properties, but also facilitates waste-reducing and chemical-saving small-volume 'green' analytical chemistry work. This is especially important for samples or analytes that are hazardous to the operator and the environment.

Thus, this microlitre volume Pt-T minicell is recommended as a 'green' replacement for the conventional, millilitre volume beaker-type electrochemical cell. More importantly it can be reused countlessly. Thus, this minicell can be viewed as a cotton bag analogue which is an environmental-friendly alternative to plastic shopping bags. With its simplicity of fabrication and operation, low cost and wide functionality, daily green voltammetry practice is no longer a question of possibility but a matter of willingness to change habits and adapt the design in routine laboratory trials.

The second part of this study successfully developed a copper microbands array electrode ( $\mu$ BAE) using cheap materials, i.e. copper foil, acrylic plate and super glue. The third generation  $\mu$ BAE was made by sandwiching a copper foil continuously in between acrylic plates forming seven continuous parallel bands. The single band of



this copper microband array electrode had a thickness of 28  $\mu\text{m}$  estimated from the scanning electron microscopic images.

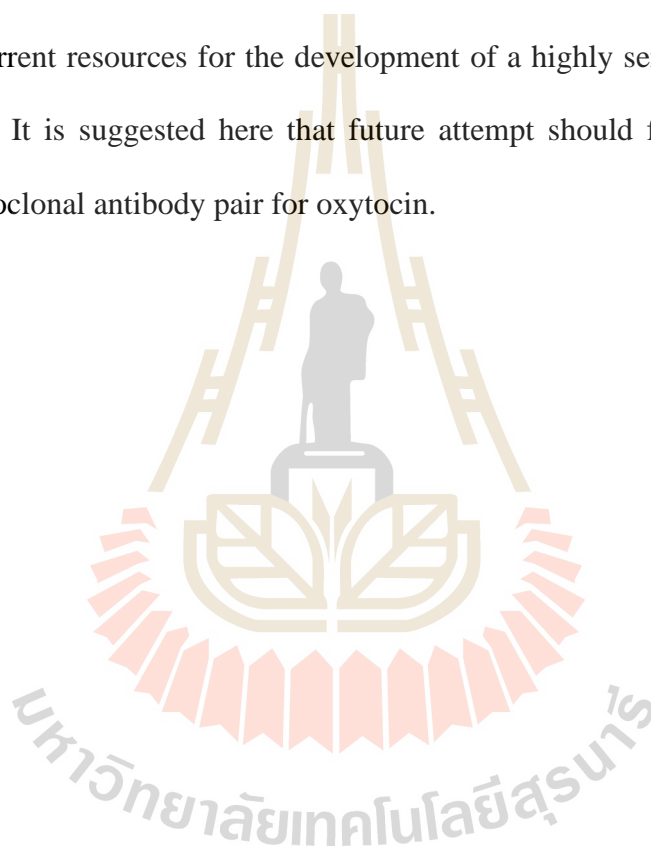
This copper  $\mu\text{BAE}$  demonstrated microelectrode behaviour with a transition into macroelectrode behaviour at a scan rate between 10 – 15  $\text{mV s}^{-1}$ , observed in linear sweep voltammetry against 5 mM hexaamineruthenium(III) chloride. This microelectrode behaviour suggested that analytes might be transported to the microbands in a hemispherical diffusion mode. This more effective delivery of analyte also led to a higher current density and sensitivity for hydrogen peroxide and dopamine detection in comparison to a macro disc electrode. The use of this  $\mu\text{BAE}$  as a platform for biosensor preparation is still a challenge as precise immobilisation of bioactive molecules on these microscale bands requires further research. However, the electrode has demonstrated a high possibility in an area like localised exocytosis, where for instance, dopamine is the major analyte.

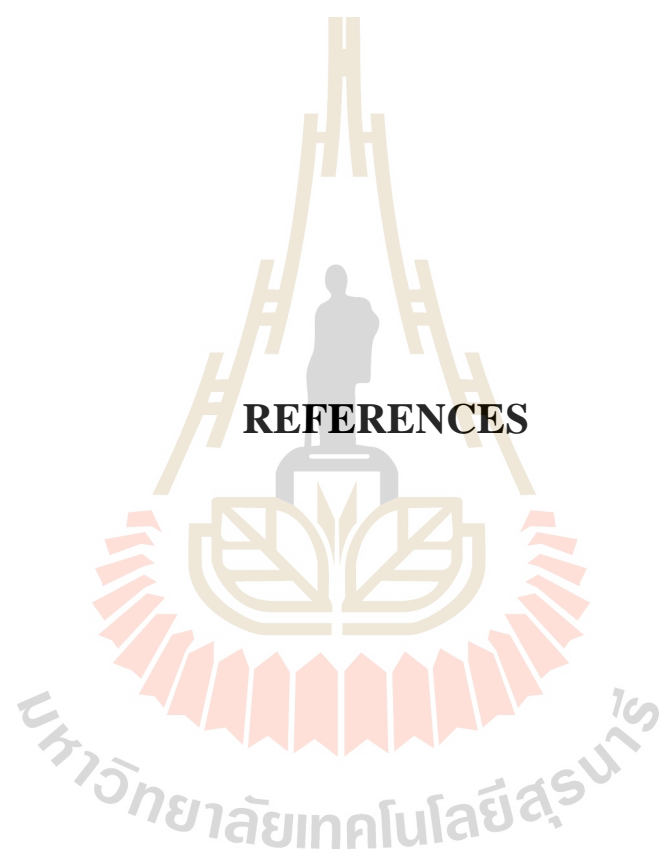
The third part of this study was the most challenging task, as the target hormones oxytocin has an ultralow concentration at 1 pM level in real rat brain dialysate. The initial attempt for the detection of oxytocin with a commercially purchased boron-doped diamond gave a detection limit of 58.6  $\mu\text{M}$  which is about 60,000 times higher than the target concentration.

The strategy was then switched to electrochemical immunosensing with a signal amplifier which was reportedly successful for some large target protein at femtomolar level. It was expected that a simple adoption of the existing method with minor tweaks would enable the detection of oxytocin at picomolar level.

However, unlike the successful cases, oxytocin is a small peptide with only 9 amino acid moieties, which has fewer binding sites for the sandwich reaction. The

antibodies used for both capture and detection antibodies were the same polyclonal antibody. This can result in a competition of binding side and led to a less effective sandwich reaction. The lack of a highly confirmed antibody pair for oxytocin for sandwich immunoassay resulted in a low analytical signal from oxytocin. Nonetheless, the blocking molecules, i.e. BSA and casein, showed non-specific interaction with the signal magnifier MB-MWCNT leading to a high blank signal which further limited the use of the current resources for the development of a highly sensitive immunosensor for oxytocin. It is suggested here that future attempt should first identify a highly specific monoclonal antibody pair for oxytocin.





**REFERENCES**

## REFERENCES

- Anastas, P. T., and Warner, J. C. (1998). *Green Chemistry: Theory and Practice*. Oxford: Oxford University Press.
- Arrigoni, O., and De Tullio, M. C. (2002). Ascorbic Acid: Much More Than Just an Antioxidant. **Biochimica et Biophysica Acta (BBA) - General Subjects**, 1569(1): 1-9.
- Arya, S. K., and Bhansali, S. (2011). Lung Cancer and Its Early Detection Using Biomarker-Based Biosensors. **Chemical Reviews**, 111(11): 6783-6809.
- Asai, K., Ivandini, T. A., and Einaga, Y. (2016). Continuous and Selective Measurement of Oxytocin and Vasopressin Using Boron-Doped Diamond Electrodes. **Scientific Reports**, 6: 32429.
- Atighilorestani, M., and Brolo, A. G. (2017). Recessed Gold Nanoring–Ring Microarray Electrodes. **Analytical Chemistry**, 89(18): 9870-9876.
- Baig, N., and Kawde, A.-N. (2015). A Novel, Fast and Cost Effective Graphene-Modified Graphite Pencil Electrode for Trace Quantification of L-Tyrosine. **Analytical Methods**, 7(22): 9535-9541.
- Bakker, E., and Qin, Y. (2006). Electrochemical Sensors. **Analytical Chemistry**, 78(12): 3965-3984.
- Balleine, B. W., and Killcross, S. (2006). Parallel Incentive Processing: An Integrated View of Amygdala Function. **Trends in Neurosciences**, 29(5): 272-279.

- Bard, A. J., and Faulkner, L. R. (2001). *Electrochemical Methods: Fundamentals and Applications*. (A. J. Bard & L. R. Faulkner Eds. 2 ed.). New York: Wiley
- Barton, J., García, M. B. G., Santos, D. H., Fanjul-Bolado, P., Ribotti, A., McCaul, M., Diamond, D., and Magni, P. (2016). Screen-Printed Electrodes for Environmental Monitoring of Heavy Metal Ions: A Review. **Microchimica Acta**, 183(2): 503-517.
- Born, J., Lange, T., Kern, W., McGregor, G. P., Bickel, U., and Fehm, H. L. (2002). Sniffing Neuropeptides: A Transnasal Approach to the Human Brain. **Nature Neuroscience**, 5(6): 514-516.
- Caldwell, H. K., and Young III, W. S. (2006). Oxytocin and Vasopressin: Genetics and Behavioral Implications. In **Handbook of Neurochemistry and Molecular Neurobiology** (pp. 573-607): Springer.
- Carson, D. S., Guastella, A. J., Taylor, E. R., and McGregor, I. S. (2013). A Brief History of Oxytocin and Its Role in Modulating Psychostimulant Effects. **Journal of Psychopharmacology**, 27(3): 231-247.
- Chunglok, W., Khownarumit, P., Rijiravanich, P., Somasundrum, M., and Surareungchai, W. (2011). Electrochemical Immunoassay Platform for High Sensitivity Protein Detection Based on Redox-Modified Carbon Nanotube Labels. **Analyst**, 136(14): 2969-2974.
- Clark, R. A., and Ewing, A. G. (1998). Characterization of Electrochemical Responses in Picoliter Volumes. **Analytical Chemistry**, 70(6): 1119-1125.
- Clark, R. A., Hietpas, P. B., and Ewing, A. G. (1997). Electrochemical Analysis in Picoliter Microvials. **Analytical Chemistry**, 69(2): 259-263.

- Coelho, R. R. R., Rosa, J. P., Souza, R. F., and Fróes, A. M. (2013). Methods to Determine Chitinolytic Activity. In A. B. Vermelho & S. Couri (Eds.), **Methods to Determine Enzymatic Activity** (pp. 39-67). Sharjah: Bentham Science Publishers.
- Connolly, P., Clark, P., Curtis, A. S. G., Dow, J. A. T., and Wilkinson, C. D. W. (1990). An Extracellular Microelectrode Array for Monitoring Electrogenic Cells in Culture. **Biosensors and Bioelectronics**, 5(3): 223-234.
- Cox, K. L., Devanarayan, V., Kriauciunas, A., Manetta, J., Montrose, C., and Sittampalam, S. (2012). Immunoassay Methods. In **Assay Guidance Manual**: National Center for Biotechnology Information, U.S. National Library of Medicine.
- Davis, R., Markham, A., and Balfour, J. A. (1996). Ciprofloxacin. **Drugs**, 51(6): 1019-1074.
- Domes, G., Heinrichs, M., Gläscher, J., Büchel, C., Braus, D. F., and Herpertz, S. C. (2007). Oxytocin Attenuates Amygdala Responses to Emotional Faces Regardless of Valence. **Biological Psychiatry**, 62(10): 1187-1190.
- Domes, G., Lischke, A., Berger, C., Grossmann, A., Hauenstein, K., Heinrichs, M., and Herpertz, S. C. (2010). Effects of Intranasal Oxytocin on Emotional Face Processing in Women. **Psychoneuroendocrinology**, 35(1): 83-93.
- Drogowska, M., Brossard, L., and Ménard, H. (1992). Effects of Phosphate Ions on Copper Dissolution and Passivation. **Journal of the Electrochemical Society**, 139(10): 2787-2793.

- Dumé, B. (2013). Scientists Delve Deeper into Carbon Nanotubes. Retrieved from <http://physicsworld.com/cws/article/news/2013/feb/19/scientists-delve-deeper-into-carbon-nanotubes>
- Eguílaz, M., Moreno-Guzmán, M., Campuzano, S., González-Cortés, A., Yáñez-Sedeño, P., and Pingarrón, J. M. (2010). An Electrochemical Immunosensor for Testosterone Using Functionalized Magnetic Beads and Screen-Printed Carbon Electrodes. **Biosensors and Bioelectronics**, 26(2): 517-522.
- Elfar, M., Zhong, Z., Li, Z., Chakrabarty, K., and Pajic, M. (2017). Synthesis of Error-Recovery Protocols for Micro-Electrode-Dot-Array Digital Microfluidic Biochips. **ACM Transactions on Embedded Computing Systems**, 16(5s): 1-22.
- Green, J. J., and Hollander, E. (2010). Autism and Oxytocin: New Developments in Translational Approaches to Therapeutics. **Neurotherapeutics**, 7(3): 250-257.
- He, L., Sarkar, S., Barras, A., Boukherroub, R., Szunerits, S., and Mandler, D. (2017). Electrochemically Stimulated Drug Release from Flexible Electrodes Coated Electrophoretically with Doxorubicin Loaded Reduced Graphene Oxide. **Chemical Communications**, 53(28): 4022-4025.
- Heinze, J. (1984a). Cyclic Voltammetry - "Electrochemical Spectroscopy". New Analytical Methods. **Angewandte Chemie, International Edition in English**, 23: 831.
- Heinze, J. (1984b). Cyclovoltammetrie — Die „Spektroskopie“ Des Elektrochemikers. **Angewandte Chemie**, 96(11): 823-840.

- Henry, C. S., and Fritsch, I. (1999). Microcavities Containing Individually Addressable Recessed Microdisk and Tubular Nanoband Electrodes. **Journal of the Electrochemical Society**, 146(9): 3367-3373.
- Ho, J.-a. A., Chang, H.-C., Shih, N.-Y., Wu, L.-C., Chang, Y.-F., Chen, C.-C., and Chou, C. (2010). Diagnostic Detection of Human Lung Cancer-Associated Antigen Using a Gold Nanoparticle-Based Electrochemical Immunosensor. **Analytical Chemistry**, 82(14): 5944-5950.
- Jaikaew, W., Patanakul, R., and Schulte, A. (2016). Electrical Cable-Based Copper Disk Electrodes as Oxidase Biosensor Platforms with Cathodic H<sub>2</sub>O<sub>2</sub> Readout. **Electroanalysis**, 28(10): 2408-2414.
- Jemelková, Z., Zima, J., and Barek, J. (2009). Voltammetric and Amperometric Determination of Doxorubicin Using Carbon Paste Electrodes. **Collection of Czechoslovak Chemical Communications**, 74(10): 1503-1515.
- Jimenez, A. I. P., Challier, L., Di Pisa, M., Guille-Collignon, M., Lemaître, F., Lavielle, S., Mansuy, C., Amatore, C., Labbé, E., and Buriez, O. (2015). Three-Electrode Analytical and Preparative Electrochemistry in Micro-Volume Hanging Droplets. **Electrochemistry Communications**, 54: 41-45.
- Ju, H., Lai, G., and Yan, F. (2017a). 1 - Introduction. In **Immunosensing for Detection of Protein Biomarkers** (pp. 1-30): Elsevier.
- Ju, H., Lai, G., and Yan, F. (2017b). 3 - Electrochemical Immunosensing. In **Immunosensing for Detection of Protein Biomarkers** (pp. 77-110): Elsevier.
- Kai, T., Chen, S., Monterroso, E., Hailu, A., and Zhou, F. (2014). Microconcentric Ring Electrode/Injector Assembly for Sensitive Voltammetric Analysis in Single Droplets of Ultrasmall Volumes. **Analytical Chemistry**, 86(16): 8037-8041.



- Kimmel, D. W., LeBlanc, G., Meschievitz, M. E., and Cliffel, D. E. (2012). Electrochemical Sensors and Biosensors. **Analytical Chemistry**, 84(2): 685-707.
- Kirsch, P., Esslinger, C., Chen, Q., Mier, D., Lis, S., Siddhanti, S., Gruppe, H., Mattay, V. S., Gallhofer, B., and Meyer-Lindenberg, A. (2005). Oxytocin Modulates Neural Circuitry for Social Cognition and Fear in Humans. **The Journal of Neuroscience**, 25(49): 11489-11493.
- Koebach, J., O'Brien, M., Muttenthaler, M., Miazzo, M., Akcan, M., Elliott, A. G., Daly, N. L., Harvey, P. J., Arrowsmith, S., Gunasekera, S., Smith, T. J., Wray, S., Göransson, U., Dawson, P. E., Craik, D. J., Freissmuth, M., and Gruber, C. W. (2013). Oxytocic Plant Cyclotides as Templates for Peptide G Protein-Coupled Receptor Ligand Design. **Proceedings of the National Academy of Sciences**, 110(52): 21183-21188.
- Kosfeld, M., Heinrichs, M., Zak, P. J., Fischbacher, U., and Fehr, E. (2005). Oxytocin Increases Trust in Humans. **Nature**, 435(7042): 673-676.
- Kovalcik, K. D., Kirchoff, J. R., Giolando, D. M., and Bozon, J. P. (2004). Copper Ring-Disk Microelectrodes: Fabrication, Characterization, and Application as an Amperometric Detector for Capillary Columns. **Analytica Chimica Acta**, 507(2): 237-245.
- Krishnamoorthy, K., Sudha, V., Senthil Kumar, S. M., and Thangamuthu, R. (2018). Simultaneous Determination of Dopamine and Uric Acid Using Copper Oxide Nano-Rice Modified Electrode. **Journal of Alloys and Compounds**, 748: 338-347.

- Kwon, W.-K., Kim, J. H., Lee, J.-H., Lim, B.-G., Lee, I.-o., Koh, S. B., and Kwon, T. H. (2016). Microelectrode Recording (Mer) Findings During Sleep–Awake Anesthesia Using Dexmedetomidine in Deep Brain Stimulation Surgery for Parkinson’s Disease. **Clinical Neurology and Neurosurgery**, 143: 27-33.
- Leng, G., and Ludwig, M. (2016). Intranasal Oxytocin: Myths and Delusions. **Biological Psychiatry**, 79(3): 243-250.
- Leng, G., Onaka, T., Caquineau, C., Sabatier, N., Tobin, V. A., and Takayanagi, Y. (2008). Oxytocin and Appetite. In I. D. Neumann & R. Landgraf (Eds.), **Progress in Brain Research** (Vol. 170, pp. 137-151): Elsevier.
- Leng, G., and Sabatier, N. (2016). Measuring Oxytocin and Vasopressin: Bioassays, Immunoassays and Random Numbers. **Journal of Neuroendocrinology**, 28(10): 13.
- Lenihan, J. S., Ball, J. C., Gavalas, V. G., Lumpp, J. K., Hines, J., Daunert, S., and Bachas, L. G. (2007). Microfabrication of Screen-Printed Nanoliter Vials with Embedded Surface-Modified Electrodes. **Analytical and Bioanalytical Chemistry**, 387(1): 259-265.
- Lourenço, C. F., Ledo, A., Laranjinha, J., Gerhardt, G. A., and Barbosa, R. M. (2016). Microelectrode Array Biosensor for High-Resolution Measurements of Extracellular Glucose in the Brain. **Sensors and Actuators B: Chemical**, 237: 298-307.
- Marathe, B. M., Lévêque, V., Klumpp, K., Webster, R. G., and Govorkova, E. A. (2013). Determination of Neuraminidase Kinetic Constants Using Whole Influenza Virus Preparations and Correction for Spectroscopic Interference by a Fluorogenic Substrate. **PLOS ONE**, 8(8): e71401.

- Mohamed, H. M. (2016). Screen-Printed Disposable Electrodes: Pharmaceutical Applications and Recent Developments. **TRAC Trends in Analytical Chemistry**, 82: 1-11.
- Mohammadian, A., Ebrahimi, M., and Karimi-Maleh, H. (2018). Synergic Effect of 2d Nitrogen Doped Reduced Graphene Nano-Sheet and Ionic Liquid as a New Approach for Fabrication of Anticancer Drug Sensor in Analysis of Doxorubicin and Topotecan. **Journal of Molecular Liquids**, 265: 727-732.
- Montenegro, I., Queirós, M. A., and Daschbach, J. L. (2012). Microelectrodes: Theory and Applications. (Vol. 197): Springer Science & Business Media.
- Neugebauer, S., Evans, S. R., Aguilar, Z. P., Mosbach, M., Fritsch, I., and Schuhmann, W. (2004). Analysis in Ultrasmall Volumes: Microdispensing of Picoliter Droplets and Analysis without Protection from Evaporation. **Analytical Chemistry**, 76(2): 458-463.
- Neumann, I. D. (2008). Brain Oxytocin: A Key Regulator of Emotional and Social Behaviours in Both Females and Males. **Journal of Neuroendocrinology**, 20(6): 858-865.
- Nicholson, R. S. (1965). Theory and Application of Cyclic Voltammetry for Measurement of Electrode Reaction Kinetics. **Analytical Chemistry**, 37(11): 1351-1355.
- Nicholson, R. S., and Shain, I. (1964). Theory of Stationary Electrode Polarography. Single Scan and Cyclic Methods Applied to Reversible, Irreversible, and Kinetic Systems. **Analytical Chemistry**, 36: 706.
- Nordhausen, C. T., Maynard, E. M., and Normann, R. A. (1996). Single Unit Recording Capabilities of a 100 Microelectrode Array. **Brain Research**, 726(1): 129-140.

- Ojeda, I., López-Montero, J., Moreno-Guzmán, M., Janegitz, B. C., González-Cortés, A., Yáñez-Sedeño, P., and Pingarrón, J. M. (2012). Electrochemical Immunosensor for Rapid and Sensitive Determination of Estradiol. **Analytica Chimica Acta**, 743(Supplement C): 117-124.
- Renedo, O. D., Alonso-Lomillo, M. A., and Martínez, M. J. A. (2007). Recent Developments in the Field of Screen-Printed Electrodes and Their Related Applications. **Talanta**, 73(2): 202-219.
- Riberi, W. I., Tarditto, L. V., Zon, M. A., Arévalo, F. J., and Fernández, H. (2018). Development of an Electrochemical Immunosensor to Determine Zearalenone in Maize Using Carbon Screen Printed Electrodes Modified with Multi-Walled Carbon Nanotubes/Polyethyleneimine Dispersions. **Sensors and Actuators, B: Chemical**, 254: 1271-1277.
- Sahlin, E., Halle, A. t., Schaefer, K., Horn, J., Then, M., and Weber, S. G. (2003). Miniaturized Electrochemical Flow Cells. **Analytical Chemistry**, 75(4): 1031-1036.
- Scholz, F., Bond, A. M., Compton, R. G., Fiedler, D. A., Inzelt, G., Kahlert, H., Komorsky-Lovrić, Š., Lohse, H., Lovrić, M., Marken, F., Neudeck, A., Retter, U., Scholz, F., and Stojek, Z. (2010). *Electroanalytical Methods*. (F. Scholz Ed. 2 ed.). Berlin: Springer.
- Sharma, P. S., Iskierko, Z., Noworyta, K., Cieplak, M., Borowicz, P., Lisowski, W., D'Souza, F., and Kutner, W. (2018). Synthesis and Application of a “Plastic Antibody” in Electrochemical Microfluidic Platform for Oxytocin Determination. **Biosensors and Bioelectronics**, 100: 251-258.

- Shein-Idelson, M., Pammer, L., Hemberger, M., and Laurent, G. (2017). Large-Scale Mapping of Cortical Synaptic Projections with Extracellular Electrode Arrays. **Nature Methods**, 14(9): 882-890.
- Shen, B., Wen, X., and Korshin, G. V. (2018). Electrochemical Oxidation of Ciprofloxacin in Two Different Processes: The Electron Transfer Process on the Anode Surface and the Indirect Oxidation Process in Bulk Solutions. **Environmental Science: Processes & Impacts**, 20(6): 943-955.
- Shitanda, I., Irisako, T., and Itagaki, M. (2011). Three-Electrode Type Micro-Electrochemical Cell Fabricated by Screen-Printing. **Sensors and Actuators B: Chemical**, 160(1): 1606-1609.
- Sina, A. A. I., Foster, M. T., Korbie, D., Carrascosa, L. G., Shiddiky, M. J. A., Gao, J., Dey, S., and Trau, M. (2017). A Multiplex Microplatform for the Detection of Multiple DNA Methylation Events Using Gold-DNA Affinity. **Analyst**, 142(19): 3573-3578.
- Skalová, Š., Gonçalves, L. M., Navrátil, T., Barek, J., Rodrigues, J. A., and Vyskočil, V. (2018). Miniaturized Voltammetric Cell for Cathodic Voltammetry Making Use of an Agar Membrane. **Journal of Electroanalytical Chemistry**, 821: 47-52.
- Soloff, M., Alexandrova, M., and Fernstrom, M. (1979). Oxytocin Receptors: Triggers for Parturition and Lactation? **Science**, 204(4399): 1313-1315.
- Somasundrum, M., Kirtikara, K., and Tanticharoen, M. (1996). Amperometric Determination of Hydrogen Peroxide by Direct and Catalytic Reduction at a Copper Electrode. **Analytica Chimica Acta**, 319(1): 59-70.

- Sripirom, J. (2013). *Carbon Fiber-Based Sensors for Trace Electroanalysis and Scanning Probe Microscopy and a Novel System for Simple Small-Volume Voltammetry*. (Doctor of Philosophy), Suranaree University of Technology, Nakhon Ratchasima. Retrieved from <http://sutir.sut.ac.th:8080/sutir/bitstream/123456789/5005/2/Fulltext.pdf>
- Sripirom, J., Sim, W. C., Khunkaewla, P., Suginta, W., and Schulte, A. (2018). Simple and Economical Analytical Voltammetry in 15 Ml Volumes: Paracetamol Voltammetry in Blood Serum as a Working Example. **Analytical Chemistry**, 90(17): 10105-10110.
- Stradiotto, N. R., Yamanaka, H., and Zanoni, M. V. B. (2003). Electrochemical Sensors: A Powerful Tool in Analytical Chemistry. **Journal of the Brazilian Chemical Society**, 14: 159-173.
- Swain, S. M., Whaley, F. S., and Ewer, M. S. (2003). Congestive Heart Failure in Patients Treated with Doxorubicin. **Cancer**, 97(11): 2869-2879.
- Takeuchi, S., Suzuki, T., Mabuchi, K., and Fujita, H. (2003). 3d Flexible Multichannel Neural Probe Array. **Journal of micromechanics and microengineering**, 14(1): 104.
- Tardi, P., Boman, N., and Cullis, P. (1996). Liposomal Doxorubicin. **Journal of Drug Targeting**, 4(3): 129-140.
- Tarhan, F., Faydacı, G., Gül, A. E., Kuyumcuoğlu, U., and Eryıldırım, B. (2011). Oxytocin Immunoreactivity in the Corpus Cavernosum of Patients with Erectile Dysfunction. **Urologia Internationalis**, 87(2): 225-229.

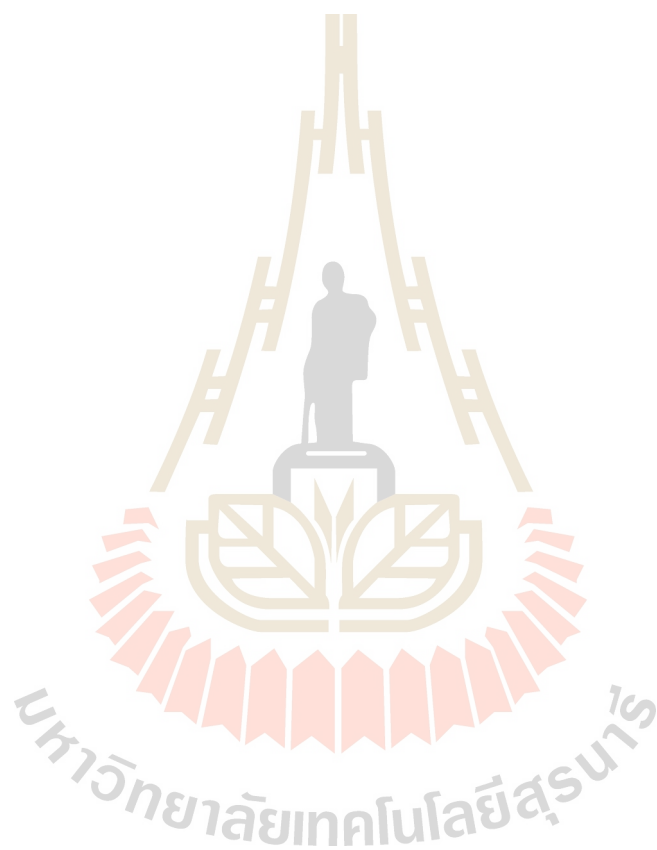
- Trojanowicz, M. (2016). Impact of Nanotechnology on Design of Advanced Screen-Printed Electrodes for Different Analytical Applications. **TRAC Trends in Analytical Chemistry**, 84: 22-47.
- Von Hoff, D. D., Layard, M. W., Basa, P., and et al. (1979). Risk Factors for Doxorubicin-Induced Congestive Heart Failure. **Annals of Internal Medicine**, 91(5): 710-717.
- Wang, J. (2006). Analytical Electrochemistry. (3rd ed.). New York: John Wiley & Sons, Inc.
- Wang, L., Li, Y., Li, G., Xie, Z., and Ye, B. (2015). Electrochemical Characters of Hymecromone at the Graphene Modified Electrode and Its Analytical Application. **Analytical Methods**, 7(7): 3000-3005.
- Ward, M. P., Rajdev, P., Ellison, C., and Irazoqui, P. P. (2009). Toward a Comparison of Microelectrodes for Acute and Chronic Recordings. **Brain Research**, 1282: 183-200.
- Weisman, O., Zagoory-Sharon, O., and Feldman, R. (2012). Intranasal Oxytocin Administration Is Reflected in Human Saliva. **Psychoneuroendocrinology**, 37(9): 1582-1586.
- Wightman, R. M., Jankowski, J. A., Kennedy, R. T., Kawagoe, K. T., Schroeder, T. J., Leszczyszyn, D. J., Near, J. A., Diliberto, E. J., and Viveros, O. H. (1991). Temporally Resolved Catecholamine Spikes Correspond to Single Vesicle Release from Individual Chromaffin Cells. **Proceedings of the National Academy of Sciences**, 88(23): 10754-10758.
- Woods, A. G., Ngounou Wetie, A. G., Sokolowska, I., Russell, S., Ryan, J. P., Michel, T. M., Thome, J., and Darie, C. C. (2013). Mass Spectrometry as a Tool for

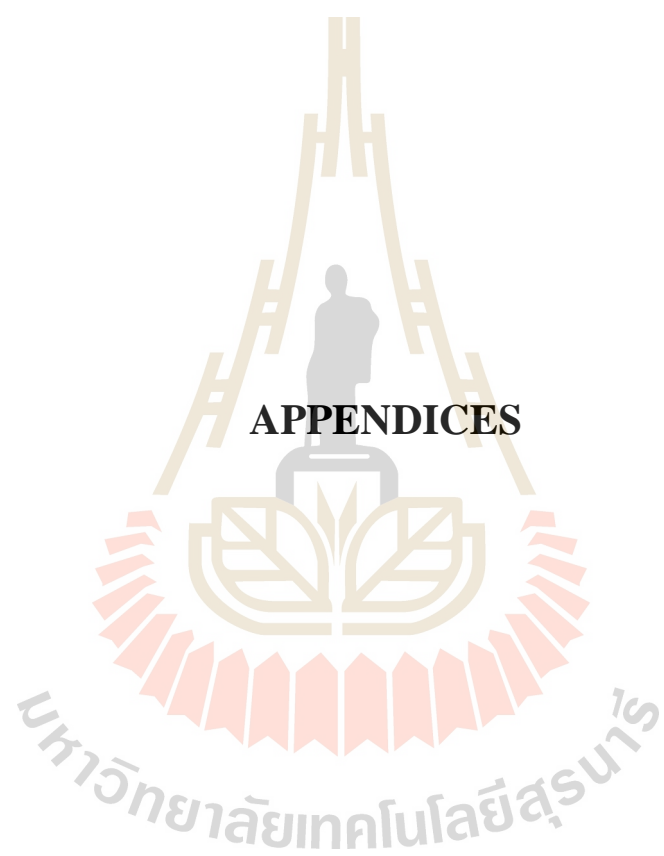


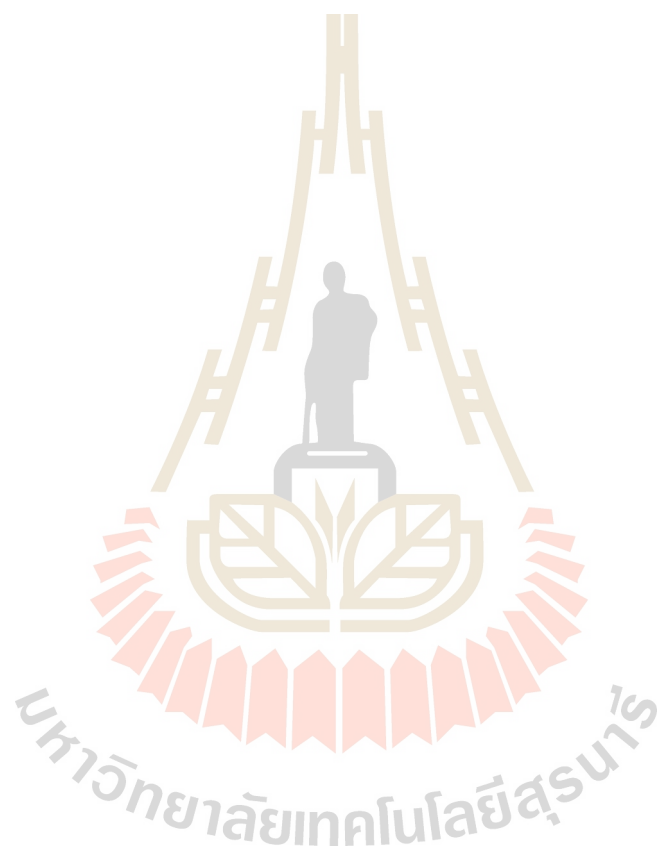
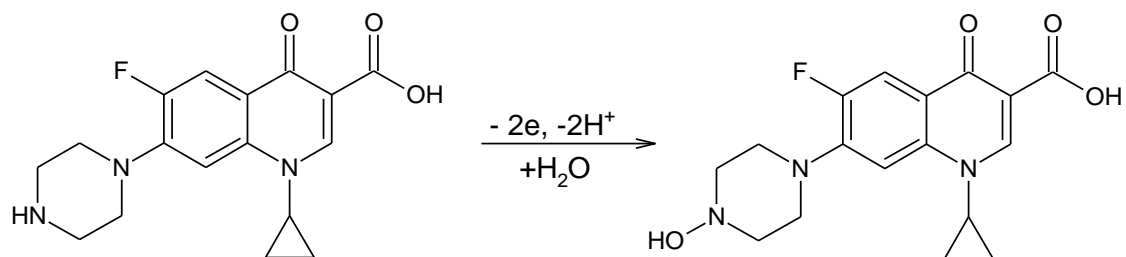
- Studying Autism Spectrum Disorder. **Journal of Molecular Psychiatry**, 1(1): 6.
- Xiang, Y., and Lu, Y. (2011). Using Personal Glucose Meters and Functional DNA Sensors to Quantify a Variety of Analytical Targets. **Nature Chemistry**, 3(9): 697-703.
- Xu, T.-Q., Zhang, Q.-L., Zheng, J.-N., Lv, Z.-Y., Wei, J., Wang, A.-J., and Feng, J.-J. (2014). Simultaneous Determination of Dopamine and Uric Acid in the Presence of Ascorbic Acid Using Pt Nanoparticles Supported on Reduced Graphene Oxide. **Electrochimica Acta**, 115: 109-115.
- Yamanaka, K., Vestergaard, M. d. C., and Tamiya, E. (2016). Printable Electrochemical Biosensors: A Focus on Screen-Printed Electrodes and Their Application. **Sensors**, 16(10): 1761.
- Yan, Y., Zhang, M., Gong, K., Su, L., Guo, Z., and Mao, L. (2005). Adsorption of Methylene Blue Dye onto Carbon Nanotubes: A Route to an Electrochemically Functional Nanostructure and Its Layer-by-Layer Assembled Nanocomposite. **Chemistry of Materials**, 17(13): 3457-3463.
- Zhang, D., Peng, Y., Qi, H., Gao, Q., and Zhang, C. (2009). Application of Multielectrode Array Modified with Carbon Nanotubes to Simultaneous Amperometric Determination of Dihydroxybenzene Isomers. **Sensors and Actuators B: Chemical**, 136(1): 113-121.
- Zhang, G., Zhang, Y., Fast, D. M., Lin, Z., and Steenwyk, R. (2011). Ultra Sensitive Quantitation of Endogenous Oxytocin in Rat and Human Plasma Using a Two-Dimensional Liquid Chromatography–Tandem Mass Spectrometry Assay. **Analytical Biochemistry**, 416(1): 45-52.

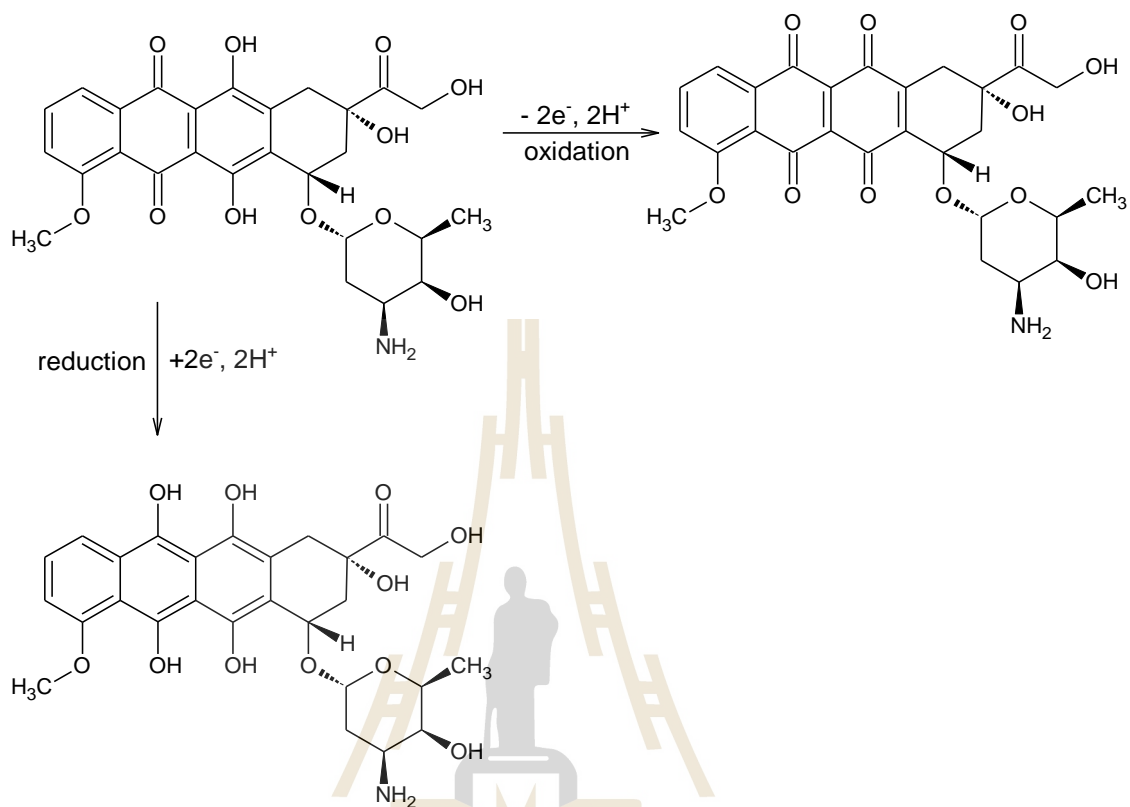


Zhang, J., Lee, J. K., Wu, Y., and Murray, R. W. (2003). Photoluminescence and Electronic Interaction of Anthracene Derivatives Adsorbed on Sidewalls of Single-Walled Carbon Nanotubes. **Nano Letters**, 3(3): 403-407.





**Appendix 1: Oxidation of ciprofloxacin**

**Appendix 2: Redox reaction of doxorubicin**

source: He *et al.* (2017); Mohammadian *et al.* (2018)

### Appendix 3: List of Publications

#### Published

1. Simple and Economical Analytical Voltammetry in 15  $\mu\text{L}$  Volumes: Paracetamol Voltammetry in Blood Serum as a Working Example  
Jiyapa Sripirom, Wei Chung Sim, Panida Khunkaewla, Wipa Suginta, Albert Schulte  
Analytical Chemistry, 2018, 90(17): 10105-10110.  
Impact factor: 6.042 (2017), Nature-Indexed Journal

#### Revised manuscript under peer-review

2. A three-electrode 30–60  $\mu\text{L}$  mini-cell for ecologically conscious analytical voltammetry with common macro- and microelectrodes  
Wei Chung Sim, Panida Khunkaewla, Albert Schulte  
Submitted to Green Chemistry  
Impact factor: 8.586 (2017)

#### Draft

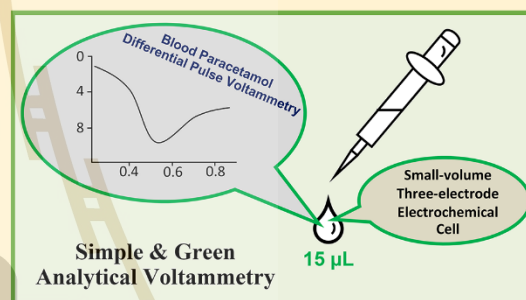
3. A copper  $\mu$ -band array electrode with microelectrode properties made by simple sandwich lamination.  
Wei Chung Sim, Panida Khunkaewla, Albert Schulte  
Planned to be submitted to Analytica Chimica Acta or Electrochimica Acta

## Appendix 3.1: Publication 1 (Page 1 of 6)

Simple and Economical Analytical Voltammetry in 15  $\mu\text{L}$  Volumes: Paracetamol Voltammetry in Blood Serum as a Working ExampleJiyapa Sripirom,<sup>†,‡,∇</sup> Wei Chung Sim,<sup>†,§,∇</sup> Panida Khunkaewla,<sup>†</sup> Wipa Suginta,<sup>†,¶</sup> and Albert Schulte<sup>\*,‡,⊙</sup><sup>†</sup>School of Chemistry, Biochemistry - Electrochemistry Research Unit - Institute of Science, Suranaree University of Technology (SUT), Nakhon Ratchasima 30000, Thailand<sup>‡</sup>School of Biomolecular Science and Engineering, Vidyasirimedhi Institute of Science and Technology (VISTEC), Rayong 21210, Thailand

## Supporting Information

**ABSTRACT:** Reported is a three-electrode mini-cell for voltammetry in 15  $\mu\text{L}$  solutions. The key device component is a rolled platinum foil of an inverted omega-shaped cross section, which functions as both the electrolyte container and the counter-electrode. The analytical assembly was completed with properly sized working and reference electrodes in the two terminals of the quasi-tubular Pt trough. Its applicability in electrochemical assays of 15  $\mu\text{L}$  solutions was verified by redox mediator voltammetry at graphite and noble metal sensors and by trace lead stripping voltammetry. Real sample analysis was adequate for drug detection in a volunteer's blood, drawn before and 1 or 4 h after ingestion of paracetamol. In line with its known pharmacokinetics, lack of drug as well as drug presence and clearance were proven correctly in the three samples. The mini-cell here is easy to assemble and operate, indefinitely reusable, and offers valuable economy in chemical usage and minimal waste. This is primarily a versatile device for electrochemical laboratory analysis of samples that are available only in small quantities, and cost-effective quantitative screens for expensive high-molecular-weight compounds, products of microsynthesis, physiological microdialysis collections, and finger-prick blood sampling are seen as feasible targets.



In the past, benchmark advances of electrochemical equipment, innovations in sensor miniaturization and surface modification, and adaptations of electrochemical cells led to great progress in the quality of analytical voltammetry. Reducing voltammetric cell volumes from mL to  $\mu\text{L}$  levels or below not only addressed “green analytical chemistry” standards in terms of chemical waste prevention/minimization and the responsible use of chemical resources<sup>1,2</sup> but also tackled budget-related needs to handle expensive redox-active compounds economically and coped with the challenges of samples that are available only in small quantities. Such cases include low yields of chemical (micro-) synthesis, fluids from microdialysis assays, rare synthetic or isolated metabolites, and finger-prick blood collections.

Present options for small-volume voltammetry range from scaled down glass- or polymer-based three-electrode vessels,<sup>3–6</sup> mini-cells for scanning probe microscopy,<sup>7,8</sup> outlets of capillary electrophoresis tubes,<sup>9–11</sup> and sophisticated flow-through cell arrangements<sup>12</sup> to microfabricated nL/pL vials with integrated two- or three-electrode assemblies.<sup>13–16</sup> From their reported performance, each of these choices has distinct advantages and works well in certain applications. Their repetitive use, however, may be hindered by the inconvenience and long

handling time of miniaturized beaker-type systems, the complexity of flow- and capillary-based variants, and the demands of nL/pL vials in terms of peripheral apparatus and operator skills. Screen-printed two- or three-electrode (SPEs) systems with bare or chemically modified carbon or noble metal detectors are, on the other hand, well-established disposable tools with the ability for testing tiny samples.<sup>17</sup> If in-house fabrication of SPEs is not possible, they can be purchased; however, frequent use may then be limited by budget, particularly in laboratories in developing countries. Recently, Perez Jimenez et al. described a low-cost, user-friendly three-electrode cell using a 50  $\mu\text{L}$  droplet, hanging by surface tension from the fritted end of a bridged saturated calomel (SCE) reference electrode, as measuring solution.<sup>18</sup> Practical working (WE) and counter (CE) electrodes for this analytical tool were slim carbon fibers or Pt microdisks or -wires. These were inserted into a freshly placed droplet from either side, enabling voltammetric measurements within the tiny blob of electrolyte. Tests of this system included standard

Received: March 13, 2018

Accepted: August 9, 2018

Published: August 9, 2018

## Appendix 3.1: Publication 1 (Page 2 of 6)

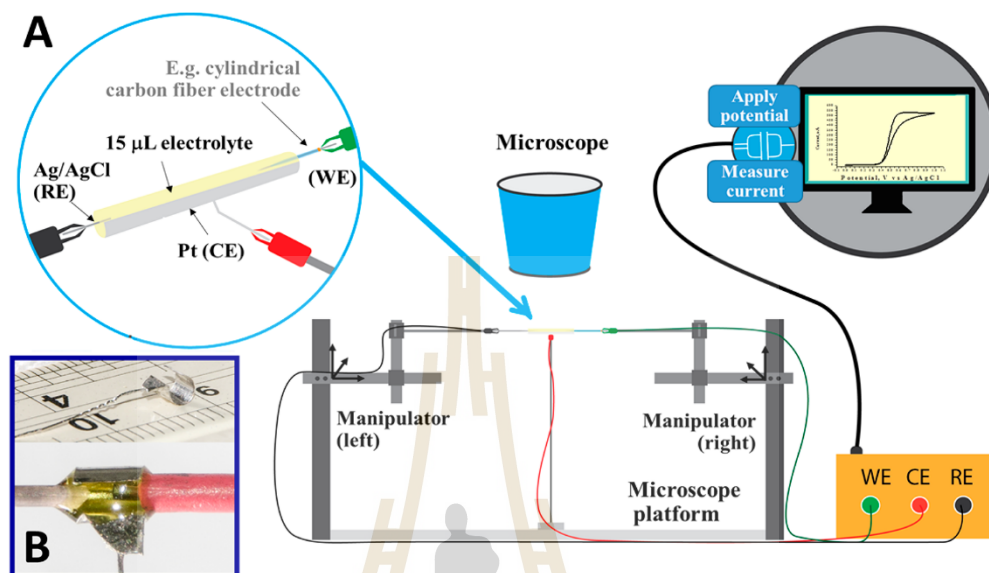


**Figure 1.** (A) Design of the miniaturized three-electrode electrochemical cell, suitable for analytical voltammetry in 15  $\mu\text{L}$  electrolyte volumes. Incorporated is, as a representative WE, a cylindrical carbon-fiber electrode, as used for serum paracetamol determinations. (B) Photograph of a completed mini-cell arrangement as used for the heavy metal stripping voltammetry trials. Visible are the yellowish ferrocyanide electrolyte (15  $\mu\text{L}$ ), the immersed end of a Ag/AgCl wire RE on the left and, on the right, an immersed 1 mm long cylindrical pencil lead electrode with red heat-shrinking tube insulation.

cyclic voltammetry (CV) in aqueous and organic electrolytes, galvanic metal plating of microelectrode disks, and CV measurements of a ferrocenyl-tagged cationic, cell-permeant peptide as a model high-value analytical target; quantitative trace voltammetry was not reported.

Here we propose a cheap, quick, and adaptable alternative to the “Perez Jimenez mini-cell”, another option for convenient and speedy low- $\mu\text{L}$  volume voltammetry, in a 3-fold smaller sample volume of just 15  $\mu\text{L}$ , for which WE and CE insertion would be hard in the hanging droplet configuration. Successful voltammetric trials with carbon and Pt or Au WEs in quasi-reversible redox mediator solutions verified the basic functionality, flexibility, and response stability of our reusable cell design. The electroanalytic capability of the proposed mini-cell was first tested by anodic stripping voltammetry of lead with carbon rod sensors. Adequate performance was confirmed with a pharmacokinetic study that followed the clearance of paracetamol (PCT), a common “over the counter” non-narcotic analgesic that is frequently the subject of intentional overdosing, from the serum of a volunteer, by means of timed blood sampling and subsequent differential pulse voltammetry (DPV) screening. Consistent with the known pharmacokinetic behavior of PCT,<sup>19–22</sup> an initial rise and subsequent fall in the serum PCT concentration after ingestion was shown by the pattern of DPV peak heights, in samples that were assessed in the microcell with cylindrical carbon-fiber microelectrodes (CFMEs) in standard addition mode.

The good outcome of the proof-of-principle studies confirmed the suitability of the innovative microcell for economic research laboratory voltammetry and suggested its use when there is a need to process samples in the microliter range, and other approaches are unfeasible.

## EXPERIMENTAL SECTION

**Chemicals, Materials, Solutions.** Paracetamol (PCT), hexammineruthenium(III) chloride, a commercial  $\text{Pb}^{2+}$  standard solution, and salts for buffer preparation were analytical grade products from various manufacturers, obtained through S. M. Chemical Supplies Co. Ltd. (Bangkok, Thailand). Aqueous buffers and analyte stock solutions were prepared with ultrapure deionized water. Precursor for disk and cylindrical CFME fabrication was a 5–7  $\mu\text{m}$  diameter polyacrylonitrile (PAN)-based carbon fiber (CF) from SGL TECHNIK GmbH, Meitingen, Germany. Also used for electrode making were 50  $\mu\text{m}$  diameter platinum (Pt) and gold (Au) microwires, thin Pt foil, and 0.25 mm diameter tungsten (W) wire (all from Goodfellow, England), glass capillaries (HEKA Elektronik Dr. Schulz GmbH, Germany), conductive carbon paint (SPI Supplies, West Chester, PA), cathodic electrodeposition paint (EDP) (Clearclad HSR, LHV Coatings Ltd., Birmingham, England), and Sylgard 184, a two-component silicone elastomer (Dow Corning Corp., Midland, MI, USA). PCT stock solutions (1 mM) were prepared by dissolving pure drug powder in DI water.

**Electrode Fabrication.** A glue-smear needle was used to pick a single CF from a multifilament bundle, which was then attached with a small drop of carbon paint to one end of a W wire that served as a holder and later electrical connection to the WE pin of the potentiostat. The CF–W wire assembly was introduced into a pulled glass capillary with a tapered tip with an inner diameter of  $\sim 20 \mu\text{m}$ , with a few mm of the CF protruding from the tip opening. The end of the W wire was glued to the top end of the glass capillary with quick-hardening two-component epoxy glue, while the CF was secured in the capillary tip with a bit of Sylgard. To construct a cylindrical CFME, the protruding CF was trimmed with a scalpel to the



## Appendix 3.1: Publication 1 (Page 3 of 6)

### Analytical Chemistry

### Technical Note

required length of, for instance, 1 mm, using a dissection microscope. Disk-shaped CFMEs were produced by insulation of the protruding graphite microfilament with a heat-cured thin film of cathodic EDP, deposited in a configuration previously described for an anodic EDP<sup>23,24</sup> but with negative fiber polarization and scalpel transection.

Carbon rod WEs were made by feeding 0.5 mm diameter pencil leads (PLs) into glass capillaries with end openings just large enough to admit the rods and a few mm left protruding. The PLs were glued to the top of the glass capillary with quick-hardening two-component epoxy glue, while a Sylgard blob formed a tight seal at the bottom, with the rod protrusion, trimmed to 1 mm, being the cylindrical sensor, similar to a design employing heat-shrinking tube insulation.<sup>25</sup> Another option was simply sealing PLs partially into heat-shrinking tubes.

Glass-insulated 50  $\mu\text{m}$  diameter Pt and Au microdisk WEs were made by heat-sealing wires of the desired diameter tightly into the ends of pulled glass capillaries and polishing the tips to expose the active surface.

For electron transfer rate constant estimation in the mini-cell, cylindrical Pt electrodes with a diameter of 250  $\mu\text{m}$  and length of 1 mm were made by sealing correspondingly thin Pt wires into the ends of pulled borosilicate glass pipettes. During the heat-sealing process, it was ensured that 1 mm of the Pt wire protruded from the glass tip. Before use, the Pt microcylinder surface was cleaned by a sequence of alumina polishing and electrochemical pretreatment procedures.

**Equipment and Electrochemical Cell Configuration.** Room temperature cyclic (CV) and differential pulse (DPV) voltammeteries used a Reference 600 potentiostat from Gamry Instruments, PA or a PSTAT 910 mini from Metrohm Siam Co., Ltd., Bangkok, Thailand. The counter-electrode was the previously mentioned homemade Pt tube with an inverted-omega-shaped cross section, and the pseudo reference electrode (RE) was a silver (Ag) wire of 1 mm diameter with a freshly prepared homogeneous AgCl coating.

Please note that for the desired quantitative PCT-DPV, the 1 mm long cylindrical CFMEs have been operated in the proposed mini-cell as a disposable type of WE. This single use was considered to avoid an unfavorable influence of electrode fouling for the voltammetric PCT measurements in the mini-cell through the formation of a contaminating surface film of polymerized products of the interfacial electrochemical process that generates the current signal for PCT analysis.

**Human Serum Samples.** Blood was collected from a volunteer before and 1 or 4 h after intake of 1000 mg of PCT (Tylenol, McNeil Consumer Healthcare, PA). The taken blood was centrifuged, the serum was collected, and the aliquots were stored at 4  $^{\circ}\text{C}$  in plastic tubes until further use. For voltammetric analysis, serum was diluted 1:1 with 0.1 M PBS, pH 7.2. Serum PCT valuation was gained by DPV in the standard addition mode.

### RESULTS AND DISCUSSION

Figure 1 shows the design of the three-electrode electrochemical mini-cell that was used for multipurpose voltammetry in 15  $\mu\text{L}$  electrolyte volumes. A rectangular piece of thin Pt foil was carefully furled into a tube with an inverted-omega-shaped cross section of 2.5 mm diameter and 3 mm length. With the opening at the top, this cell has the capacity for the specified 15  $\mu\text{L}$  of liquid. A Pt wire, spot-welded to the wall at one end of the tube, served as a gripping point for an alligator clip and

connector to the CE cable. A 1 mm diameter Ag wire with a homogeneous AgCl surface coating and a WE of an appropriate contour and size were inserted into the quasi-tubular Pt CE from the left and right, respectively. As shown in Supplementary Figure S1, handling of the mini-cell and RE and WE placement were facilitated by incorporation of the system into a stereomicroscope/micromanipulator platform. Although this makes operation easier, it is not essential, and mini-cell assembly and handling for measurements can be achieved using simpler manipulators or by careful application of simple “three hand” assembly aids, for instance, such as those used for delicate soldering actions. Data acquisition with the mini-cell for CV and DPV used the measuring cycle that is shown in Supplementary Figure S2. The procedure started with mini-cell assembly and pipetting of 15  $\mu\text{L}$  of a particular test solution into the Pt trough, followed by a voltammetry run, cell disassembly, Pt counter-electrode cleaning, and finally system reassembly and cycle repetition.

The feasibility of the 15  $\mu\text{L}$  Pt trough for electrochemical analysis was first tested by CV of 1 mM hexammineruthenium(III), with 0.1 M KCl as electrolyte and a scan speed,  $v$ , of 50  $\text{mV s}^{-1}$ . Consistent with theory, CV with a 1 mm long 0.5 mm diameter PL macroelectrode produced a symmetrical, reversible reduction and oxidation waves (Supplementary Figure S3A). Use of a carbon fiber and Pt or Au microdisk electrodes, on the other hand, led to steady state CVs of sigmoidal shape (Supplementary Figure 3B–D), as predicted for miniaturized sensors with improved delivery of redox species to the electrode surface. This proof of normal macro- and microelectrode performance was the first indication of mini-cell suitability for common voltammetry.

For a freshly polished and electrochemically cleaned cylindrical Pt microwire electrode with a diameter of 250  $\mu\text{m}$  and length of 1 mm, the quality of mini-cell voltammetry was further evaluated through CV acquisition for the ferrocyanide/ferricyanide redox couple, which is often used as stable quasi-reversible model system for characterization of new electrode materials and of mass transfer kinetics in electrochemical reactors. Supplementary Figure S4A is a display of 11 CVs that were recorded with the Pt microwire electrode in 15  $\mu\text{L}$  of 1 mM  $\text{K}_3[\text{Fe}(\text{CN})_6]/0.1$  M KCl solution, with scan rate,  $v$ , varied between 5 and 100  $\text{mV s}^{-1}$ . Symmetric anodic and cathodic current waves were verified for all tested scan rates. In Randles–Sevcik plots, the mined anodic ( $i_{p,a}$ ) and cathodic ( $i_{p,c}$ ) peak currents increased with about the same slope, consistently linear with  $v^{1/2}$  (Supplementary Figure S4B), and the statistics of a peak current analysis (Supplementary Figure S5) revealed the average  $i_{p,c}/i_{p,a}$  ratio for the CV set as  $1.06 \pm 0.01$  ( $n = 11$ ). As explained through Supplementary Figure S6, the experimental peak separations for the various scan rates were computed into electron transfer rate constants,  $k$ , for the redox interaction of the iron species with the Pt microwire electrode of the mini-cell, using the well-known Nicholson and Shain mathematical routine for the calculation.<sup>26</sup> With  $\sim 1 \times 10^{-2}$   $\text{cm s}^{-1}$ , the average  $k$  for the CV data set of this mini-cell trial was actually well within the proposed range of  $10^{-1} > k > 10^{-5}$   $\text{cm s}^{-1}$  for systems with quasi-reversibility,<sup>27</sup> and the good linearity of the Randles–Sevcik plot and the peak current ratio close to 1 confirmed this feature of the Fe (II/III)/Pt redox in the mini-cell, too.

A concern with  $\mu\text{L}$  volume electroanalysis is solvent vaporization, as associated concentration variations may critically affect signal stability. This was looked at for the



## Appendix 3.1: Publication 1 (Page 4 of 6)

### Analytical Chemistry

### Technical Note

mini-cell by reversible 1 mM hexammineruthenium(III) CV with a disk-shaped CFME as the WE. Six CVs were recorded, one immediately after loading the Pt trough with 15  $\mu\text{L}$  of test solution and the other five sequentially, with 2 min intervals in between the scans. [Supplementary Figure S7](#) shows a typical set of CVs for such an evaporation trial. The different current ( $I$ ) vs potential ( $E$ ) plots were superimposable, with plateau currents spread randomly around the computed average value,  $\pm 2\%$ . For the tested 10 min continuous unprotected operation in air, evaporation was apparently not a critical issue for practical voltammetry in the mini-cell.

DPV or square wave (SWV) stripping voltammetry is widely used for heavy metal quantification. The feasibility of this assay in the 15  $\mu\text{L}$  mini-cell was confirmed by  $\text{Pb}^{2+}$  anodic stripping voltammetry at in situ bismuth-plated 0.5 mm diameter PL electrodes of 1 mm length as sensors. Lead was gathered by controlled electrodeposition and then stripped off the electrode in a SWV scan. [Supplementary Figure S8](#) shows SWVs as obtained in the mini-cell for solutions of progressively increasing  $\text{Pb}^{2+}$  levels. Even 100 ppb produced a nice anodic current wave significantly above background. Like for published  $\text{Pb}^{2+}$  stripping voltammetry, the SWV peak currents increased over a range of 100–1500 ppb linearly with  $\text{Pb}^{2+}$  concentration. Mini-cell heavy metal stripping voltammetry is thus practicable, and the device is a promising novel electrochemical accessory for simplified green environmental sample electroanalysis.

A special sample for further mini-cell quality testing was human blood serum, obtained after uptake of 1000 mg of PCT. PCT ingestion is followed by absorption from the gastrointestinal tract into the bloodstream, metabolism in the liver, and excretion of the products in the urine or bile. The balance of drug uptake and clearance is accountable for a distinct pharmacokinetic fingerprint, with an initial rise in plasma PCT level followed by a drop. The aim here was to show by mini-cell voltammetry the time course of serum PCT values via inspection of blood samples from the various phases of medication. The PCT electroanalysis trial used 1 mm long cylindrical CFMEs as drug sensors, and before the serum measurements, their PCT signaling was verified by CV ([Supplementary Figure S9](#)). [Figure 2](#) shows for an exemplary CFME calibration that for samples with up to 1500  $\mu\text{M}$  PCT, the height of the recorded DPV peak was directly proportional to the PCT concentration, with a correlation coefficient,  $R^2$ , of 0.998. The sensitivity of the CFME voltammetry toward PCT, equal to the slope of the regression line in [Figure 2](#), was 0.1599  $\text{nA } \mu\text{M}^{-1}$  PCT, and the lowest detectable PCT level was 0.1  $\mu\text{M}$ ; below this value, the current raised not significantly above the system background. A repetition of the calibration trial with another CFME of the same (not shown) and three CFMEs of a new batch (refer to [Supplementary Figure S10](#) for the data) confirmed 1500  $\mu\text{M}$  PCT as the upper limit of linearity and 0.1  $\mu\text{M}$  as the detection limit and delivered 0.1607 and 0.2294  $\text{nA } \mu\text{M}^{-1}$  as the second old and new batch sensor sensitivity and evidence for reasonable CFME fabrication and operation reproducibility. Further application for mini-cell blood PCT voltammetry, but in standard addition mode, was therefore approached with confidence.

The methodology was then applied to the serum from the blood of a volunteer who had ingested 1000 mg of PCT. Blood samples were collected at the start of the trial, immediately before PCT was consumed, at 1 and 4 h after dose uptake, and an aliquot of the 1 h sample was also supplemented with PCT.

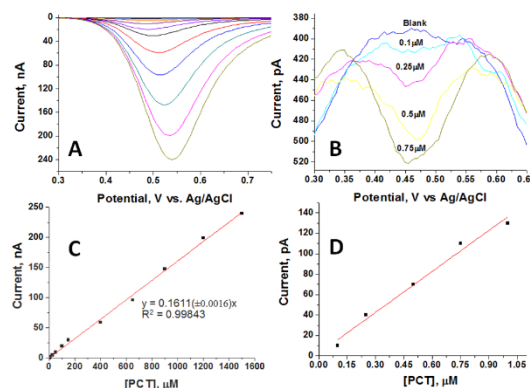


**Figure 2.** 15  $\mu\text{L}$  mini-cell paracetamol differential pulse voltammetry. WE was a cylindrical 5–6  $\mu\text{m}$  diameter carbon-fiber microelectrode of 1 mm length. (A) Set of 18 DPV traces for PCT levels of 0.1 to 1500  $\mu\text{M}$ . (B) Zoomed-in view of the DPVs for the 0.1, 0.25, 0.5, and 0.75  $\mu\text{M}$  samples. (C) Calibration plot from data in (A) and (B). (D) Zoomed-in view of the low-level region of the calibration plot in (C). Electrolyte was 0.1 M PBS, pH 7, and the scan speed for DPV acquisition without particular accumulation was 50  $\text{mV s}^{-1}$ .

The resulting set of four DPV recordings is shown in [Figure 3](#). Within the potential range used for data acquisition, a slight

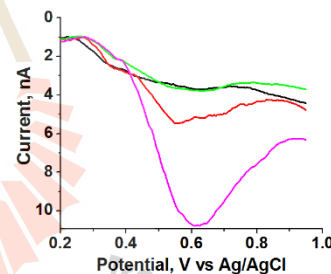


**Figure 3.** 15  $\mu\text{L}$  mini-cell voltammetry as a serum drug assay. Paracetamol (PCT) was screened in the serum of a volunteer before and after oral administration. DPV acquisition used parameters as listed in [Figure 2](#). Samples assayed included serum from blood taken before ingestion of 1000 mg (black trace), 1 h after uptake (red trace), and 4 h after (green trace). The purple trace refers to the 1 h serum supplemented with 50  $\mu\text{M}$  PCT.

anodic current activity was observed for the zero-time sample, indicating the presence of low levels of oxidizable species other than PCT and/or slight reactivity of the graphitic electrode material. The “spiked” 1 h sample showed a bell-shaped PCT-DPV with a peak maximum around +0.62 V vs RE. The curve for the 1 h sample without added PCT was less symmetrical than that of the “spiked” equivalent but was also noticeably above reference level, confirming the presence of PCT and the expected rise in serum PCT concentration on digestion of the tablet and PCT absorption. In contrast, the DPV of the 4 h sample was superimposable on the zero-time trace, indicating the metabolism and clearance of PCT from the blood.

The PCT level in the 1 h serum sample was determined via quantitative mini-cell voltammetry in standard addition mode. [Figure 4](#) shows one of the five sets of voltammograms that were acquired during a 5-fold replication of the specific serum

## Appendix 3.1: Publication 1 (Page 5 of 6)

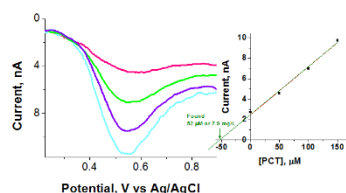


**Figure 4.** Serum paracetamol quantification by differential pulse voltammetry in the 15  $\mu\text{L}$  mini-cell in standard addition mode. Serum from blood taken 1 h after 1000 mg of PCT uptake was diluted 1:1 with phosphate buffer. DPV acquisition used parameters listed in Figure 2. The purple curve refers to unmodified sample, while the green, blue, and azure traces are samples with the addition of 50, 100, and 150  $\mu\text{M}$  PCT. The inset to the right is the corresponding standard addition calibration curve with the regression graph.

valuation. Analysis of the pool of standard addition plots, an example of which is shown in Figure 4 to the right, gave the 1 h serum PCT level as  $105.0 \pm 1.2 \mu\text{M}$  or, in the more commonly used clinical units,  $15.7 \pm 0.2 \text{ mg L}^{-1}$ , which is well within the literature reference range of 10–20  $\text{mg L}^{-1}$  1 to 2 h after uptake of a 1000 mg dose.<sup>28</sup> Use of the mini-cell for voltammetric serum analysis not only succeeded in following the distinct phases of the PCT pharmacokinetic profile but also achieved quantification of the drug in blood samples taken after oral drug administration.

In this study, we tested the proposed mini-cell for analyte measurements in aqueous electrolytes. However, the main functional entity of the device, namely, the small-volume Pt tube of inverted omega shape, is chemically resistant to organic solvents. Application for 15  $\mu\text{L}$  organic electrolyte voltammetry should thus be feasible, if the sizes of the ends of the necessary REs and WEs are suitably adapted to the dimension of the narrow opening of the mini-cell. This would reduce critical solvent waste, and further exploration of this aspect would be valuable.

### CONCLUSION

A 15  $\mu\text{L}$  volume three-electrode electrochemical cell has been developed as a tool for cheap qualitative and quantitative small-volume analytical voltammetry that is easy and quick to make and assemble. In combination with modern software-controlled potentiostats, the entire range of voltammetry schemes is applicable to electroanalysis in this “mini-cell” device. Its general applicability to redox mediator (cyclic) voltammetry was demonstrated for disk-shaped CFMEs, disk-shaped Pt and Au microelectrodes, and macroscopic cylindrical pencil lead-based carbon rod electrodes. With the last of these as WE, the mini-cell was successfully used for trace  $\text{Pb}^{2+}$  stripping voltammetry, and with cylindrical carbon-fiber microelectrodes, it was also applicable to drug voltammetry, with a performance suitable for pharmacokinetic profiling of blood samples. The electrochemical cell we describe is a simple construction for  $\mu\text{L}$  volume and thus “green” voltammetric work. The unique advantages of the cell are its simplicity of fabrication and use and, through careful choice of WEs and voltammetry procedures, flexibility in analyte targets. The established three-electrode cell solution is thus a useful miniaturized option for research laboratory voltammetry, in particular for economic electroanalytical trials with expensive molecular targets or for the measurement of samples that are available only in small quantities.

### ASSOCIATED CONTENT

#### Supporting Information

The Supporting Information is available free of charge on the ACS Publications website at DOI: 10.1021/acs.analchem.8b01135.

Portrayal of the use of the mini-cell for voltammetry with a sketch of the measuring cycle, CVs in the mini-cell for various electrodes, a description and data of the rate constant determination for the ferri-/ferrocyanide redox at a Pt microcylinder electrode in the mini-cell, the data for mini-cell  $\text{Pb}^{2+}$  stripping voltammetry and CVs from the signal stability test/electrolyte evaporation trial, a CFME-PCT cyclic voltammogram, and differential pulse PCT voltammograms of a calibration trial for cylindrical CFMEs with corresponding calibration plots (PDF)

### AUTHOR INFORMATION

#### Corresponding Author

\*E-mail: albert.s@vistec.ac.th.

#### ORCID

Wipa Suginta: 0000-0001-5927-7192

Albert Schulte: 0000-0002-3034-6075

#### Present Addresses

<sup>1</sup>Jiyapa Sripirom, Division of Chemistry, Faculty of Science, Udon Thani Rajabhat University, Udon Thani 41000, Thailand.

<sup>8</sup>Wei Chung Sim, Malaysian Agricultural Research and Development Institute, 88460 Kota Kinabalu, Sabah, Malaysia; currently on approved study leave to Suranaree University of Technology, Nakhon Ratchasima, Thailand.

#### Author Contributions

<sup>7</sup>J.S. and W.C.S. contributed equally to the laboratory experiments for this work. The manuscript was written through contributions of all authors. All authors have given approval to the final version of the manuscript.

#### Notes

The authors declare no competing financial interest.

### ACKNOWLEDGMENTS

The authors acknowledge the valuable core financial support of this work by the Thailand Research Fund (TRF) through Basic Research Grant BRG 568000013 to A.S. as well as supportive “Biochemistry-Electrochemistry Research Unit” budget allocations from Suranaree University of Technology (SUT) and SUT’s ‘Center of Excellence (CoE) in Advanced Functional Materials’ to A.S. and W.S. Extra funding for W.C.S. through the SUT-Ph.D. Scholarship Program for ASEAN, is gratefully acknowledged. Sincere appreciation also goes to LHV Coatings Limited, Birmingham, United Kingdom, for kindly supplying the cathodic electrodeposition paint for research purposes and Dr. David Apps, quondam Reader, Centre for Integrative Physiology, Edinburgh Medical School: Biomedical Sciences, Edinburgh, Scotland, for his critical manuscript reading and language improvements.

### REFERENCES

- (1) Galuszka, A.; Migaszewski, Z.; Namiesnik, J. *TrAC, Trends Anal. Chem.* **2013**, *50*, 78–84.
- (2) Tobiszewski, M.; Mechlinska, A.; Namiesnik, J. *Chem. Soc. Rev.* **2010**, *39*, 2869–2878.

### Appendix 3.1: Publication 1 (Page 6 of 6)

#### Analytical Chemistry

Technical Note

- (3) Miner, D. J.; King, W. P.; Kissinger, P. T. *Anal. Lett.* **1979**, *12*, 213–217.
- (4) Feldman, B. J.; Gheller, S. F.; Bailey, G. F.; Newton, W. E.; Schultz, F. A. *Anal. Biochem.* **1990**, *185*, 170–175.
- (5) Habermueller, K.; Schuhmann, W. *Electroanalysis* **1998**, *10*, 1281–1284.
- (6) Huber, B.; Drueschler, M.; Roling, B. *Nachr. Chem.* **2012**, *60*, 1213–1214.
- (7) Yaniv, D. R.; Jung, P. S. *Electroanalysis* **1995**, *7*, 260–263.
- (8) Turcu, F.; Schulte, A.; Schuhmann, W. *Anal. Bioanal. Chem.* **2004**, *380*, 736–741.
- (9) Wang, J. *Electroanalysis* **2005**, *17*, 1133–1140.
- (10) Lin, Y.; Trouillon, R.; Safina, G.; Ewing, A. G. *Anal. Chem.* **2011**, *83*, 4369–4392.
- (11) Cecala, C.; Sweedler, S. V. *Analyst* **2012**, *137*, 2922–2929.
- (12) Del Campo, F. J. *Electrochem. Commun.* **2014**, *45*, 91–94.
- (13) Cai, X.; Glidle, A.; Cooper, J. M. *Electroanalysis* **2000**, *12*, 631–639.
- (14) Clark, R. A.; Hietpas, P. B.; Ewing, A. G. *Anal. Chem.* **1997**, *69*, 259–263.
- (15) Henry, C. S.; Fritsch, I. J. *Electrochem. Soc.* **1999**, *146*, 3367–3373.
- (16) Yasukawa, T.; Glidle, A.; Cooper, J. M.; Matsue, T. *Anal. Chem.* **2002**, *74*, S001–S008.
- (17) Metters, J. P.; Kadara, R. O.; Banks, C. E. *Analyst* **2011**, *136*, 1067–1076.
- (18) Perez Jimenez, A. I.; Challier, L.; Di Pisa, M.; Guille Collignon, M.; Lemaitre, F.; Lavielle, S.; Mansuy, C.; Amatore, C.; Labbe, E.; Buriez, O. *Electrochem. Commun.* **2015**, *54*, 41–45.
- (19) Ward, B.; Alexander-Williams, J. M. *Acute Pain* **1999**, *2*, 139–149.
- (20) Clissold, P. S. *Drugs* **1986**, *32*, 46–59.
- (21) Prescott, L. F. *Br. J. Clin. Pharmacol.* **1980**, *10*, 291S–298S.
- (22) Bertolini, A.; Ferrari, A.; Ottani, A.; Guerzoni, S.; Tacchi, R.; Leone, S. *CNS Drug Rev.* **2006**, *12*, 250–275.
- (23) Schulte, A.; Chow, R. H. *Anal. Chem.* **1996**, *68*, 3054–3058.
- (24) Schulte, A.; Chow, R. H. *Anal. Chem.* **1998**, *70*, 985–990.
- (25) Theanponkrang, S.; Suginta, W.; Weingart, H.; Winterhalter, M.; Schulte, A. *Int. J. Nanomed.* **2015**, *10*, 859–868.
- (26) Nicholson, R. S.; Shain, I. *Anal. Chem.* **1964**, *36*, 706–723.
- (27) Heinze, J. *Angew. Chem., Int. Ed. Engl.* **1984**, *23*, 831–847.
- (28) Meredith, T. J.; Goulding, A. *Postgrad. Med. J.* **1980**, *56*, 459–473.

### Appendix 3.2: Publication 2 (Page 1 of 7)



# Green Chemistry

## A three-electrode 30–60 $\mu\text{L}$ mini-cell for ecologically conscious analytical voltammetry with common macro- and microelectrodes

Journal:	<i>Green Chemistry</i>
Manuscript ID	GC-ART-04-2019-001323
Article Type:	Paper
Date Submitted by the Author:	21-Apr-2019
Complete List of Authors:	Sim, Wei Chung; Institut Penyelidikan and Kemajuan Pertanian, Technical Services and Commercialisation Centre; Suranaree University of Technology Institute of Science, School of Chemistry Khunkaewla, Panida; Suranaree University of Technology Institute of Science, School of Chemistry Schulte, Albert; Vidyasirimedhi Institute of Science and Technology, School of Biomolecular Science and Engineering

SCHOLARONE™  
Manuscripts

มหาวิทยาลัยเทคโนโลยีสุรนารี



## Appendix 3.2: Publication 2 (Page 2 of 7)



Journal Name

ARTICLE

## A three-electrode 30–60 $\mu\text{L}$ mini-cell for ecologically conscious analytical voltammetry with common macro- and microelectrodes

Wei Chung Sim,<sup>a,b</sup> Panida Khunkaewla<sup>a</sup> and Albert Schulte<sup>c\*</sup>Received 00th January 20xx,  
Accepted 00th January 20xx

DOI: 10.1039/x0xx00000x

www.rsc.org/

A 30–60  $\mu\text{L}$  three-electrode electrochemical mini-cell for analytical voltammetry is described. The main module is a platinum tube (Pt-T) of 4 mm diameter and 5 mm height, which when placed on an inverted working electrode serves both as the counter-electrode and as the electrolyte container. A fritted mini Ag|AgCl reference electrode completes the electrochemical cell by contacting the electrolyte through the top opening of the Pt-T cell. The Pt-T mini-cell produced typical cyclic voltammograms for 30  $\mu\text{L}$  hexacyanoferrate(III) with all types of working electrode tested, i.e. Pt, Au, boron-doped diamond and glassy carbon disk macroelectrodes, a cylindrical pencil lead electrode and Pt disk microelectrodes. The mini-cell was also shown to be suitable for drug, hormone, antioxidant and redox label voltammetry, operation of a glucose biosensor and quantitative differential pulse voltammetric analysis of paracetamol in standard addition mode. The significant technical advantages of the mini-cell are its cheapness and simplicity of construction, unlimited reusability, wide analyte adaptability and ability to incorporate practically all standard macro- and microelectrode designs. Consequently, the mini-cell is not only a valuable option for voltammetry work in general, but more importantly it facilitates, in a simple and inexpensive manner, electrochemical analysis of samples with a mass or volume constraint or when the chemicals involved are costly. Obviously, the  $\mu\text{L}$ -volume electrochemical cell described in this study helps waste reduction and reduces chemical usage and, compared with conventional mL-volume beaker-type cells, is a 'green' electroanalytical tool that supports eco-friendly practice in research, commercial and teaching laboratories.

### 1. Introduction

The continuously growing world population is now confronted with increasing environmental pollution and acute natural habitat destruction. Obviously, awareness of this environmental crisis has stimulated interest in ecological life styles and in clean food, energy and chemical production and use in large sections of global society. Among scientists of all disciplines, especially chemists, it is clear that the adoption of green practices in routine tasks offers the chance to contribute personally to the minimisation of waste generation, to energy saving and to thoughtful resource utilisation, as well as inspiring others by example. Over the past few decades, electrochemical (EC) analytical chemistry has exploited the power of modern microelectronics and micro- and nano-fabrication in advancing instrumentation and accessories for better analytical performance. Innovation in electrode miniaturisation, for example, has boosted the quality of scanning electrochemical

microscopy (SECM)<sup>1–3</sup>, improved the signal-to-noise ratio and temporal resolution of voltammetric measurements<sup>4–8</sup>, and advanced physiological microelectrode voltammetry in laboratory animal brains or individual cultured cells<sup>9–14</sup>. On the other hand, the reduction in size of the measuring amplifiers has enabled the construction of portable, hand-held devices for field applications and home health care<sup>15</sup>. The ability to perform analysis on site has greatly reduced the need for sample preservation, storage and transportation to laboratories. Nevertheless, it was the shrinking of the volumes of voltammetric cells from mL to  $\mu\text{L}$  or below that really gave EC analytical chemists the option to significantly reduce analyte and reagent consumption and minimise waste generation in accordance with green chemistry standards<sup>16–21</sup>. In terms of practicability, EC cell miniaturisation is beneficial for the EC analysis of volume- or mass-limited samples. Voltammetry of these samples in larger beaker-type cells would not produce assessable current signals, since dilution may lower the analyte concentration below the detection limit.

The feasibility of accommodating functional two- or three-electrode mini-cells within vials of pL to nL volume has already been reported<sup>22–25</sup>, but this is achievable only with complex fabrication procedures and requires specially adapted working stages for cell operation, which limits the practicability of these systems for routine laboratory applications. In contrast, bulk-fabricated, screen-printed electrode devices (SPEs) are a convenient platform for voltammetry in 25–100  $\mu\text{L}$  test solutions.<sup>26–30</sup> The high purchase cost of SPEs tends to

<sup>a</sup> Biochemistry and Electrochemistry Research Unit & School of Chemistry, Institute of Science, Suranaree University of Technology, 30000 Nakhon Ratchasima, Thailand.

<sup>b</sup> Technical Services & Commercialisation Centre, Malaysian Agricultural Research and Development Institute, 88460 Kota Kinabalu, Sabah, Malaysia.

<sup>c</sup> School of Biomolecular Science & Engineering, Vidyasirimedhi Institute of Science and Technology, 21210 Rayong, Thailand.

\* Corresponding email: albert.s@vistec.ac.th

Electronic Supplementary Information (ESI) available: Additional figures. See DOI: 10.1039/x0xx00000x

## Appendix 3.2: Publication 2 (Page 3 of 7)

ARTICLE

Journal Name

discourage their daily use, as does the significant demand for equipment, time and material input, in the case of in-house manufacture. Furthermore, single-use SPE strips contribute to laboratory waste, although not to a very great extent.

Strategies for more economical  $\mu\text{L}$ -volume electroanalysis with systems other than SPEs are the subject of three recent reports. Jimenez *et al.* completed a three-electrode mini-cell by introducing the slim tips of carbon or noble metal microelectrodes and part of a platinum microwire into a 50  $\mu\text{L}$  electrolyte droplet, hanging from the bottom disc of an inverted glass-fritted reference electrode (RE)<sup>31</sup>. Skalova *et al.* sealed the tip of a tapered glass tube with agar gel, injected 20–50  $\mu\text{L}$  of test solution into the compartment thus formed and inserted disc-type working electrodes (WE) into the trapped liquid. In order to obtain voltammetric data, the sensor/sample assembly was operated in a beaker with the addition of electrolyte and a reference/counter electrode<sup>32</sup>. Most recently, Sripirom *et al.* utilised an inverted  $\Omega$ -shaped Pt tube of approximately 2 mm diameter as the container for 15- $\mu\text{L}$  sample solution and also as the counter electrode (CE). RE and WE of appropriate diameter were inserted from the left- and right-hand ends of the tube so as to complete the EC cell<sup>33</sup>. The three distinct mini-cell designs resulted in the detection of a ferrocene-labelled, cell-penetrating peptide and the electrodeposition of gold nanocrystals<sup>31</sup>, the accurate voltammetric determination of chemotherapeutic anthraquinone in urine<sup>32</sup> and pharmacokinetic drug profiling in human blood following paracetamol tablet consumption<sup>33</sup>, thus verifying the potential of  $\mu\text{L}$ -volume voltammetry as a practical alternative to conventional measurements in mL-capacity beakers. The benefits of (bio)-electroanalysis in satisfying the criteria of green, ecological and economic practice were also apparent. However, although these three types of mini-cell work well for  $\mu\text{L}$  'green' voltammetry, they all require specially-prepared tapered working electrodes for successful operation. The demand for dedicated working electrodes limits the usefulness of these systems and may thus be a reason for electrochemists not to switch from regular beaker-type EC cells to one of the suggested options for eco-friendly voltammetric sample testing.

Elimination of this drawback, so as to allow the use of commercial or homemade electrodes of standard geometries and sizes commonly available in an electrochemical laboratory, is obviously crucial in encouraging the wider adoption of  $\mu\text{L}$  voltammetry for daily 'green' electroanalysis. Accordingly, we propose a simple roll-and-fold platinum tube (Pt-T) EC cell of 30–60  $\mu\text{L}$  volume (Figure 1) that can incorporate the full range of electrodes typically available to ordinary laboratories for electroanalytical applications. The potential beneficiaries of our new EC cell are research groups that work with samples of limited availability, with expensive and/or high molecular weight analytes, have restricted budgets for the repetitive purchase of electrode consumables or need portability for instant *in situ* analyses. Furthermore, teaching laboratories in schools and universities could also benefit from the Pt-T mini-cell as a cheap, easily-made and simple-to-use option for introducing and demonstrating the ideas and values of 'green' (electro-) analytical chemistry. As good education is the key to

character building, early nurturing of green awareness in school-pupils and young scientists at universities is a valuable opportunity of inculcating environmentally friendly practices, in both their private and their professional life.

## 2. Experimental

### 2.1 Reagents and solutions

All chemicals used in this study were of analytical grade. Ultrapure water for aqueous solution preparation was obtained from a reverse osmosis-deionization system. For stock solution preparation and for most measurements in the study the electrolyte was 0.1 M phosphate buffer, pH 7.0, made by mixing solutions of sodium dihydrogen phosphate ( $\text{NaH}_2\text{PO}_4$ ) and disodium hydrogen phosphate ( $\text{Na}_2\text{HPO}_4$ ). Stock solutions of 1 M potassium hexacyanoferrate (III) ( $\text{K}_3[\text{Fe}(\text{CN})_6]$ ), 10 mM hexammineruthenium (III) chloride ( $[\text{Ru}(\text{NH}_3)_6]\text{Cl}_3$ ), 1 mM paracetamol, 1 mM ciprofloxacin, 0.1 mM doxorubicin, 0.1 mM 4-methylumbelliferone, 1 mM glucose and 0.5 M ascorbic acid were prepared in 0.1 M phosphate buffer. 15 mM oxytocin was prepared in 0.1 M phosphate buffer, divided into 100  $\mu\text{L}$  aliquots and kept in vials at  $-20^\circ\text{C}$ . Glucose oxidase from *Aspergillus niger*, of specific activity 228  $\text{U mg}^{-1}$ , was used to prepare amperometric glucose biosensors.

### 2.2 Electrodes and instrumentation

**Boron-doped diamond, noble metal and carbon working electrodes.** The 3 mm disc boron-doped diamond (BDD) electrode (S/N: D-638-SA) used in this study was purchased from Windsor Scientific Ltd. (Slough, UK). The percentage of boron dopant was listed as 0.1%. Additionally, 3 mm gold (product no.: 932-0002), 3 mm platinum (product no.: 932-0003), and 10  $\mu\text{m}$  platinum disc electrodes from Gamry Instruments (Warminster, PA, US) and a 3 mm glassy carbon disc electrode from Metrohm AG (Herisau, Switzerland) were tested with the proposed Pt-T mini-cell. The surfaces of all disc electrodes were thoroughly cleaned by polishing with 0.4  $\mu\text{m}$  alumina paste on a soft polishing mat in a continuous eight-shaped motion, before every use. A 2-mm-long cylindrical carbon electrode was made by insulating a 0.9 mm Pentel Hi-Polymer E 2B pencil lead with heat-shrink tube, leaving a 2 mm portion exposed.

**Glucose biosensor.** 5  $\mu\text{L}$  of 5  $\text{mg mL}^{-1}$  glucose oxidase (GOx) in 2 % Nafion<sup>®</sup> was dropped onto a polished 3-mm platinum disc electrode. The modified electrode was then dried in air at room temperature. This process was then repeated 4 times, giving a total loading of 125  $\mu\text{g}$  GOx on the conductive surface. Completed biosensors were immersed in 0.1 M sodium phosphate buffer, pH 7.0 containing 0.1 M KCl with stirring for 30 min before transfer to a refrigerator for overnight acclimation.

**Mini reference electrode.** The reference electrode in all measurements was a home-made  $\text{Ag}|\text{AgCl}|3\text{ M KCl}$  electrode, made by oxidising the surface of an Ag wire to AgCl by anodizing exposure to +1.0 V in 1 M HCl solution. The resultant  $\text{Ag}|\text{AgCl}$

## Appendix 3.2: Publication 2 (Page 4 of 7)

Journal Name

ARTICLE

wire was immersed in 3 M KCl solution in a glass Pasteur pipette with the narrow tip tightly sealed by a fitted porous ceramic frit.

**Potentiostat.** Electrochemical analyses in this report were conducted with a pocket-sized USB-powered 910 PSTAT mini-potentiostat from Metrohm AG (Herisau, Switzerland). The selection of this potentiostat also demonstrated the portability of the system.

### 2.3 Pt-tube mini-cell design and operation

Construction of the proposed Pt-T mini-cell simply involves rolling a rectangular piece of Pt foil ( $22 \times 5$  mm, 0.1 mm thickness) along its longer side from one end, to form a rigid cylinder of 4 mm diameter and 5 mm length. If necessary, a rod of 3 mm diameter (e.g. of Cu wire) can be used to assist in forming the shape. The remaining flat section (approx.  $10 \times 5$  mm) at the other end is folded to form a plane normal to the tube circumference (see Figure S1). The end product is a tubular Pt-T mini-cell with two open ends and a grip area for electrical connection using an alligator clip. Before use, the Pt-T mini-cell is cleaned by heating in a flame until bright red, then cooled. It is then attached to a simple height-adjustable holder and carefully brought to rest on the circular insulating housing surrounding the working electrode surface, held in an upright position. No sealing material is needed to support the intimate contact. Note also that any conductive foil could function in a minicell of our design as long as it is chemically inert, recyclable and also ductile and malleable into the required tube geometry. If stainless steel, for instance, is a suitable counter-electrode in a conventional setup, then using stainless steel sheet/plate to make this minicell is fine (although, of course, it cannot be flame-cleaned in the same way as Pt).

For electroanalysis, the Pt-T mini-cell serves both as the sample solution holder and as the counter-electrode. An Ag|AgCl|3 M KCl reference-electrode is placed in contact with the sample/electrolyte filling from the top. Working-, reference- and counter-electrodes are connected to the potentiostat leads with alligator clips. All measurements were performed at room temperature. To perform cyclic voltammetry (CV), differential pulse voltammetry (DPV) and amperometry analyses, the Pt-T mini-cell was arranged as shown in detail in ESI Figures S2 and S3. The Ag|AgCl reference-electrode was held with a simple coarse micromanipulator and slowly lowered until it dipped into the supporting electrolyte or sample solution in the mini-cell tube. Care was always taken that the tip of the reference electrode did not touch the surface of the working electrode below and was high enough to ensure that the active area of working electrode was fully accessible to the target analyte. For trials in de-aerated electrolytes the glove-box operation of the minicell should be a feasible solution.

## 3. Results and discussion

Cheap construction materials, ease of fabrication (Figure 1), wide compatibility of WE (ESI Figure S1) and simplicity of operation (ESI Figure S2) are determining factors for the acceptance of the proposed miniaturised EC cells as 'green'

substitutes for conventional beaker options. The proposed Pt-T cell can be made at a cost of \$US 50–100, at current prices, for a  $22 \times 5$  mm piece of 0.1 mm-thick Pt foil. Furthermore, the use of the mini-cell in a three-electrode arrangement requires only placement on an upright WE, pipetting of the electrolyte and insertion of the tip of a miniaturised RE into the upper opening of the Pt-T tube. The time required for reassembly between two measurements is just 2 min, inclusive of flaming the Pt-T mini-cell and polishing a 3-mm disc WE. An assembled Pt-T mini-cell was able to hold a sample of volume 30–60  $\mu$ L with no observable leakage, due to the capillary force of fluid within the thin cylinder. A tube diameter of 4 mm and height of 5 mm was suitable for common commercial disc electrodes and containing the 30–60  $\mu$ L sample. Mini-cells of significantly larger dimensions would be likely to suffer electrolyte leakage as the capillary force might fail to retain the larger liquid mass, although this was not tested. Operating the Pt-T mini-cell with sample volumes below 30  $\mu$ L was inconvenient since the immersion of the RE from the tube top was difficult without clear visualisation of physical contact.

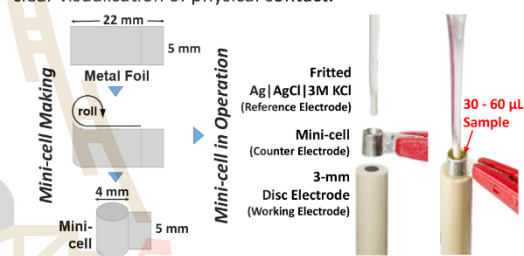


Figure 1 The construction of Pt-T mini-cell and operational assembly for electrochemical experiments.

Eight different WEs (ESI Figure S1) were tested with the Pt-T mini-cell for various voltammetry applications. Commercial disc electrodes of diameter  $\leq 3$  mm and an outer diameter  $\geq 4$  mm can easily be coupled with the Pt-T mini-cell. Electrodes of smaller diameter or different geometry may also be fitted with the help of an extra support, such as an O-ring or a short length of polymer rod with an appropriate perforation at the centre. It is worth mentioning that with tailor-made adaptors, virtually any common nano-, micro- or macroelectrode form is adaptable to the Pt-T mini-cell, which is of the utmost importance for the general applicability of the tool in electroanalysis laboratories.

Cyclic voltammograms (CVs) of 30  $\mu$ L of 12.5 mM hexacyanoferrate(III) in 0.1 M phosphate buffer, pH 7 in the Pt-T mini-cell were recorded with 3-mm diameter Pt, Au, boron-doped diamond (BDD) and glassy carbon (GC) disc macroelectrodes, a 10- $\mu$ m-diameter Pt disc microelectrode and a 2-mm-long, 0.9-mm diameter cylindrical pencil lead macroelectrode. CVs from all except the pencil lead electrode showed the peak-shaped or sigmoidal waves that are characteristic of hexacyanoferrate(III) voltammetry at disc-shaped noble metal and macro- and micro-electrodes (ESI Figure S4). The absence of distinct peaks in CVs with the pencil-lead sensor, made of a less redox-sensitive composite of



## Appendix 3.2: Publication 2 (Page 5 of 7)

ARTICLE

Journal Name

graphitic carbon and polymer binder, was also apparent in the mini-cell.

Two sets of three hexaammineruthenium(III) CVs were taken with a 3-mm boron-doped diamond disc electrode with 5 mL of solution in the beaker cell and 30  $\mu$ L in the Pt-T mini-cell, for the evaluation of reproducibility between cell reassembly. The Pt-T mini-cell delivered a set of virtually superimposable CVs, while in the beaker small but noticeable peak shifts occurred between individual runs and the CVs did not exactly overlap each other (ESI Figure S5). Also, the separation of anodic and cathodic peak maxima was a little greater for scans in the beaker cell, which can be attributed to effects related to ohmic (IR) drop and EC reversibility of electron transfer inherent in the design of the two cells. Based on specific design details, the WE-RE and WE-CE spacings for the Pt-T mini-cell are very small and thus the CVs from the repetitive cell assemblies are virtually identical. For the beaker option, however, these spacings are somewhat larger and less reproducible. The technical details suggest that the ohmic drop in the beaker cell, which is slightly larger than that in the mini-cell, is the reason for the Ru(III)/(II) redox wave shift.

To compare EC reversibility for sensor operation in the large- and small-volume systems, two sets of CV experiments were performed with 1 mM hexacyanoferrate(III) in 0.1 M KCl, with a 3-mm Pt disc electrode respectively in a 5 mL beaker and with the Pt-T mini-cell, with scan rates from 2 to 100  $\text{mV s}^{-1}$  (ESI Figure S6). For both CV sets, cathodic ( $i_{pc}$ ) and anodic ( $i_{pa}$ ) peak currents were directly proportional to the square root of the scan rate. Peak separations for the two cell options varied between  $\sim 70$  and  $\sim 100$  mV, while the average ratios of  $i_{pa}/i_{pc}$  were 1.39 and 1.08, respectively for the 5-mL beaker and Pt-T mini-cell. Using standard methodology<sup>34, 35</sup>, peak separations were converted to electron transfer rates ( $k$ ) which were  $\sim 0.009$  and  $\sim 0.015$   $\text{cm s}^{-1}$  as the mean values for hexacyanoferrate(III) redox in the beaker and mini-cell, respectively. Both cell systems showed pronounced linearity of the Randles-Sevcik plot, an  $i_{pa}/i_{pc}$  close to 1 and rate constant values within the required range of  $10^{-1}$  to  $10^{-5}$   $\text{cm s}^{-1}$ . This agrees with the expected quasi-reversibility of the redox interaction of dissolved hexacyanoferrate(III) with Pt, though the mini-cell produced a slightly better result. Reproducibly, the minicell produced about 30 % larger currents than the beaker-type equivalent. Although the reason for this is not clear the observed current enhancement was not a problem but an advantage of minicell application. In summary, the minimal manifestation of ohmic iR drop, excellent reproducibility of voltammetric response and superior quasi-reversibility make the mini-cell a valuable alternative for practical applications.

Solvent evaporation is a critical factor for electroanalysis in a small volume as it may significantly affect concentrations of dissolved species in the remaining electrolyte and thus disturb the response stability of the WE. The Pt-T mini-cell gave stable differential pulse voltammogram (DPV) peak currents over 30 min, for a 30  $\mu$ L test solution with no other measures to minimise solvent loss. This is a valuable side-effect of the special Pt-T mini-cell design as the only opening at the top of the cell is

largely blocked by the ceramic frit tip of the RE, thus minimising the surface area of solution in contact with air.

The practical functionality of the Pt-T mini-cell was further evaluated through voltammetric inspection of six electroactive compounds with relevance to basic electroanalysis and EC testing in medicine and pharmacy. These compounds were chosen because biological samples are often of limited size and low target analyte concentration, making small-volume screening a good option. The samples were (1) ciprofloxacin (CIP), a fluoroquinolone antibiotic<sup>36</sup>; (2) doxorubicin (DOX), a widely prescribed and effective anticancer agent<sup>37</sup>; (3) oxytocin (OXT), a neurohypophyseal peptide hormone involved in the regulation of emotional and social behaviours and of childbirth<sup>38</sup>; (4) ascorbic acid (AA), an antioxidant that is essential to human health through its roles in collagen biosynthesis, iron absorption, radical scavenging and immune response activation<sup>39</sup>; (5) 4-methylumbelliferone (4MU), a chemifluorescent and redox-active label of synthetic substrates used in enzyme activity assays<sup>40, 41</sup>; and (6) glucose, a central metabolic energy source for mammals and the main factor in human diabetes<sup>42</sup>.

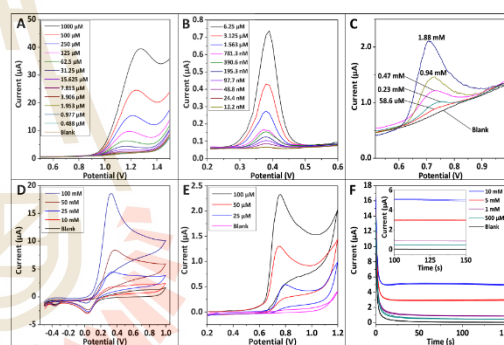


**Figure 2** Differential pulse (DPV) or cyclic (CV) response of Pt-T mini-cell with **A** ciprofloxacin (DPV), **B** doxorubicin (DPV), **C** oxytocin (DPV), **D** ascorbic acid (CV), **E** 4-methylumbelliferone (CV) and **F** mini cell glucose oxidase biosensor testing in 0.1 M phosphate buffer, pH 7.0.

Figure 2 demonstrates that the mini-cell is an attractive routine laboratory tool for 'green' electroanalysis, with the potential for the cheap and easy detection of a wide range of analytes with oxidisable and/or reducible structures. The DPVs for the two drugs and the hormone all display well-formed anodic peaks, with current directly proportional to the respective compound concentration (ESI Figure S7). In the CVs of AA and 4MU, the concentration-dependent anodic peak current are evident (ESI Figure S7), but equivalent reduction peaks are vague, which agrees with the known irreversible nature of the related interfacial charge transfer processes for these two compounds. As expected in a potential-step experiment, all five amperometric glucose oxidase biosensor recordings start with the onset of a large but fast-decaying capacitive current spike. The plateau currents are faradaic currents, contributed by the oxidation of hydrogen peroxide that is generated continuously in the biosensor's active surface coating by the enzyme-catalysed reaction. This current is directly proportional to the glucose concentration in the blank and standard samples, with



## Appendix 3.2: Publication 2 (Page 6 of 7)

Journal Name

ARTICLE

a linear range up to about 5 mM (ESI Figure S7) and can thus be utilised for quantitative analysis. Furthermore, heavy metal stripping voltammetry<sup>33</sup> and electrodeposition<sup>31</sup>, which were recently achieved in other miniaturised three-electrode EC cells of microliter volume, should also be feasible in the proposed Pt-T assembly used in this study. With the evidence presented above, it is apparent that the Pt-T mini-cell possesses the essential characteristic of general applicability.

Paracetamol (PCT), an ingredient of cold and 'flu medications, over-the-counter analgesic and a frequent choice for suicidal overdose<sup>43</sup>, was chosen as a model redox species to demonstrate the practicability of the Pt-T mini-cell for voltammetric analyte quantification. The calibration plot for PCT oxidation peak currents (ESI Figure S8) indicates that the BDD electrode coupled with Pt-T mini-cell had a dynamic range up to 250  $\mu\text{M}$  of the drug, with a linear correlation of 0.9998.

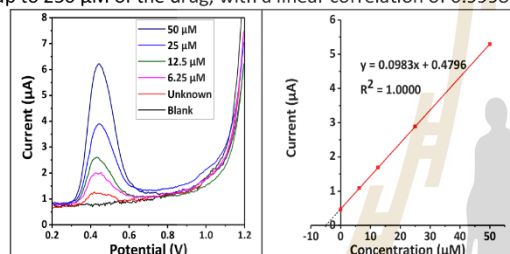


**Figure 3** DPVs and peak current vs concentration plot for quantification of paracetamol (PCT) in 0.1 M phosphate buffer, pH 7.0 by standard addition method.

Because of the small sample volume, the conventional standard addition method for the quantification of analyte in the Pt-T mini-cell was not practical, as even a small addition of standard solution to the sample would affect the analyte concentration adversely. Therefore, equal volumes of sample and standard solutions of various concentrations were mixed prior to the EC detection by DPV. A detailed illustration of this sample preparation is provided in ESI Figure S9. Since equal volumes were mixed, the initial concentrations of both sample and standard concentrations were halved. As shown in Figure 3, the PCT sample with a nominal concentration of 10  $\mu\text{M}$  produced a standard plot with an x-intercept at  $-4.98 \mu\text{M}$ , which translated into a sample concentration of 9.96  $\mu\text{M}$  and a recovery of 99.6%. Repetitions of the recovery experiment with 10  $\mu\text{M}$  PCT gave a mean recovery at 98.11% with RSD 6.60% (n=5). Similarly, a sample of 50  $\mu\text{M}$  PCT had a mean recovery of 100.67% with RSD 6.97% (n=3).

#### 4. Conclusions

An advanced  $\mu\text{L}$ -volume Pt-T mini-cell for waste-reducing and chemical-sparing small-volume 'green' analytical work was successfully demonstrated. The small tool is well suited to routine electroanalysis in common laboratories, particularly those with low budgets and no access to high-end facilities for sensor fabrication. With only 30-60  $\mu\text{L}$  of test solution needed, the mini-cell is ideal for analytes of low sample availability, high molecular weight, high toxicity or low concentration that

cannot be further diluted for measurements in conventional beaker-type cells. Accordingly, the mini-cell is recommended as a 'green' replacement for the conventional, mL-volume beaker-type electrochemical cell, just as cotton bags are an environmentally-friendly alternative to plastic shopping bags. With its simple and cheap fabrication, ease of operation and wide functionality, realisation of green voltammetry practice as a standard is thus no longer a question of possibility but a matter of willingness to abandon current approaches and adopt the proposed mini-cell for daily laboratory trials. The cheap, simple and reusable Pt-T mini-cell is also suitable for consideration in secondary and tertiary educational institutions worldwide as a device that demonstrates the principles of *Green Electrochemistry* and *Green Analytical Chemistry* to young scholars. Our future work with the developed three-electrode minicell will address the move from common indoor laboratory to special on-site field applications.

#### Conflicts of interest

There are no conflicts to declare.

#### Acknowledgements

W.C.S. acknowledges a scholarship and research budget awarded by Suranaree University of Technology (SUT) under the SUT-Ph.D. Scholarship Program for ASEAN. The authors acknowledge the financial support of this work by "Biochemistry Electrochemistry Research Unit" budget allocations from SUT and Thailand Research Fund (RTA5980007). Special thanks goes to Dr. David Apps, quondam Reader at the Centre for Integrative Physiology, Edinburgh Medical School: Biomedical Sciences, University of Edinburgh, Scotland, for manuscript proofreading and valuable language improvements.

#### Notes and references

1. T. Kai, C. G. Zoski and A. J. Bard, *Chem. Commun.*, 2018, **54**, 1934-1947.
2. J. Izquierdo, P. Knittel and C. Kranz, *Anal. Bioanal. Chem.*, 2018, **410**, 307-324.
3. C. G. Zoski, *Curr. Opin. Electrochem.*, 2017, **1**, 46-52.
4. R. J. Forster, *Chem. Soc. Rev.*, 1994, **23**, 289-297.
5. S. Daniele, M. A. Baldo and C. Bragato, *Current Analytical Chemistry*, 2008, **4**, 215-228.
6. R. M. Wightman and D. O. Wipf, in *Electroanalytical chemistry*, ed. A. J. Bard, Marcel Dekker, New York, 1989, vol. 15, pp. 267-353.
7. R. M. Wightman, *Anal. Chem.*, 1981, **53**, 1125A-1134A.
8. M. A. Dayton, J. C. Brown, K. J. Stutts and R. M. Wightman, *Anal. Chem.*, 1980, **52**, 946-950.
9. S. Majdi, A. Larsson, M. Hoang Philipsen and A. G. Ewing, *Electroanalysis*, 2018, **30**, 999-1010.
10. N. T. N. Phan, X. Li and A. G. Ewing, *Nat. Rev. Chem.*, 2017, **1**, 0048.
11. M. L. Huffman and B. J. Venton, *Analyst*, 2009, **134**, 18-24.

## Appendix 3.2: Publication 2 (Page 7 of 7)

ARTICLE

Journal Name

12. D. L. Robinson, A. Hermans, A. T. Seipel and R. M. Wightman, *Chem. Rev.*, 2008, **108**, 2554-2584.
13. C. Amatore, S. Arbault, M. Guille and F. Lemaître, *Chem. Rev.*, 2008, **108**, 2585-2621.
14. R. M. Wightman, *Science*, 2006, **311**, 1570-1574.
15. J. Wang, *Talanta*, 2002, **56**, 223-231.
16. M. de la Guardia and S. Garrigues, *Challenges in green analytical chemistry*, Cambridge, 2011.
17. S. Armenta, S. Garrigues and M. de la Guardia, *TrAC, Trends Anal. Chem.*, 2008, **27**, 497-511.
18. M. de la Guardia and S. Garrigues, *Handbook of Green Analytical Chemistry*, John Wiley & Sons, Ltd, West Sussex, UK, 2012.
19. A. Galuszka, Z. Migaszewski and J. Namieśnik, *Trends Anal. Chem.*, 2013, **50**, 78-84.
20. M. Tobiszewski, A. Mechlińska and J. Namieśnik, *Chem. Soc. Rev.*, 2010, **39**, 2869-2878.
21. J. Wang, *Acc. Chem. Res.*, 2002, **35**, 811-816.
22. J. S. Lenihan, J. C. Ball, V. G. Gavalas, J. K. Lumpp, J. Hines, S. Daunert and L. G. Bachas, *Anal. Bioanal. Chem.*, 2007, **387**, 259-265.
23. R. A. Clark and A. G. Ewing, *Anal. Chem.*, 1998, **70**, 1119-1125.
24. R. A. Clark, P. B. Hietpas and A. G. Ewing, *Anal. Chem.*, 1997, **69**, 259-263.
25. C. S. Henry and I. Fritsch, *J. Electrochem. Soc.*, 1999, **146**, 3367-3373.
26. M. Trojanowicz, *TrAC, Trends Anal. Chem.*, 2016, **84**, 22-47.
27. K. Yamanaka, M. d. C. Vestergaard and E. Tamiya, *Sensors*, 2016, **16**, 1761.
28. H. M. Mohamed, *TrAC, Trends Anal. Chem.*, 2016, **82**, 1-11.
29. J. Barton, M. B. G. García, D. H. Santos, P. Fanjul-Bolado, A. Ribotti, M. McCaul, D. Diamond and P. Magni, *Microchim. Acta*, 2016, **183**, 503-517.
30. O. D. Renedo, M. A. Alonso-Lomillo and M. J. A. Martínez, *Talanta*, 2007, **73**, 202-219.
31. A. I. P. Jimenez, L. Challier, M. Di Pisa, M. Guille-Collignon, F. Lemaître, S. Lavielle, C. Mansuy, C. Amatore, E. Labbé and O. Buriez, *Electrochem. Commun.*, 2015, **54**, 41-45.
32. Š. Skalová, L. M. Gonçalves, T. Navrátil, J. Barek, J. A. Rodrigues and V. Vyskočil, *J. Electroanal. Chem.*, 2018, **821**, 47-52.
33. J. Sripirom, W. C. Sim, P. Khunkaewla, W. Suginta and A. Schulte, *Anal. Chem.*, 2018, **90**, 10105-10110.
34. J. Heinze, *Angew. Chem.*, 1984, **96**, 823-840.
35. R. S. Nicholson, *Anal. Chem.*, 1965, **37**, 1351-1355.
36. R. Davis, A. Markham and J. A. Balfour, *Drugs*, 1996, **51**, 1019-1074.
37. P. Tardi, N. Boman and P. Cullis, *J. Drug Targeting*, 1996, **4**, 129-140.
38. D. S. Carson, A. J. Guastella, E. R. Taylor and I. S. McGregor, *J. Psychopharm.*, 2013, **27**, 231-247.
39. O. Arrigoni and M. C. De Tullio, *Biochim. Biophys. Acta Gen. Subj.*, 2002, **1569**, 1-9.
40. B. M. Marathe, V. Lévêque, K. Klumpp, R. G. Webster and E. A. Govorkova, *PLOS ONE*, 2013, **8**, e71401.
41. R. R. Coelho, J. P. Rosa, R. F. Souza and A. M. Fróes, in *Methods to Determine Enzymatic Activity*, eds. A. B. Vermelho and S. Couri, Bentham Science Publishers, Sharjah, 2013, ch. 3, pp. 39-67.
42. S. F. Clarke and J. R. Foster, *Br. J. Biomed. Sci.*, 2012, **69**, 83-93.
43. S. P. Clissold, *Drugs*, 1986, **32**, 46-59.

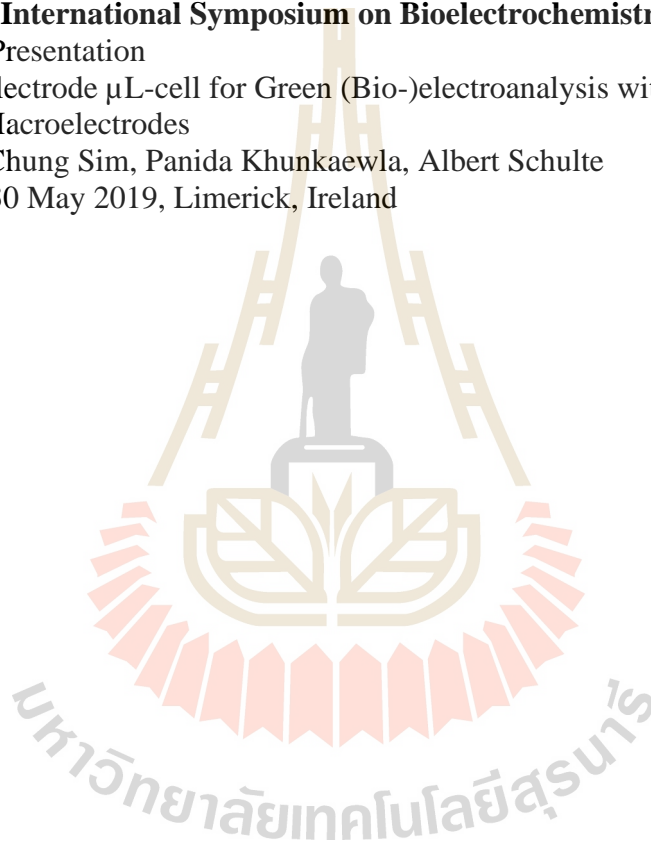
#### Appendix 4: List of Conferences

##### Attended

- 1. Pure and Applied Chemistry International Conference (PACCON 2019)**  
Poster Presentation  
A Laminated Copper Microband Array Electrode for Electrochemical Detection with Microelectrode Properties  
Wei Chung Sim, Panida Khunkaewla, Albert Schulte  
7 – 8 February 2019, BITEC Bangkok, Thailand

##### Attending soon

- 2. XXV International Symposium on Bioelectrochemistry and Bioenergetics**  
Oral Presentation  
A 3-electrode  $\mu$ L-cell for Green (Bio-)electroanalysis with Common Micro- and Macroelectrodes  
Wei Chung Sim, Panida Khunkaewla, Albert Schulte  
26 – 30 May 2019, Limerick, Ireland



# CURRICULUM VITAE

**Name:** WEI CHUNG SIM  
**Status:** Ph.D. Candidate in Chemistry  
**Date of Birth:** 12th June 1984  
**Place of Birth:** Sarawak, Malaysia  
**Nationality:** Malaysian

## Educations:

- Primary Education 1992-1996 : Chung Hwa Middle School, BSB, Brunei.
- Secondary Education  
Lower form: 1997-1999 : Chung Hwa Middle School, BSB, Brunei  
Higher form: 2000-2001 : Chung Hua Middle School, Miri, Sarawak  
Form 6: 2002-2003 : Riam Middle School, Miri, Sarawak
- Tertiary Education  
BSc. (Hons.) Petroleum Chemistry, 2007, Universiti Putra Malaysia  
MSc. Chemistry, 2010, Universiti Putra Malaysia
- Enrolled as a Ph.D. student at Suranaree University of Technology, Thailand,  
in July 2016

## Awards and Scholarships

SUT-PhD Scholarship for ASEAN, Thailand, 2016-2019.